THE CHEMICAL CHARACTERISATION OF AUTHIGENIC CARBONATES FROM THE WITBANK NO.2 COAL SEAM: ENVIRONMENTAL AND DIAGENETIC IMPLICATIONS.

by

DAVID VAN DER SPUY

Thesis submitted in fulfilment of the requirements

for the degree of

Master of Science

Department of Geochemistry

University of Cape Town

March 1991

DECLARATION

I hereby declare that all the work presented in this thesis is my own, except where otherwise stated.

Signed by candidate

D. VAN DER SPUY

Abstract

Six different types of authigenic carbonate were identified associated with the no.2 coal seam in the Witbank basin. These are:1) cell-filling carbonate, 2) early formed spherulites, 3) massive carbonates, 4) cleat-filling carbonate, 5) fracture-filling carbonates and 6) carbonate cement of associated sands. The textural relationships, depth of burial and chemical evolution of these carbonates were studied with the aid of X-ray diffraction, total organic carbon analysis, vitrinite reflectance, reflected and transmitted light microscopy, scanning electron microscopy and electron microprobe analysis.

Comparison with the studies of Matsumoto and Iijima (1981), Curtis and Coleman (1986) and other literature showed the Witbank carbonates to have followed a fairly complex path in terms of chemical evolution. The chemistry of the earliest cell-filling carbonates is indicative of an early brackish, alkaline environment with high sulphate levels, with occasional local oxidising conditions prevailing during precipitation.

Spherulite chemistry is largely representative of the continuation of alkaline conditions with high sulphate supply. Those forming closer to palaeohighs are sideritic and possibly reflect the input of fresher run-off water, allowing more acidic conditions locally. Compositional zonation of some examples indicates initial acidic conditions and later alkaline conditions. Massive carbonates are

considered to have formed, at least in some cases, from amalgamations of these earlier spherulites. They are high-Ca carbonates, siderite or dolomite. A number of the high-Ca massive carbonates were found to be aragonite. These are considered to have precipitated from water with high ionic strength, in the presence of humic acids. The chemistries of these massive carbonates are representative of the continuation of relatively alkaline conditions, or, in some cases, represent a strong brackish or marine imprint over the earlier fresh water chemistries. Chemical trends and isotope data suggest continued formation with burial.

Later formed carbonates filling cleats and fractures show more diverse compositions and are interpreted as the results of mixing of pore waters at depth, primary silicate dissolution and later percolation of groundwaters after uplift.

The overall evolution of the authigenic carbonates in the Witbank no.2 seam leads to the interpretation that the early swamp was only locally "fresh", and provides strong evidence for a marine influence at both early and late stages of deposition and diagenesis.

CONTENTS

1. INTRODUCTION..... 1

1.1 PREVIOUS MODELS..... 2

1.1.1 The study of Matsumoto and Iijima..... 2

1.1.1.a Initial sedimentary facies..... 3

1.1.1.b Diagenetic changes with burial.. 4

1.1.2 The work of Curtis and Coleman..... 5

1.2 THE DEPOSITIONAL AND DIAGENETIC ENVIRONMENTS OF THE WITBANK BASIN: A REVIEW..... 8

1.2.1 Location, age and stratigraphy..... 8

1.2.2 Sedimentary systems..... 11

2. EXPERIMENTAL SECTION..... 18

2.1 SAMPLE COLLECTION..... 18

2.2 SAMPLE PROCESSING..... 21

2.2.1 Crushing for X-ray diffraction (XRD) and Total organic carbon (TOC) analyses..... 21

2.2.2 Composite particulate blocks..... 23

2.2.3 Polished blocks..... 23

2.2.4 Polished thin sections..... 23

2.3 ANALYTICAL TECHNIQUES..... 23

2.3.1 X-ray diffraction..... 23

2.3.2 Total organic carbon determination..... 24

2.3.3 Reflected light microscope observation.. 25

2.3.4 Scanning electron microscope and energy dispersive XRF analyses..... 25

2.3.5 Electron microprobe analyses..... 26

2.3.6 Transmitted light observation and staining..... 26

2.3.7 Vitrinite reflectance..... 27

3. RESULTS..... 28

3.1 XRD AND TOTAL ORGANIC CARBON DETERMINATIONS..... 28

3.2 REFLECTANCE MEASUREMENTS AND MAXIMUM BURIAL..... 31

3.3 CARBONATES - OCCURRENCE, TEXTURES, MINERAL/MACERAL RELATIONSHIPS..... 37

3.3.1 Cell-filling carbonates..... 37

3.3.1.a Mineral compositions..... 37

3.3.1.b Associated minerals..... 39

3.3.2 Small authigenic carbonite bodies (spherulites)..... 39

3.3.2.a Mineral compositions..... 40

3.3.2.b Relationship to macerals..... 45

3.3.2.c Relationship to other minerals.. 46

3.3.3 "Massive carbonate" bodies..... 47

3.3.3.a Massive carbonate textures..... 47

3.3.3.b Mineral compositions..... 49

3.3.3.c Relationship to macerals..... 58

3.3.3.d Relationship to other minerals.. 58

3.3.4 Cleat carbonates..... 61

3.3.4.a Mineral compositions..... 61

3.3.4.b Relationship to macerals..... 68

3.3.4.c Relationship to other minerals.. 68

3.3.5 Vein and fracture fill..... 70

3.3.6 Capping sandstone cement..... 70

3.3.7 Isotope data..... 75

3.3.8 Summary..... 78

4. DISCUSSION..... 85

4.1 TEXTURAL RELATIONSHIPS AND RELATIVE TIMING OF CARBONATE FORMATION..... 85

4.1.1 Cell-filling carbonate..... 85

4.1.2 Small, spherical bodies (spherulites) associated with vitrinite..... 86

4.1.3 Massive carbonate bodies..... 87

4.1.4 Cleats..... 89

4.1.5 Fracture-filling carbonate..... 90

4.1.6 Carbonate cement in a capping sandstone above a coal seam..... 90

4.1.7 Summary..... 90

4.2 CARBONATE GEOCHEMISTRY..... 91

4.2.1 Cell-filling carbonate..... 91

4.2.2 Early spherulites..... 94

4.2.3 Massive carbonates..... 96

4.2.3.a High-Ca carbonates..... 96

4.2.3.b Siderites..... 100

4.2.3.c Dolomite..... 103

4.2.4 Cleat mineralisation..... 103

4.2.5 Fracture-filling carbonates..... 107

4.2.6 Capping sandstone cement..... 107

4.3 CHEMICAL EVOLUTION OF THE WITBANK CARBONATES..... 108

4.3.1 Siderite chemistry..... 108

4.3.2 Calcite chemistry..... 112

4.3.3 Chemical evolution of carbonates..... 116

5. CONCLUSIONS AND RECOMMENDATIONS..... 125

5.1 CONCLUSIONS..... 125

5.2 RECOMMENDATIONS FOR FURTHER RESEARCH..... 128

APPENDICES

Appendix A.....Sample descriptions

Appendix B .....Electron microprobe operating conditions and standards and X-ray diffractometer operating conditions

Appendix C.....Vitrinite reflectance data

Appendix D.....Electron microprobe analyses

Appendix E.....Plates

Appendix F.....Paper in press

van der Spuy, D. and Willis, J.P. (1991). The occurrence of aragonite in carbonate lenses in coals from the Witbank area. Trans. Geol. Soc. S. Afr.

LIST OF FIGURES

Figure 1: Summary chart showing the origin and diagenetic evolution of authigenic carbonates in Japanese coal measures, from figure 11, Matsumoto and Iijima (1981).....6

Figure 2: Map showing the location of the study area. Adapted from Falcon (1989) and Le Blanc Smith (1980).....9

Figure 3: Generalised stratigraphic column of the Vryheid Formation, from Cairncross and Cadle (1988).....10

Figure 4: Sample localities.....19

Figure 5a: An example of the classification of minerals as major, secondary and "other", on the basis of their relative XRD peak heights.....30

Figure 5b: The effect of differences in organic carbon content on peak heights in X-ray diffractograms.....32

Figure 6: Predicted vitrinite curves for early Permian sediments with increasing burial at gradients of a) 2.5°C/100m and b) 3°C/100m.....35,36

Figure 7: Cell-filling carbonate compositions.....38

Figure 8: Spherulite compositions.....41 - 44

Figure 9: Compositional distribution of spherulites across the study area.....45

Figure 10: Massive carbonate compositions - Group ia) high-Ca carbonates.....50-51

Figure 11: Massive carbonate compositions - Group ib) high-Ca carbonates with significant Mg content.....52-53

Figure 12: Massive carbonate compositions - Group ic) high-Ca carbonates with significant Fe+Mn content.....53

Figure 13: Massive carbonate compositions: Group ii) siderite.....55

Figure 14: Massive carbonate compositions: Group iii) dolomite.....56

Figure 15: Compositional distribution of massive carbonates across the study area.....57

Figure 16: $SrCO_3$-$(FeMn)CO_3$-$BaCO_3$ plot of the Sr-rich "exsolution lamellae" in sample 35.....60

Figure 17: Cleat-fill carbonate compositions: Group i) high-Ca carbonates.....62,63

Figure 18: Cleat-fill carbonate compositions: Group ii) high-Ca carbonates with significant Mg content.....64,65

Figure 19: Cleat-fill carbonate compositions: Group iii) dolomite...66,67

Figure 20: Cleat-fill carbonate compositions: Group iv) ankerite.....69

Figure 21: Fracture-fill carbonate compositions.....71-73

Figure 22: Capping sandstone carbonate cement composition.....74

Figure 23: Isotope values from detailed sampling across sample 6, from figure 7, Falcon and Verhagen (1990).....77

Figure 24: Stability relations of Fe-oxides, sulphides and carbonate in water at 25°C and 1 atmosphere pressure. Total dissolved sulphur = 10^{-6}. Total dissolved carbonate = 10^{0}. From figure 7.21, Garrels and Christ (1965).....102

Figure 25: Comparison of Japanese siderites with Witbank no.2 seam siderites.....109

Figure 26: Mg/Fe - Mn/Fe variation diagrams for 2 early spherulites and all siderites analysed.....111

Figure 27a: Diagenetic stages and the chemical composition of Japanese calcites in various sedimentary facies. From figure 10, Matsumoto and Iijima (1981).....113

Figure 27b: Chemical evolution of some Witbank calcites.....115

Figure 28: Carbonate evolution paths identified in the Witbank no.2 coal seam.....118

Figure 29a: Annotated diagrammatic summary of evolutionary path 1.....121

Figure 29b: Annotated diagrammatic summary of evolutionary path 2.....122

Figure 29c: Annotated diagrammatic summary of evolutionary path 3.....123

Figure 29d: Annotated diagrammatic summary of evolutionary path 4.....124

LIST OF TABLES

Table 1: X-ray diffraction results and Total organic carbon determinations.....29

Table 2: Vitrinite reflectance values..... 34

Table 3: Bulk sample isotope values across some massive carbonates, from table 1, (Falcon and Verhagen, 1990).....76

Table 4: Summary of results.....79-81

Table 5: Sequence of precipitation of authigenic carbonates in Japanese Coalfields, from table 1, (Matsumoto and Iijima, 1981).....117

1 INTRODUCTION

The chemical and physical nature of sedimentary rocks is determined by its depositional environment and later diagenetic history. In the case of coal, the chemical and physical properties imposed upon the sediment by these factors must ultimately affect its beneficiation. These properties include hardness, friability, ash content and composition and fusion temperatures (Ward,1984; Falcon, pers. comm.).

Although extensive work has been undertaken on the sedimentological aspects of the depositional environments of coals in the Permian Vryheid formation, Transvaal, South Africa (Holland, et al., 1989; Cairncross and Cadle, 1988), and the diagenetic environments from the point of view of coalification and macerals (Falcon, 1989), little attention has been paid to the geochemistry of the depositional and diagenetic environments as reflected by the authigenic minerals and their chemical evolution.

In a paper entitled "Origin and diagenetic evolution of Ca-Mg-Fe carbonates in some coalfields of Japan", (Matsumoto and Iijima, 1981), the authors discussed changes in carbonate chemistry in direct response to depositional and later diagenetic environments. They constructed a systematic framework for initial deposition, and described a progression in carbonate chemistry with these changes. A

similar study by Curtis and Coleman (1986), of siderite concretions from organic-rich clastic sediments in the Westphalian A, U.K., described a similar progression in carbonate chemistry with changes in diagenetic environment, but stressed the importance of sulphate availability as a control on the carbonate mineral species precipitated.

This study, which concentrates on carbonates specifically from carbonate-rich horizons in the no.2 seam of the central Witbank basin, is an attempt to relate and compare the mineral parageneses, and carbonate chemistry in particular, to the models suggested by Matsumoto and Iijima (1981) and Coleman and Curtis (1986) and other literature. Conclusions will be drawn concerning the influence of fresh, brackish and/or marine waters on the depositional and diagenetic environments of the Witbank no.2 seam coal deposit.

1.1 Previous models of carbonate diagenesis in organic rich sedimentary rocks

1.1.1 The study of Matsumoto and Iijima

From a study of carbonate concretions, lenses and bands in Pleistocene, Palaeogene and upper Triassic coalfields of Japan, Matsumoto and Iijima (1981) arrived at a systematic progression in carbonate chemistry in direct response to initial depositional environment/sedimentary facies and later diagenetic evolution of pore water with increasing depth of burial. Their study included samples

Marine conditions result in the following relative abundances of early carbonates:- calcite > dolomite >> siderite. This progression is produced in the same manner as for a brackish environment.

1.1.1.b Diagenetic changes with burial

Further influence on carbonate chemistry was exerted by changes in pore water composition with burial. Matsumoto and Iijima (1981) identified the following three stages:

i) Less than 500m burial - carbonate chemistries reflect initial sedimentary facies as outlined above, with low Ca-Mg siderite occurring in fresh water as there is an abundant supply of Fe from lateritic soils surrounding the basin. Brackish and marine environments are dominated by Mg-calcite and dolomite, which are attributed to the relatively high concentrations of the Ca^{2+} and Mg^{2+} ions in sea water [(400 ppm and 1310 ppm, respectively) (Garrels and Thompson, 1962)], due to dissolution of invertebrate shells.

ii) 500 to 2000m burial - compaction causes migration and mixing of pore waters, supplying Fe^{2+} and bicarbonate (bacterial fermentation and later decarboxylation) from fresh water and Mg^{2+} and Ca^{2+} from marine waters. Carbonates formed during this stage in freshwater environments include high Ca-Mg siderite, ankerite, Fe dolomite and Fe-Mg calcite. The assemblage in brackish and marine environments was found to be similar.

iii) Greater than 2000m burial - Carbonates formed during this stage were Fe calcite and, in marine mudstones, extremely high Ca-Mg siderite. Thermal decarboxylation, reduction of Fe^{3+}, oxidation of organic materials and thermal alteration of silicates provide the necessary ions.

Later uplift allows low-Mg calcite to precipitate in extensional cracks from percolating groundwater. The above is summarised in Figure 1.

1.1.2 The work of Curtis and Coleman

From a study of compositional variation in some siderite concretions in the Westphalian A of Yorkshire, Curtis and Coleman (1986) came to the following conclusions. Post-depositional chemical alteration in coal measures was extensive and varied and diagenetic mineralogy was strongly controlled by the availability of sulphur, and thus by depositional water composition. Slow detrital sediment accumulation allowed active sulphate reduction and Fe was precipitated as pyrite, while Fe-poor carbonates precipitated. As Mg^{2+} and Ca^{2+} were also plentiful, high-Mg calcite was the norm.

In fresh water, sulphate is scarce and pore waters of sediments deposited in fresh water contain lower concentrations of solutes. Solute availability is thus strongly controlled from within the sediment itself by the breakdown of detrital constituents, with the most unstable reacting first. Thus hydrated iron oxides are reduced, raising Fe^{2+} concentrations, the Fe/Ca ratio and alkalinity. Early carbonates are thus Fe and Mn-rich siderites.

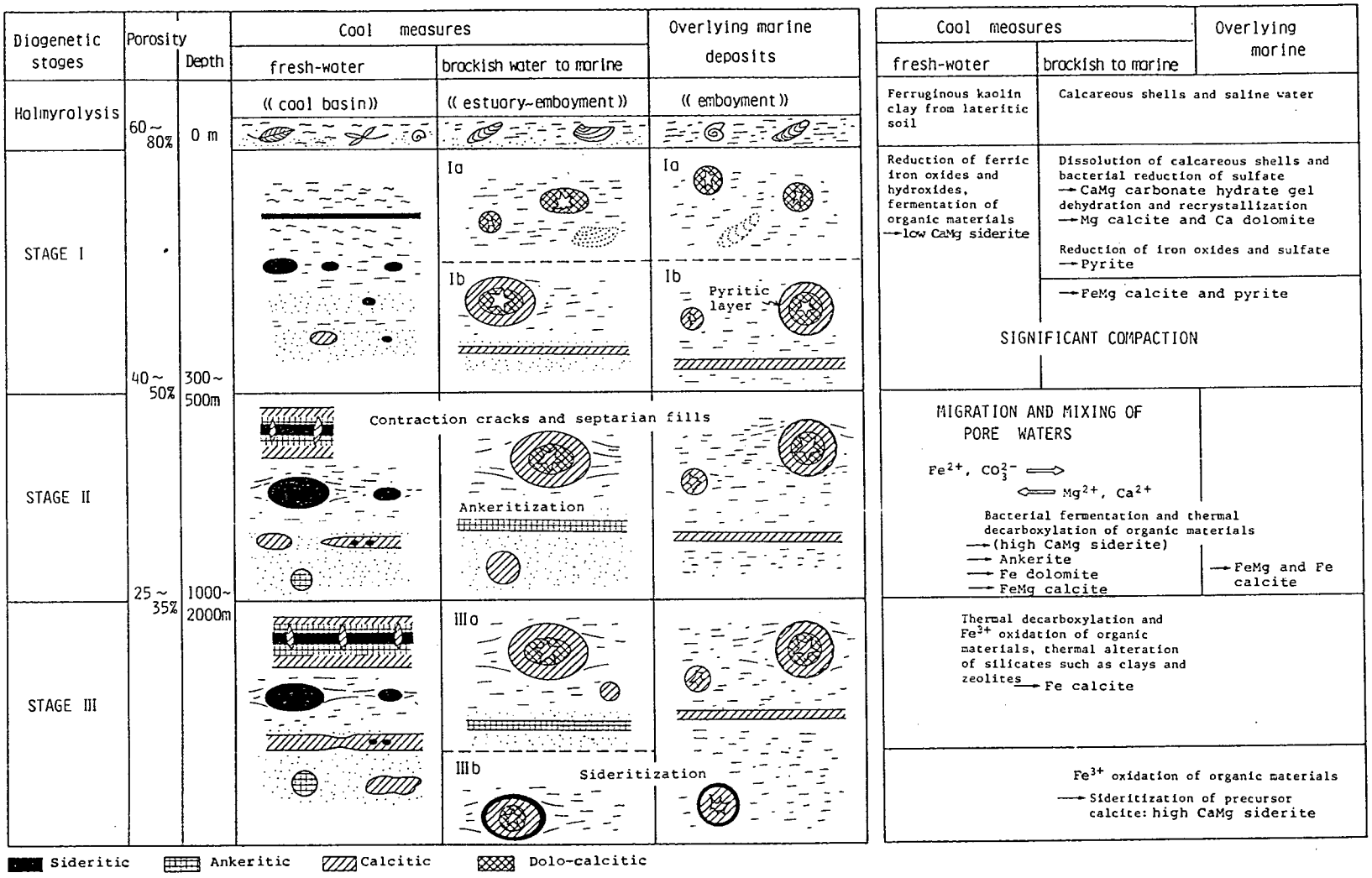

Figure 1: Summary chart showing the origin and diagenetic evolution of authigenic carbonates in Japanese coal measures, from figure 11, Matsumoto and Iijima (1981).

These simple patterns are overprinted by rapid changes in depositional environment as sediment pore waters become mixed by downward diffusion or upward flow due to compaction and dewatering. This effect is most clearly seen after marine transgressions when early diagenesis in freshwater coal peats is entirely marine in character, i.e. calcite and pyrite. In mixed waters, the principal control appears to be sulphate concentrations in the pore water; high levels result in the precipitation of Mg calcite and lower levels in dolomite formation.

Later diagenetic products such as Mg siderite, only apparent in the non-marine sequences studied, indicate that by this stage the more reactive Fe oxides occur in lower concentration and Fe^{2+} is no longer in "oversupply". Microbial decomposition eventually declines and thermal sources of carbonate become increasingly important.

The patterns of diagenetic precipitation of carbonates described in the studies above are similar. Curtis and Coleman simply placed the stress on the availability of solutes while Matsumoto and Iijima approached the problem from an environmental point of view. It is important to note, as pointed out by Curtis and Coleman, that the original depositional (and earliest diagenetic) environment may be easily masked by rapid changes such as transgressions or uplift and may find no expression in the chemistry of early carbonates at all.

1.2 The depositional and diagenetic environments of the Witbank Basin - A review.

1.2.1 Location, age and stratigraphy

The Witbank coalfield is situated south of Witbank and Middelburg but north of the Smithfield Ridge in the central Transvaal, South Africa (Figure 2). It consists of up to six coal seams interspersed with shales, sands, granulestones and conglomerates, overlying the glaciogenic Dwyka, while the Proterozoic Bushveld felsite forms positive ridges and escarpments. A generalised stratigraphic column for the sequence is presented in Figure 3.

The sedimentary package, known as the Vryheid Formation, is typically 80 to 100m thick and seldom exceeds 200m in thickness. The Vryheid Formation is middle Permian in age (Falcon, 1989; Cairncross, 1989; Falcon et al., 1984), with coal seams occurring in the late Dwyka and Ecca Groups of the Karoo Supergroup, deposited in an asymmetric, intracratonic basin (Cairncross, 1989; Falcon, 1989; Holland et al., 1989; Falcon et al., 1983). In the main Karoo Basin, coals are confined to the stable, passive, northern margin.

Palaeomagnetic reconstructions have shown that during this time, relative to Gondwana, the south pole moved from central to southern Africa, and then eastwards to Antarctica (Falcon, 1987; Hobday, 1987). This high latitude position of southern Africa in the early Permian gradually changed, resulting in a retreat of the Dwyka glaciation to the north and

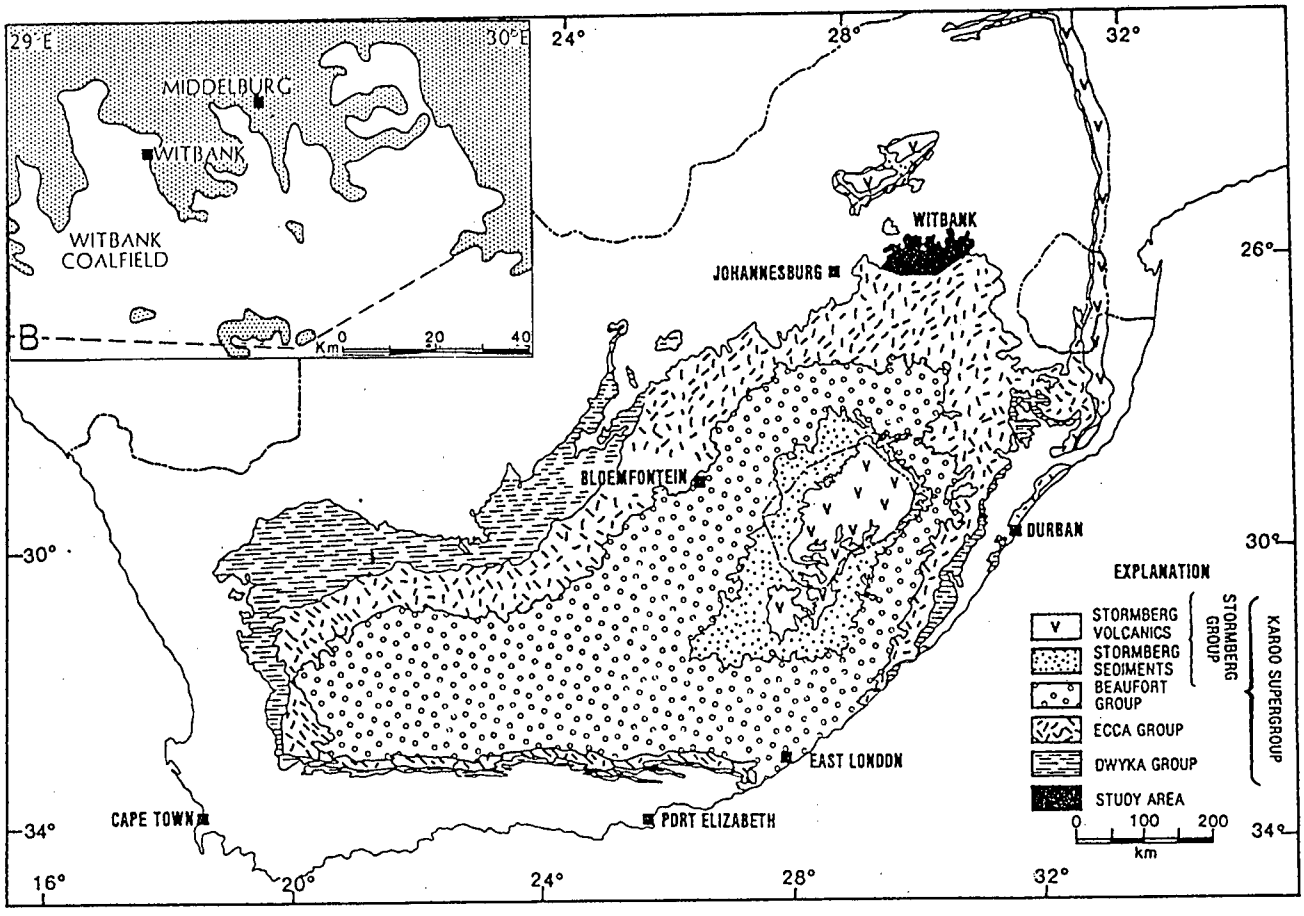

Figure 2: Map showing the location of the study area. Adapted from Falcon (1989) and Le Blanc Smith (1980).

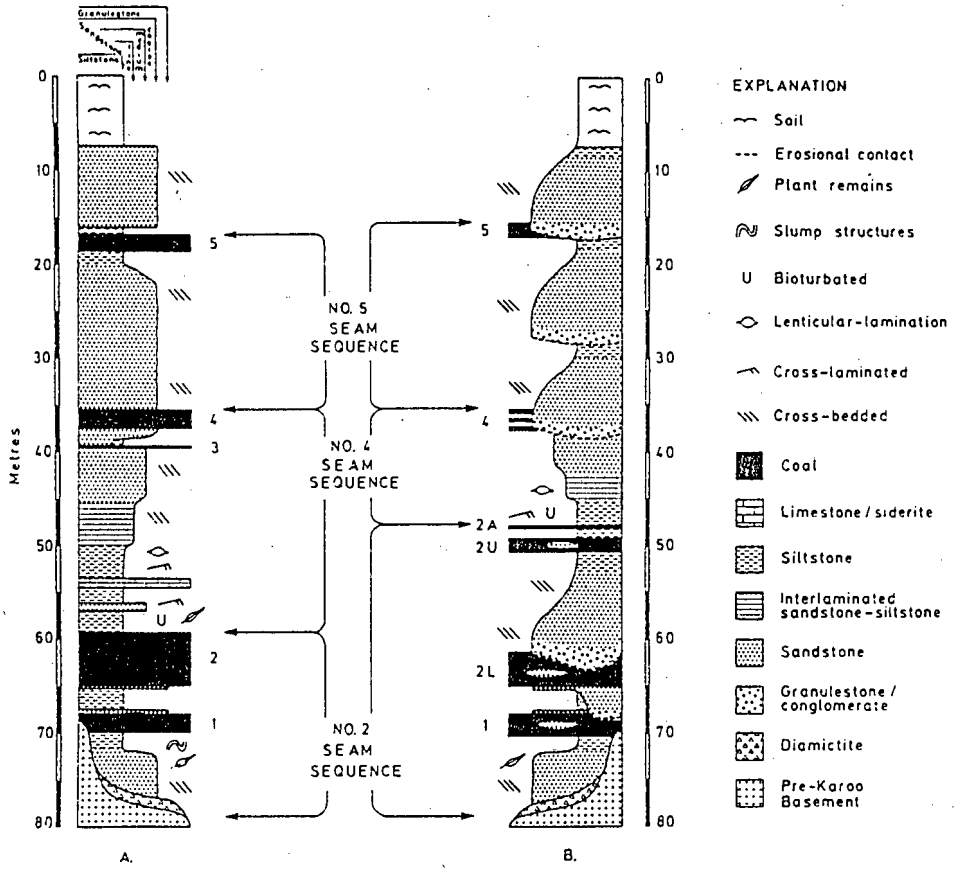

Figure 3: Generalised stratigraphic column of the Vryheid Formation, from Cairncross and Cadle (1988).

Falcon (1989) is of the opinion that subarctic, cold winters alternated with warm, humid summers resulting in wide temperature ranges and short growing seasons. High proportions of semi-reactive inertinite are typical of Gondwana coals and this has been interpreted as a result of exposure of partly gellified peat to oxidising conditions (Holland et al., 1989, Falcon, 1989). Slow plant growth and degradation alternating with relatively hot summers resulted in the formation of semi-reactive inertinite as partially gellified peat was later exposed.

Some Gondwana coals from Brazil and Australia show a close association of alginite and semi-reactive inertinite. Wet and dry conditions alternated with minimal oxidation occurring. Humified tissue is thought to have been freeze dried, resulting in a semi-reactive inertinite (Taylor et al., 1989).

These early coals are closely associated with coarse grained sandstones and conglomerates of glaciogenic origin (Cairncross, 1989), yet are relatively low in ash content. This may be the result of peat formation not being contemporaneous with clastic input, or the pH differences between swamp and flood waters resulting in the flocculating out of clays in the channel margins, thus shielding the swamp from major clastic contamination.

Clastic contamination could also be avoided if the peat were raised or floating, a common phenomenon in peats forming under cool, temperate conditions. In low pH swamps, pods of peat are floated by biogenic methane and may eventually form lenses or pods of relatively low ash coal (Cairncross and Cadle, 1988).

the coal seams is consistent with transgressive events as the transgressive waters could carry clastic material into the swamp in suspension (Falcon et al., 1983).

Falcon (1989) suggested a cyclothem model, controlled by the waxing and waning of major glaciation, for deposition in the basin from this point onwards. The number 2 seam is seen as the point of change over from glacially dominated to cyclic coal deposition. She pointed out that glauconitic deposits overlie three of the major seams in the basin.

Cairncross and Hart (1988) claimed that an increase in Br content from the base to the top of the no.2 seam in two out of six profiles, is indicative of less acidic, more marine conditions towards the top of the seam. Those profiles not showing the increase are considered to have been shielded from the marine influence by fluvial sediments. Pyritic upper surfaces of coal seams are also seen as evidence of marine transgression (Hobday, 1987).

However, this conclusion is not reached by Roberts (1988) who studied the relationship between pyrite and vitrinite in the no.4 lower, 4 upper and 5 seams, which are obviously well into the postulated marine transgressive cyclic sequence. There is a positive correlation between vitrinite and sulphur content in these coals, and as the same flora formed both vitrinite and inertinite, total sulphur contents must reflect early diagenetic conditions. A high water table and low Eh conditions would allow bacterial sulphate reduction (sulphur fixed in the original plant tissue) with H_2S and Fe^{2+} eventually forming pyrite and organic sulphur compounds. A low water table and high Eh conditions would

encourage aerobic respiration and little H_2S would be produced. Thus the variations in sulphur content (pyrite) may simply reflect oscillating water levels due to climatic changes and not necessarily variations in marine sulphur supply.

The Secunda coalfield, to the south of Witbank (further into the main basin and thus less protected from transgressions), is interpreted as having been deposited in a meandering fluvial environment (Hagelskamp et al., 1988). Coal quality varies in correspondence with fluvial depositional features and sideritic nodules occur in distinct horizons. Glauconite is not regarded as exclusively indicative of marine conditions, having been reported from nonmarine sediments and alluvial and lacustrine palaeoenvironments (Keller, 1958), and is neither persistent nor concentrated in channel belts where marine ingression would be expected to have the greatest effect.

Coupled with this suggested cyclic system of coal deposition and transgressions was a stepped, progressive amelioration in climate accompanied by an increase in diversity of flora with a change to largely disaccate species (Falcon et al., 1983; Falcon, 1989). Sediments were deposited by fluviodeltaic systems prograding towards the south and southwest, and include beach barrier deposits, bed-load braided fluvial deposits, anastomosed river deposits and high-constructive deltaic complexes (Cairncross, 1989). The central basin was dominated by high-constructive deltaic sedimentation while the eastern areas were dominated by bed-load braided fluvial deposits.

Holland et al. (1989) grouped the seams according to palaeodepositional environments. The no.1, 2 and 4 seams are thick and laterally continuous and are regarded as having been deposited in fluvial environments (whether glaciofluvial or upper delta) while the thinner laterally discontinuous no.3 seam is interpreted as a lower delta plain coal. Its higher vitrinite content is a result of subsidence keeping pace with changes in the water table, preserving anaerobic conditions.

The alternating sedimentary succession described above ends with a massive marine transgression (Falcon, 1989). From the above discussion it is clear that many and varied initial geochemical environments could thus be expected in any one seam, and from one seam to another. The two lowermost seams were deposited under largely freshwater, paraglacial fluvial conditions while climatic conditions were cold. The later seams were deposited in deltaic systems, during a period of climatic amelioration characterised by cyclic deposition and transgressions, thought to be marine in nature. These major patterns are further complicated and obscured by the existence of varied micro-environments. The close association of all these coals with coarse clastic rocks would facilitate the movement and mixing of pore fluids during further burial, perhaps enabling the later transgressions to overprint entirely the early diagenetic chemistry.

It was with this uncertainty regarding the original depositional environment and the later diagenetic environment in mind, that this study was undertaken. The chemistries and mineral and maceral associations of authigenic carbonates which formed at different stages in the evolution of the coalbeds are compared with those discussed in the literature.

Conclusions are drawn regarding the effect of fresh, brackish or marine waters on the coal sediments and on the evolution of pore fluids.

2 EXPERIMENTAL SECTION

2.1 Sample collection

Samples used for this study were collected from a number of different areas, the localities of which are shown in Figure 4. The sample set has been divided into a number of groups according to their location, and these are described below.

Samples 1 to 16

A set of sixteen "whole rock" samples of carbonate and pyritic "concretions" was collected. These samples of specific mineral "concretions" were taken from carbonate-rich marker horizons within the number 2 seam. They include coal from both above and below the mineral rich zones and typically consisted of between 1 and 3 kg of coal and mineral material. Sample orientation and positions were carefully recorded. Typical "concretions" are elongate parallel to coal bedding planes in section and are tens of centimetres to metres wide and centimetres to tens of centimetres thick. Their dimensions at right angles to the coal face could not be determined. Examples of these mineral-rich bodies are illustrated in Plate 1 (Appendix E).

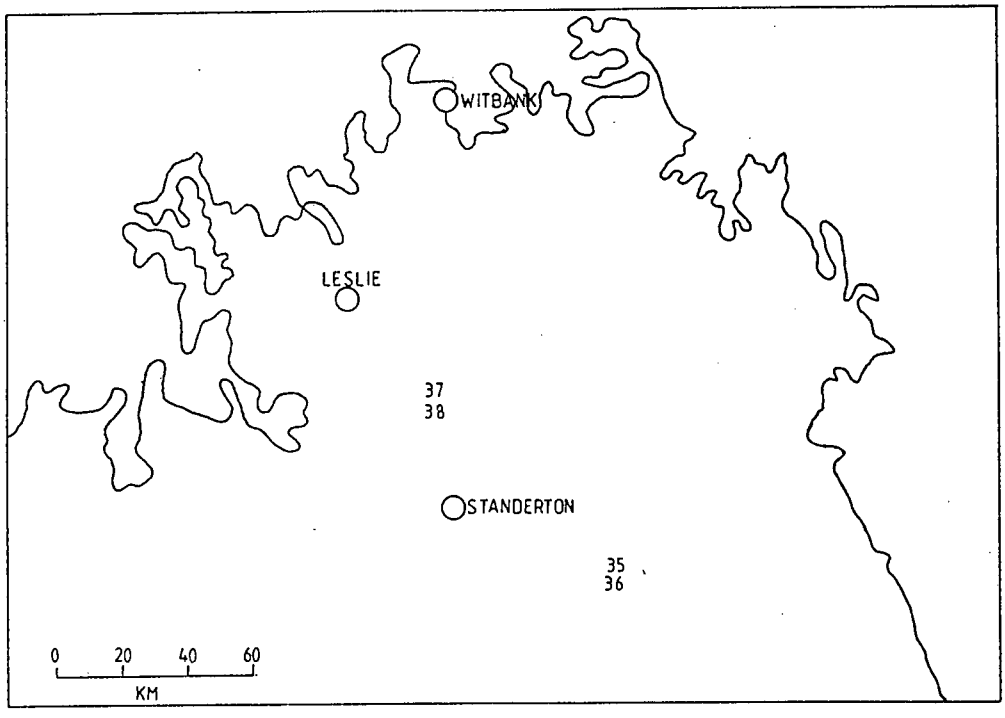

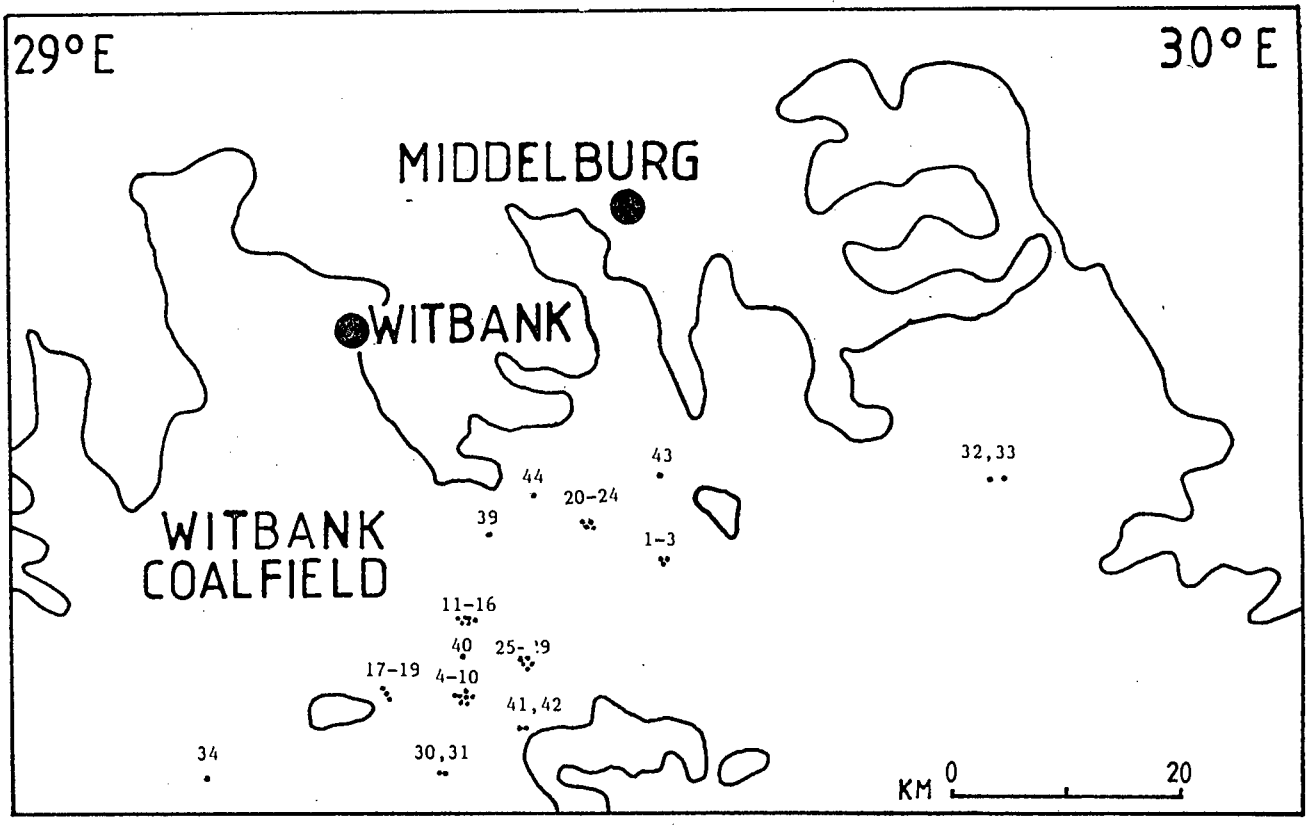

Figure 4: Sample localities.

Samples 17 to 29

These channel samples comprise a set of crushed composites representative of the complete seam at the localities shown in Figure 4. The coal face was first cleared of dust and oxidized coal before the samples were collected by progressively chipping the coal face from top to bottom. The chips were later crushed and split.

Samples 30 to 34

Uncrushed coal/mineral channel samples were collected and supplied by various mine geologists from the number 2 seam. A number of these samples were supplied clearly marked with their orientations, while others could be used only for less specific interpretation.

Samples 35 to 36

Two coal and mineral samples were collected from the Vryheid coalfield, Natal. Data from these samples can only lead to general interpretation as their relation to coal seams in the vicinity is not known.

Samples 37 to 38

These coal and mineral samples were collected from the Highveld coalfield. Again, these samples can only lead to generalised interpretation as their relationship to the enclosing coal seam has not been described.

Samples 39 to 44

Composite samples were collected from the number 2 seam from well described localities in the Witbank Basin. These samples were already supplied as crushed and split composites and any inferences regarding original orientation is difficult, but may occasionally be made by observation of draping and the preferential direction of elongation of authigenic mineral grains.

Detailed descriptions of samples containing large mineral concretions and their relationship to coal above and below them are given in Appendix A.

2.2 Sample processing

2.2.1 Crushing for X-ray diffraction (XRD) and Total organic carbon (TOC) analyses

Representative 150g samples were taken from each of the large "concretions" and crushed for 3 minutes in a mechanical mortar fitted with an agate bowl and pestle. The powdered sample was passed through a 250 micron mesh sieve and the residue returned to the mortar until all material passed through the sieve. The entire sample was then passed five times through a stainless steel sample splitter to ensure homogeneity.

2.2.2 Composite particulate blocks

Those samples in 2mm particulate form (samples 17 to 29 and 39 to 44) were mixed with Midbond, a cold-setting epoxy resin and cast in teflon moulds. The resin and hardener had been mixed at a 5:1 ratio by weight to produce a hardness similar to that of coal. Once the mounting medium had cured, the samples were ground and polished in the Soekor geochemistry laboratory in the following manner for reflected light observation. The mount was first ground down on a Dap-2 grinder using Struers 1200 paper and distilled water to expose sufficient sample. It was then rinsed in an ultra-sonic bath and polished on Texmet polishing paper with 25 micron diamond paste for 1 minute to remove scratches. After a second rinsing, the sample was polished for 1 to 2 minutes on a velvet cloth with Buehler 0,05 mm micropolish and distilled water. This was followed by a third rinsing and a final polish on a velvet cloth using distilled water only.

2.2.3 Polished blocks

Polished blocks were prepared from all solid samples for reflected light study. A 1cm cross-sectional slice of each sample was further subdivided into blocks of a suitable size for observation under the microscope and in the SEM/EDS. Where possible, the coal was not impregnated with any resin, to avoid the possibility of confusing this with mineral emplacement.

X-ray tube operating parameters were 40kV and 30mA. The range and scan speed were adjusted to produce the clearest possible traces. Pure calcite and aragonite were used as control samples.

2.3.2 Total organic carbon determination

Total organic carbon determinations were carried out on a number of the powdered samples to determine the weight percent of organic carbon associated with the larger carbonates and the effect of this on the intensities of XRD peaks. 0.16g to 0.17g of each crushed sample was accurately weighed out and transferred to ceramic crucibles. The sample was then leached three times with hot 10% HCl until no further reaction was apparent to remove all carbonates from the sample. After rinsing five times with deionised water, the samples were left overnight in an oven at 52° C to dry.

About 1g of pure copper chips was added to each sample to speed up the reaction in the furnace and the crucibles loaded into a Leco WR 112 carbon determinator. The sample then underwent combustion in a high frequency induction furnace and the generated CO_2 was selectively trapped in a molecular sieve. Once the reaction was complete, the CO_2 was released from the sieve by heating and thermal conductivity was measured. This was automatically recalculated to give the weight percent C content of the original sample.

2.3.3 Reflected light microscope observation

All polished blocks, polished composite sample mounts and polished thin sections were examined under white reflected light to determine the relationships between minerals, minerals and macerals, and multiple episodes of single mineral emplacement. A binocular microscope was used for low power (5x, 8x and 10x) observation and a Leitz Orthoplan coal petrographic microscope equipped with oil immersion lenses for high power (100x, 500x and 1200x) observation.

2.3.4 Scanning electron microscopy and energy dispersive XRF analyses

Back scattered electron image observation coupled with energy dispersive XRF analyses proved to be the most useful technique for the elucidation of mineral paragenetic sequences and the identification of the minerals involved. Many of the authigenic mineral phases present in coal are completely contained within a single maceral and are impossible to identify by optical means, and are often overlooked as the opacity of the coal obscures them.

Scanning electron microscope (SEM) observation was performed using an ISI-SX 30 instrument, at an accelerating voltage of either 15 or 30kV. Polished mounts were methodically scanned and mineral to maceral and mineral to mineral relationships described. Minerals were identified with the aid of a Link Analytical AN 10 000 energy

dispersive spectrometer (EDS). This instrument is equipped with a 10mm², 155 eV resolution Si/Li detector and a 8.0 micron Be window.

2.3.5 Electron microprobe analyses

Microprobe analyses were undertaken using the U.C.T. Earth Sciences Cameca Camebax Microbeam electron microprobe. Operating conditions of an accelerating voltage of 15 kV and 40 nA beam current were employed. The electron beam was defocussed to provide a spot size of between 5 and 10 microns in an attempt to avoid or at least minimise the vaporisation of volatile carbonate phases. Five second counts on either side of an element peak constituted the total 10 second background count. Peak counts were also of 10 second duration except in the case of Ba, Sr and Zn where counts were of 30 second duration. All samples were carbon coated. Details of corrections, standards and calculations are described in Appendix B.

2.3.6 Transmitted light observation and staining

Polished thin sections were observed under transmitted light to elucidate mineral paragenetic sequences further, as well as to locate suitable mineral grains and positions for microprobe analyses. Once microprobe work was complete, the slides were stained using Feigl's solution to clarify the relationship of aragonite to calcite, and Alizarin red to distinguish calcite from dolomite (Bouma, 1969).

2.3.7 Vitrinite reflectance

Vitrinite reflectance measurements were made on all polished composite mounts and blocks to compare the burial history of no.2 seam coals to those of coals studied by Matsumoto and Iijima (1981). A Leitz Orthoplan coal petrographic microscope equipped with a photometer, 560 nm filter and electronic readout was used. Calibration was against standards ranging from 0.299 to 1.672 percent reflectance. Fifty readings were taken per sample and all reflectance values quoted are mean values, measured in oil of refractive index 1.518 at 23° Celsius. The raw reflectance data are tabulated in Appendix C.

3 RESULTS

3.1 XRD and total organic carbon determinations

All the large carbonate "lenses" appeared to be macroscopically fairly similar, falling into two groups, either dark greyish-brown carbonate or pyritic concretions, with little further indication of their mineral compositions. The initial step in the characterisation of these concretions was XRD analysis coupled with the determination of the total organic carbon content of each of the samples. The results are presented in Table 1. Minerals were classified as major, secondary and other on the basis of their relative XRD peak heights (no quantitative XRD analyses were performed), as illustrated in Figure 5a.

The important features of the data set can be summarised as follows.

i) The major carbonate concretionary minerals are either calcite, siderite, aragonite or, rarely, dolomite. Both Matsumoto and Iijima (1981) and Curtis and Coleman (1986) performed XRD analyses on carbonate concretions from coals. Neither mentioned the occurrence of aragonite, and no reference to its association with coal, other than in shelly material, could be found in the literature.

Table 1 X-ray diffraction (XRD) results and Total Organic Carbon (TOC) determinations.

Sample	Major Minerals	Secondary Minerals	Other Minerals	TOC1 Weight%	TOC2 Weight%
1	siderite	pyrite	calcite	25.49	25.14
2	siderite	none	pyr/calc	5.67	5.78
4	calcite	none	none	12.68	11.71
6	calcite	none	dolomite	23.88	22.86
7	aragonite	calcite	pyrite	14.59	14.22
8	calcite	none	dolomite	19.22	18.62
9	aragonite	calcite	none	15.69	12.81
11	calcite	none	none	45.42	44.21
12	calcite	dolomite	none	14.06	13.95
13	pyrite	none	calcite	23.11	22.46
14	calcite	dolomite	none	14.92	12.70
15	siderite	pyrite	none	nd	
32	aragonite	calcite	pyrite	12.08	9.77
33	aragonite	calcite	pyrite	nd	
39	dolomite	pyrite	siderite	nd	
40	calcite	dolomite	pyrite	nd	
42	calcite	none	pyrite	nd	
43	cal/dol	none	none	nd	
45	dolomite	none	pyrite	nd	

TOC1 - First analysis
TOC2 - Repeat analysis
nd - not determined

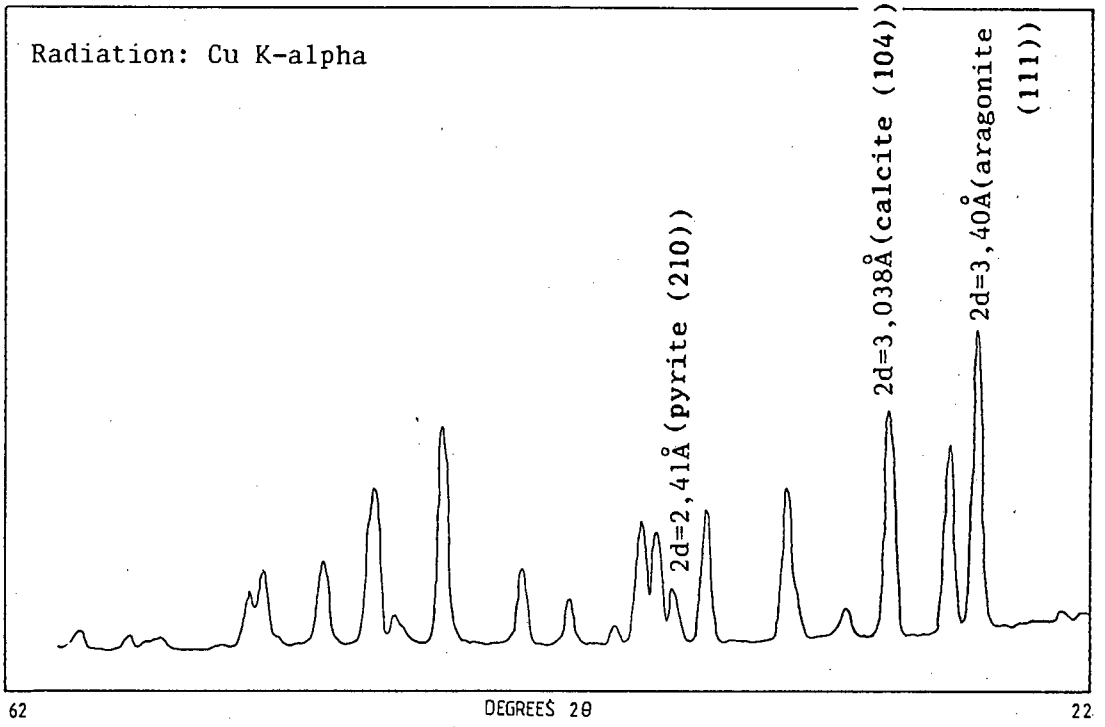

Figure 5a: An example of the classification of minerals as major, secondary and "other", on the basis of their relative XRD peak heights. In this example (sample 7), aragonite is classified as the major mineral, calcite as the secondary mineral, and pyrite as "other".

ii) Secondary minerals are calcite, dolomite and pyrite.

iii) Large concretions with siderite as the major mineral are always associated with pyrite and calcite. The single concretion with pyrite as the major mineral has calcite as an "other" mineral.

iv) Where aragonite is the major mineral, calcite is always the secondary mineral. It is possible that aragonite is common in smaller concentrations, but its presence may be masked by the diffractograms of other minerals. For more detailed discussion, see Appendix F (van der Spuy and Willis, in press).

v) Total organic carbon contents of the concretions vary widely, ranging from about 5% to 25% by weight. The effect of differences in organic carbon content on XRD traces is shown in Figure 5b. Samples 1a and 2 have similar relative mineral proportions but 1a has an organic carbon content five times that of 2. The 2.80 A d-spacing peak of siderite for sample 2 has an intensity almost four times that of sample 1a.

3.2 Reflectance measurements and maximum burial

It was impracticable to measure the porosities of the carbonates for burial depth estimation. Because of the high organic carbon contents, elongate morphology and the preferential directions of growth of the carbonate bodies, preferentially developed porosities

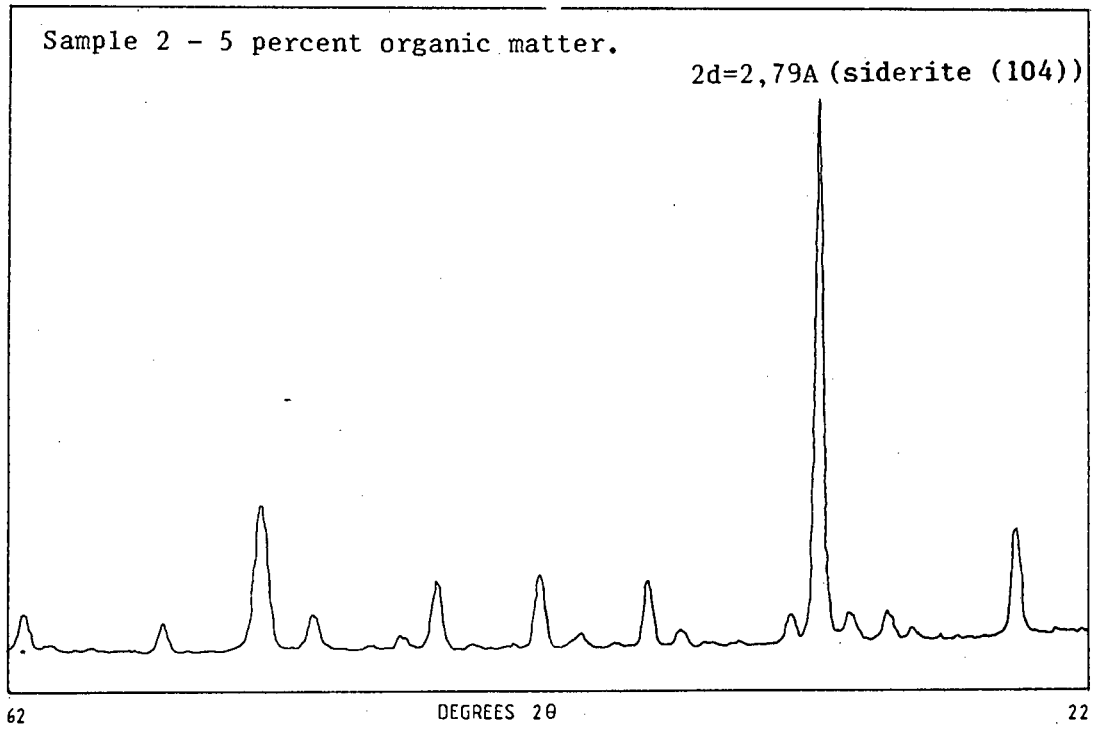

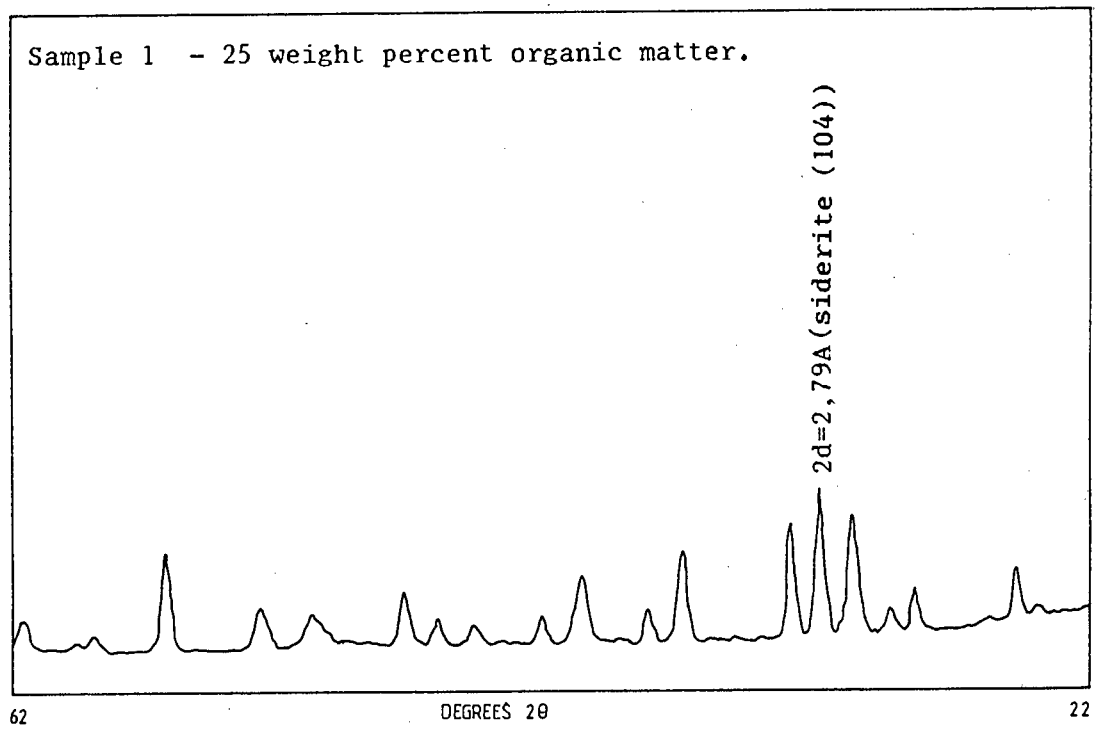

Figure 5b: The effect of differences in organic carbon content on peak heights in X-ray diffractograms.

Radiation: Cu K-alpha

would result. For burial history modelling, vitrinite reflectance measurements were taken and the methods of Lopatin and Waples (Waples, 1980) employed to calculate the maximum depth of burial. Vitrinite reflectance (%RO) allows the determination of coal rank. Rank is a result of the burial (pressure and time) and temperature history of the coal. Thus, knowing the rank and age, it is possible to model this burial and temperature history. Reflectance measurements are presented in Table 2.

Mean reflectances for the sample set cover a range of 0.50% to 0.72% i.e. the coals are high volatile-bituminous in rank (Stach et al., 1975). These coals have been dated as early Permian in age (Falcon et al., 1984). Thus, using the predictive model of Lopatin as adapted by Waples and TTI/vitrinite reflectance correlations from the literature (Waples, 1985; Royden et al., 1980; Hood et al., 1975; Goff, 1983 and Issler, 1984), over a range of assumed average geothermal gradients of 2.5° to 3° C per 100 metres, the maximum burial depth of the coal can be calculated. Unfortunately, this type of model cannot give an indication of the depth of formation of specific carbonates, but it does give an indication of the maximum depth of burial and thus the possibility of the coal having passed through the burial stages described by Matsumoto and Iijima (1981).

Figure 6a and b show the predicted vitrinite curves for early Permian sediments with increasing burial for a range of geothermal gradients, for each of the TTI/reflectance correlations. The measured reflectances are plotted over these curves and maximum burial depths of 1400m to more than 3000m are indicated.

Table 2 Vitrinite Reflectance

Sample	Vitrinite Reflectance (mean, random, in oil)
17	0.57 ±0.05
18	0.60 ±0.09
19	0.56 ±0.06
20	0.70 ±0.06
21	0.59 ±0.09
22	0.60 ±0.06
23	0.72 ±0.10
24	0.67 ±0.06
25	0.67 ±0.07
26	0.70 ±0.08
27	0.69 ±0.08
28	0.67 ±0.07
29	0.58 ±0.09
32	0.63 ±0.09
37	0.53 ±0.04
38	0.53 ±0.06
39	0.50 ±0.07
40	0.61 ±0.07
41	0.56 ±0.08
42	0.50 ±0.07
43	0.51 ±0.06
44	0.59 ±0.10

A-Waples (1985)

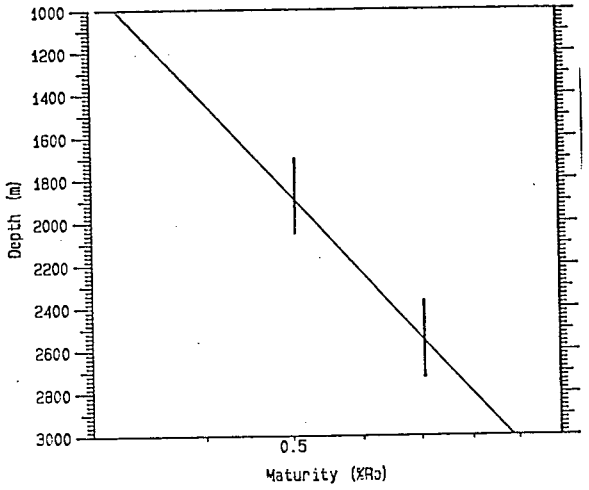

B-Royden, et al. (1980)

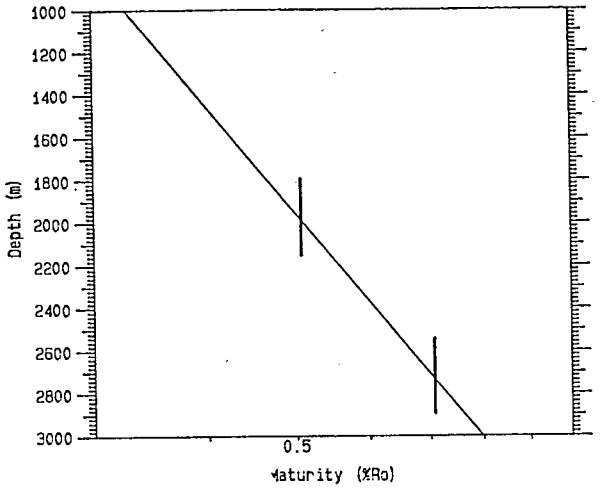

Vertical lines define the limits of vitrinite reflectance measured in this study.

C-Goff (1983)

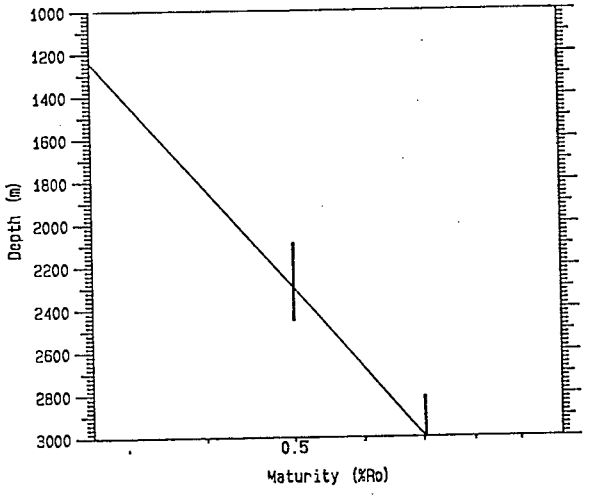

D-Hood, et al.(1975)

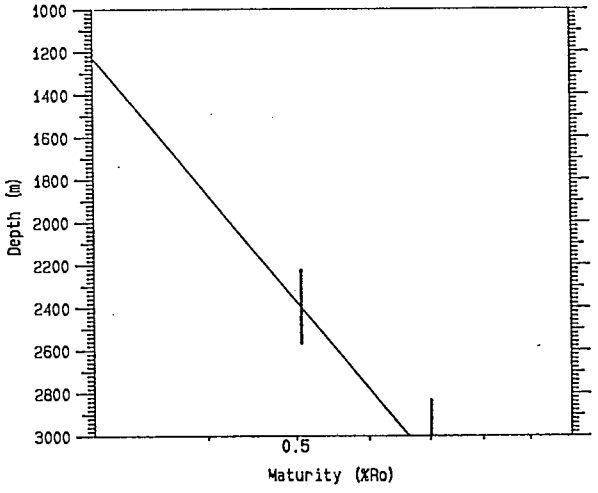

E-Issler (1984)

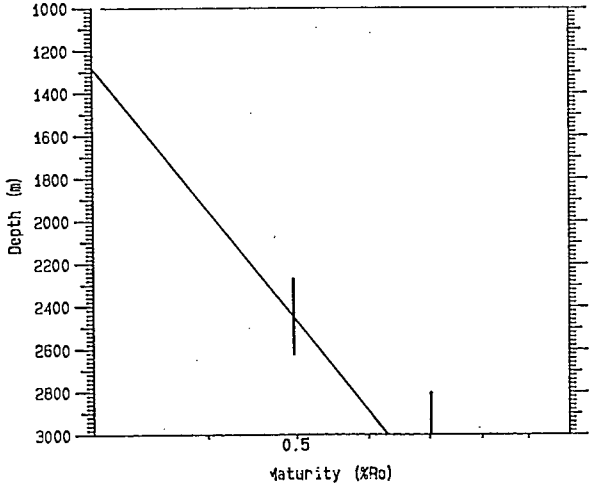

Figure 6a: Predicted vitrinite reflectance curves for early Permian sediments with increasing burial at a gradient of 2.5°C/100m.

A-Waples (1985)

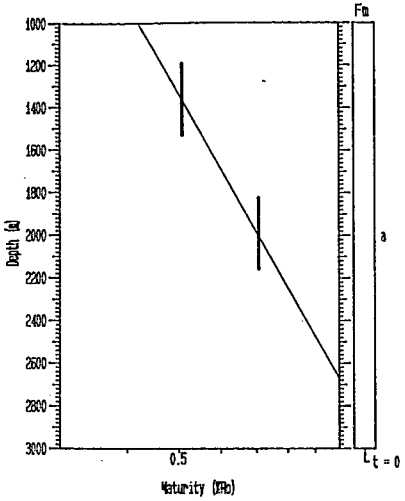

B-Royden, et al. (1980)

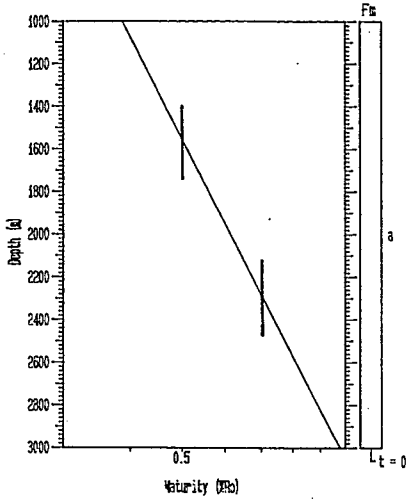

Vertical lines define the limits of vitrinite reflectance measured in this study.

C-Goff (1983)

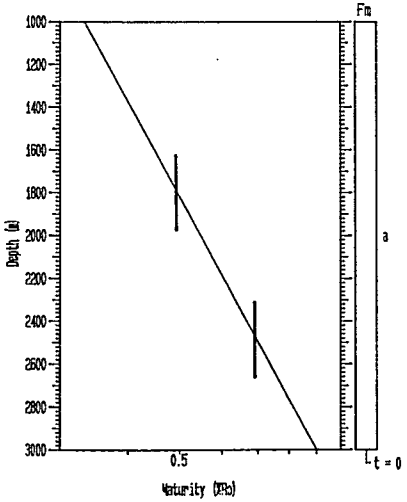

D-Hood, et al.(1975)

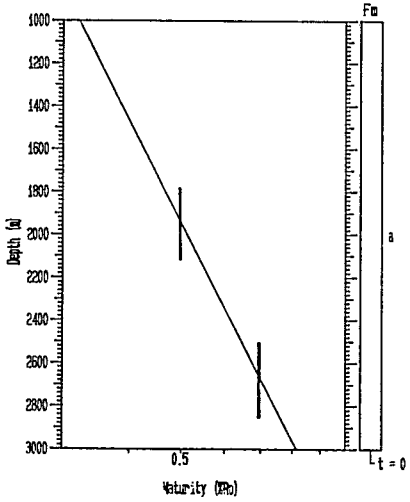

E-Issler (1984)

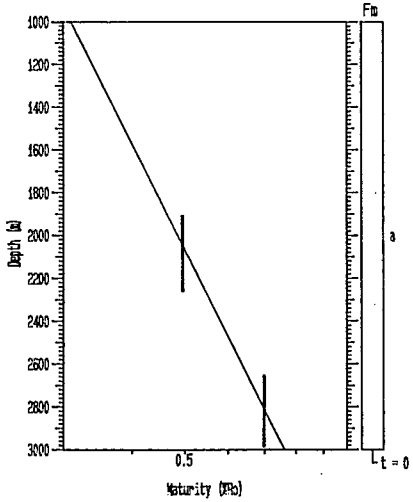

Figure 6b: Predicted vitrinite reflectance curves for early Permian sediments with increasing burial at a gradient of 3°C/100m.

3.3 Carbonates - occurrence, textures, mineral/maceral relationships

3.3.1 Cell-filling carbonates

Carbonates filling undeformed tracheid cell lumens and lumens in sclerotinite are regarded as the products of early authigenic precipitation from the earliest diagenetic fluid. If this is not the case, they must be regarded as replacements of some early cell-filling mineral capable of supporting cell structure during burial and compaction. Where the mineralisation occurs as an infill of collapsed fusinite or bogen structures, it must be regarded as a later event. Most occurrences of cell-filling carbonates are very small and difficult to find, and are best observed using high magnification reflected light and SEM observation. They are often too small for accurate analysis by electron microprobe.

3.3.1.a Mineral compositions

EDS traces for a number of cell-filling carbonates are shown in Figure 7. The carbonates are relatively pure Ca carbonates, either with no other elements present, or more commonly, with small amounts of Mg and Fe. Also shown in Figure 7 are probe data for cell-infills from sample 7. These plot as pure Ca carbonates on the carbonate triangle although one of the analyses shows a 4.4% $SrCO_3$ content.

3.3.1.b Associated minerals

Cell-filling carbonate was often found to occur adjacent to cells filled with kaolinite. Such a case is illustrated in Plate 2, which suggests that the precipitation of kaolinite continued during compaction and deformation of the cell lumens (kaolinite-filled cells are more deformed) while that of the carbonate did not. This effect could also be explained by differences in compactional strength of calcite and kaolinite. Tiny euhedral pyrite crystals commonly occur in these carbonates. These may be responsible for the small Fe peaks observed on some EDS traces. Other early cell-filling minerals include illite, possibly altered kaolinite, pyrite and gorceixite. Some examples of these are shown in Plate 3. Gorceixite was identified by SEM EDS in a number of analyses in more than one sample. Thus the possibility that the EDS profile was produced by beam interaction with a multiple mineral phase is considered to be small.

3.3.2 Small authigenic carbonate bodies (spherulites)

Small, authigenic carbonate bodies occur in almost all the samples studied. They vary in size and shape from submicroscopic, near-spherical bodies to a few millimetres in size, slightly elongate in the plane of coal bedding. They are very closely associated with vitrinite and, with one exception, occur exclusively within bands of this maceral.

3.3.2.a Mineral compositions

Microprobe data for spherulitic carbonates are plotted on carbonate triangles in Figure 8 together with EDS traces for samples 7, 8 and 1a. Compositions fall into three groups:

i) low-Fe, low-Mg Ca carbonates. This group includes samples 4, 5, 6a and b, 7, 8, 12b and 14a.

ii) siderites with $CaCO_3$ contents ranging from 4% to 10% and $MgCO_3$ contents ranging from 4% to 8%. Samples 1a, 2, 3 and 39 make up this group.

iii) dolomite - sample 30.

No pure $FeCO_3$ siderites were found. Only one sample, 39, showed any compositional zoning, with sideritic centres (with 3-4% $CaCO_3$ and 6-8% $MgCO_3$) and dolomitic or ankeritic outer edges containing up to 0.45% $SrCO_3$. BSE images of this zonation are shown in Plate 4.

Figure 9 shows the distribution of the three compositional groups across the study area. Low-Mg Ca carbonates and dolomite occur in the south west and centre of the study area while siderites occur in the north and north east, closer to large basement highs.

Sample 4: ☐ Spherulites

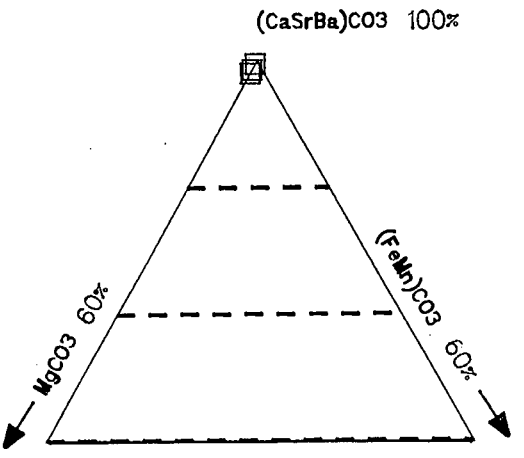

Sample 5: ☐ Spherulites

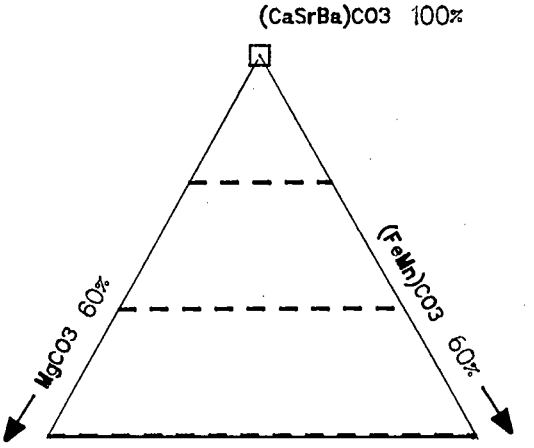

Sample 6a ☐ Spherulites

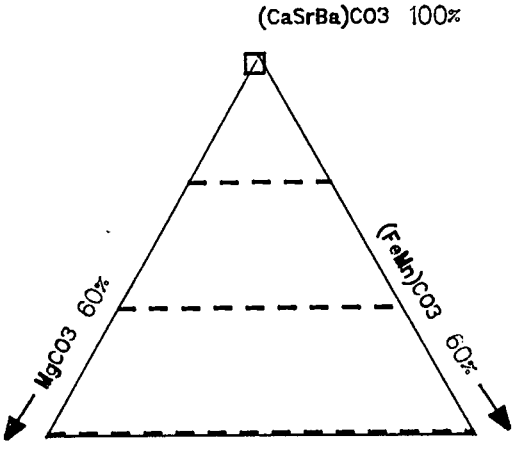

Sample 6b: ☐ Spherulites

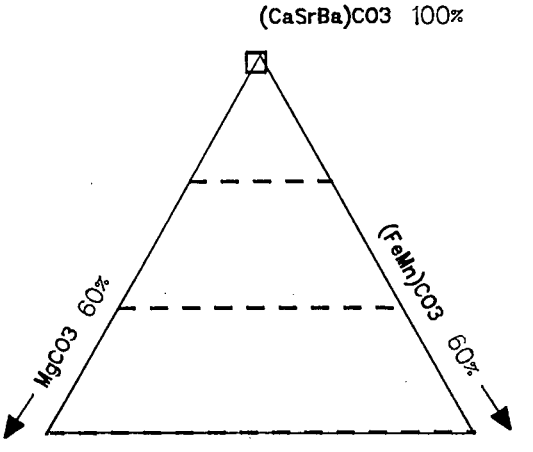

Sample 12b: ☐ Spherulites

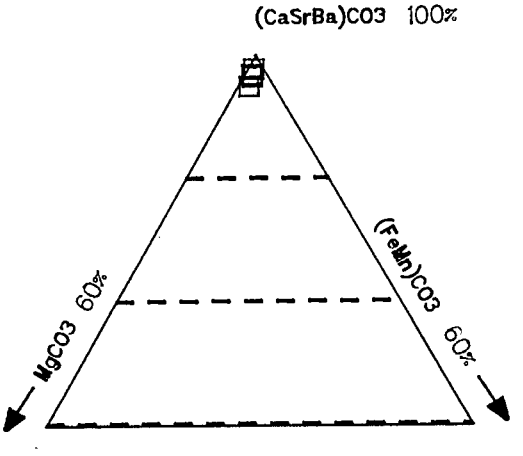

Sample 14a: ☐ Spherulites

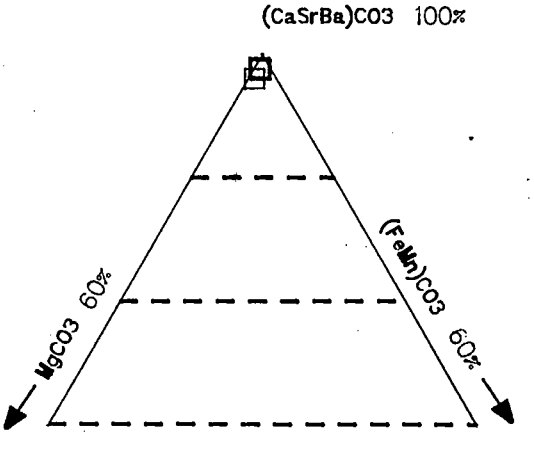

Figure 8: Spherulite compositions.

Group i) low-Mg Ca carbonates

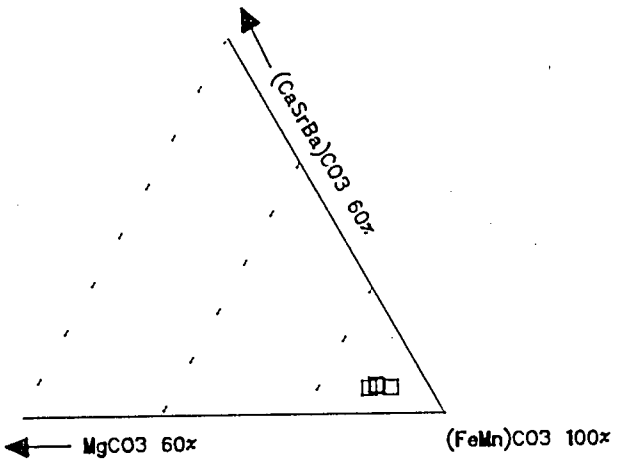

Sample 2: □ Spherulites

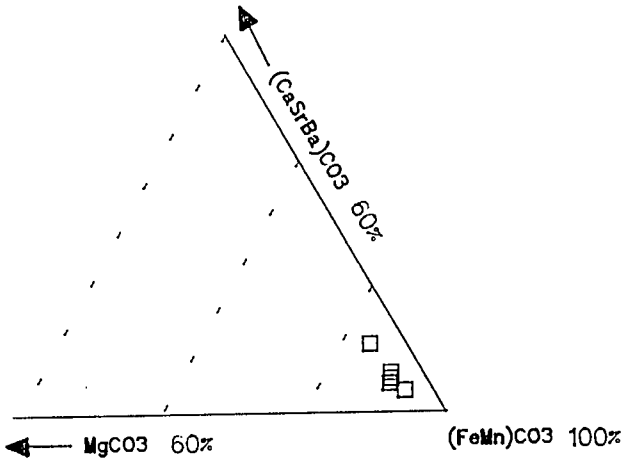

Sample 3: □ Spherulites

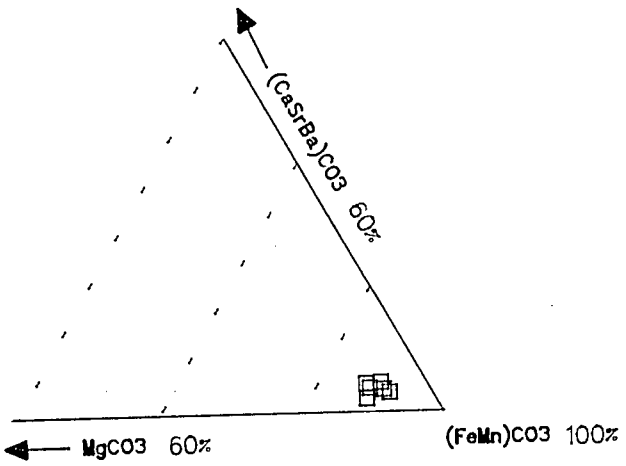

Sample 39: □ Spherulite centres

Group ii) siderite

Sample 30: □ Spherulites

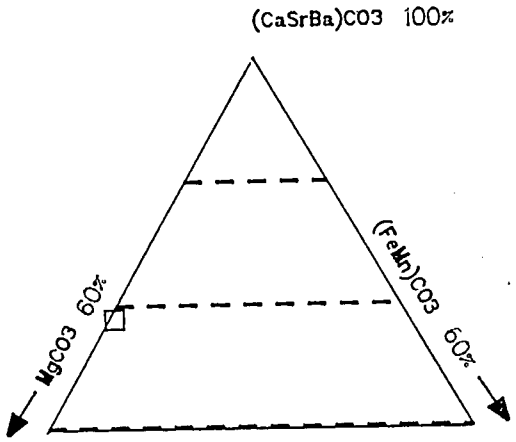

Group iii) dolomite

Figure 8 (cont.): Spherulite compositions.

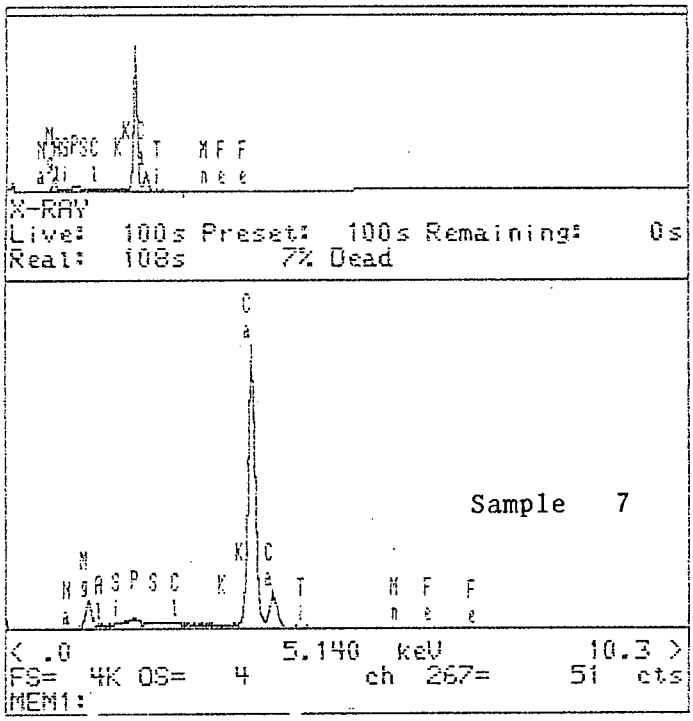

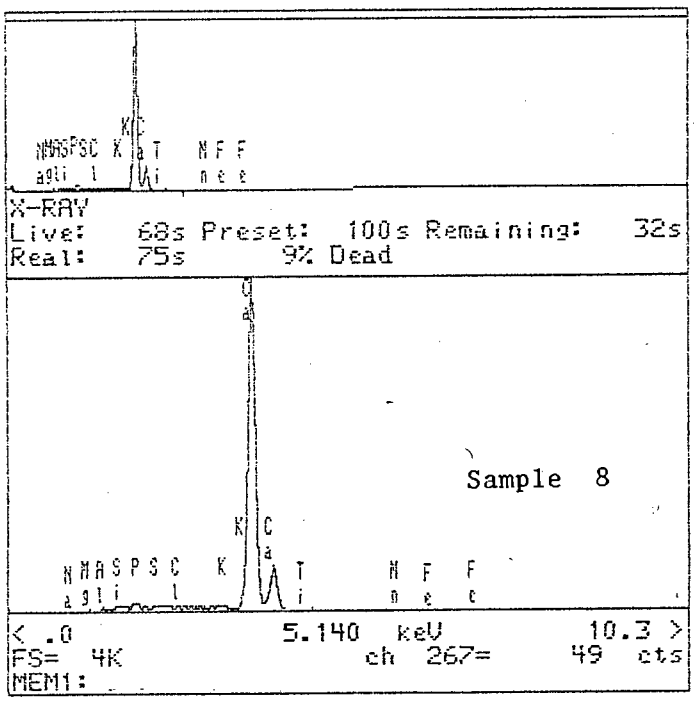

Figure 8 (cont.): SEM-EDS traces of group (i) spherulites.

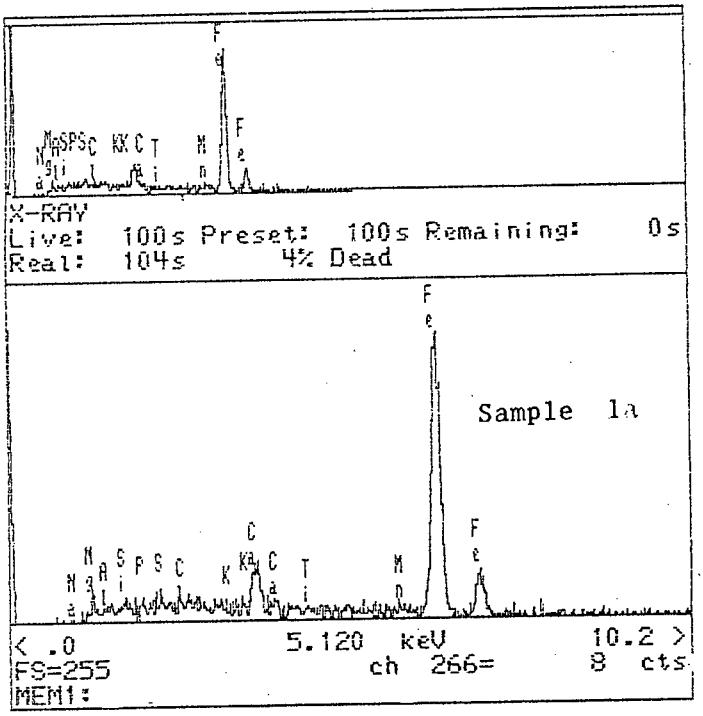

Figure 8 (cont.): ; SEM-EDS trace of a group (ii) spherulite.

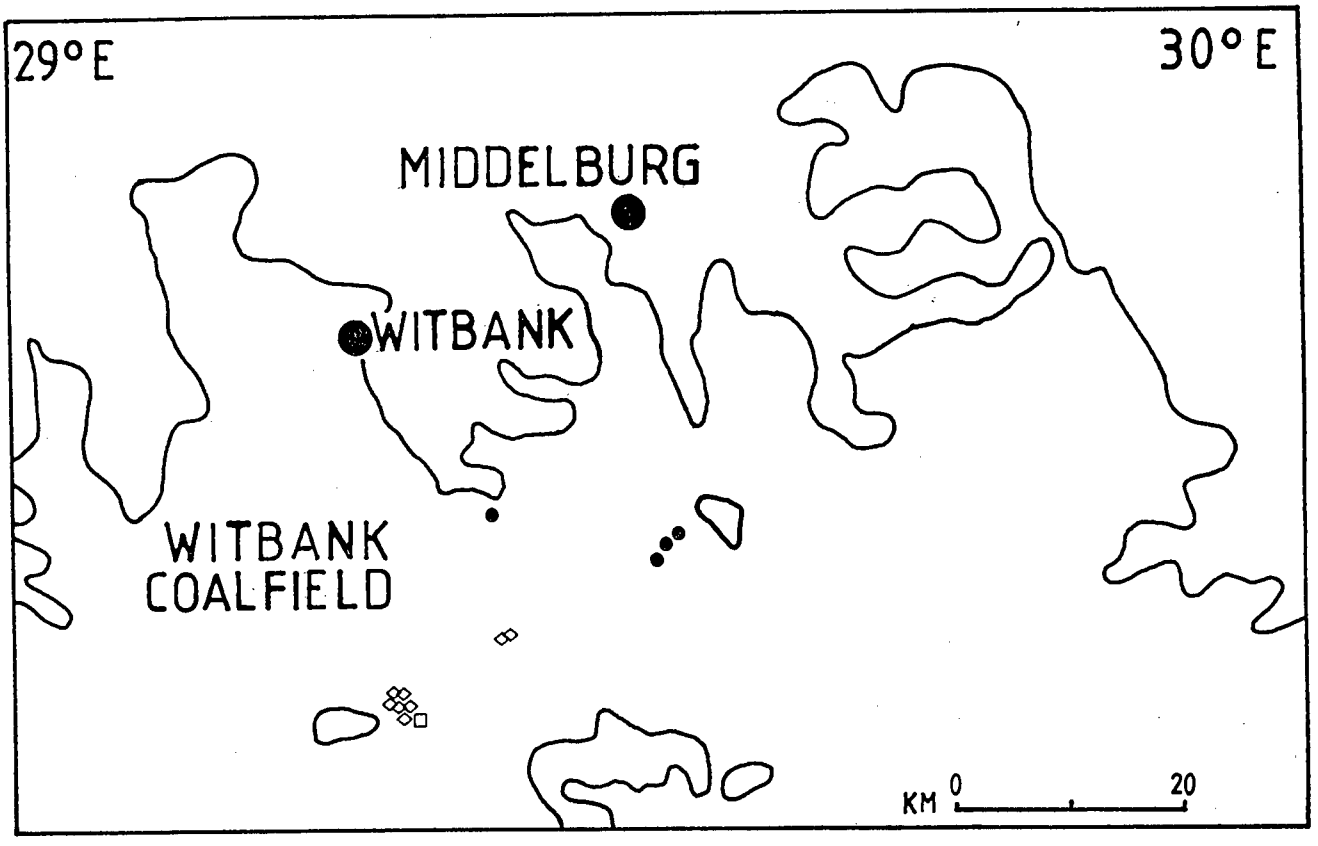

◇ low-Mg Ca carbonates

● siderites

□ dolomites

Figure 9: Compositional distribution of spherulites across the study area.

ii) kaolinite, occurring in similar manner as described for apatite as well as in some cases, intimately associated with carbonate growths.

iii) TiO_2 (either rutile or anatase), chalcopyrite, and pyrite all riddle vitrinite bands, commonly occurring as tiny euhedral crystals within vitrinite, and, in the case of pyrite, as larger growths and pseudo-framboids.

Examples of some of these mineral occurrences are shown in Plates 8 to 11.

3.3.3 " Massive carbonate " bodies

Macroscopically, these bodies appear to be solid carbonate or pyrite-rich bodies up to 15cm thick in the middle and tapering outwards to reach a width of up to a metre. However, the total organic carbon results demonstrate that they may contain from 5 to almost 30% organic matter by weight.

3.3.3.a Massive carbonate textures

Microscopic and SEM observation revealed a number of different textures within these bodies:-

i) non-destructive cell fill, of semi-fusinite and fusinite on a large scale, which has undergone some compaction and deformation (Plate 12).

ii) destructive infill of semi-fusinite and fusinite, where cell walls appear to have been forced apart by carbonate growth (Plate 13). (i) and (ii) may occur together in the same carbonate body. Inclusions of vitrinite, with cleat development, are fairly common. Areas of reduced organic material content or feeder veins often occur while some samples show the development of small, horizontal but otherwise cleat-like bodies, relatively free of organic inclusions .

iii) groups of small, elongate bodies similar to the small authigenic carbonates and usually found in association with vitrinite. These occur in far greater numbers than the smaller authigenic carbonates, often amalgamated into a larger elongate body at the centre of the "concretion". They may be surrounded by many, smaller satellite bodies. The whole group is generally elongate in the plane of coal bedding and tapers towards the outer edges (Plate 14).

iv) masses of spherical, small carbonate bodies in very close proximity or joined to one another by a network of pyrite overgrowths and rims. Dendritic pyrite-rich feeder veins which are relatively free of organic matter occur throughout the structure (Plate 15).

3.3.3.b Mineral compositions

131 electron microprobe analyses of carbonates in 22 coal samples showed large carbonate "concretions" or "massive" carbonates to fall into the following groups on the basis of their chemical compositions:-

i) high-Ca carbonates

ia) either pure Ca carbonates or high-Ca carbonates containing small percentages of $MgCO_3$ and in a few cases, $FeCO_3$. Samples 4, 6a, 6b, 7, 8, 9, 11 and 12b fall into this group, as shown in Figure 10. These samples all fall into textural groups (i) and (ii).

ib) high-Ca carbonates displaying trends of increasing Mg content. This group includes samples 12c, 14b, 32, 34, 40, 42 and 43. Samples 12c, 14a and 43 contain low percentages of Fe, but the Fe content shows little variation even with fairly large variations in Mg content, as can be seen in Figure 11. These samples fall into textural groups (i) and (ii).

ic) two samples, 35 and 36, show high-Ca carbonate with a trend of increasing FeMn content. This is shown in Figure 12. These samples fall into textural group (ii).

Sample 4: ▫ Massive carbonate

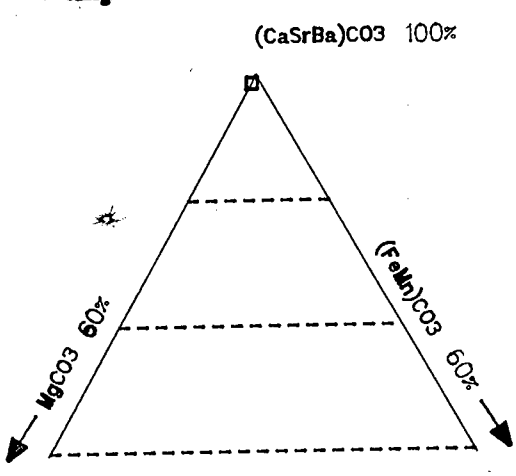

Sample 6a: ☐ Massive carbonates

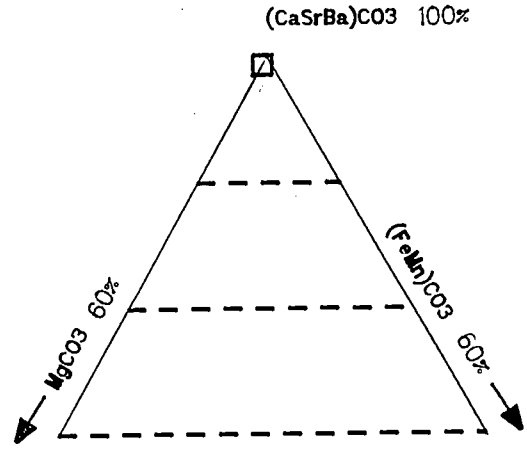

Sample 6b: ☐ Massive carbonates

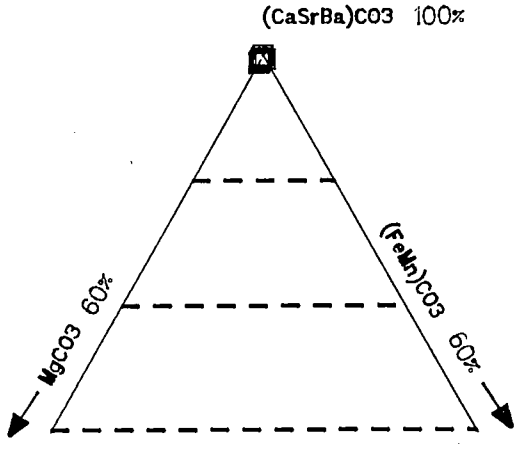

Sample 7: ☐ Massive carbonates

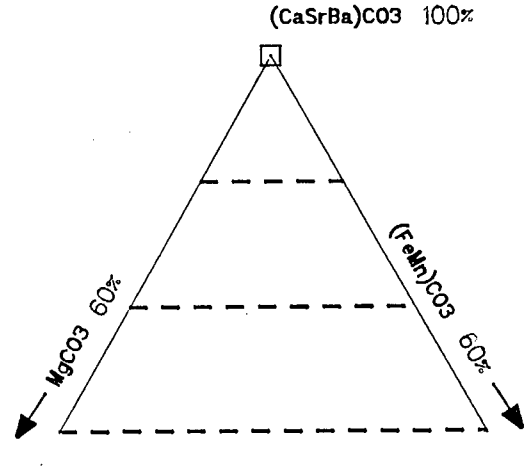

Sample 8: ☐ Massive carbonates

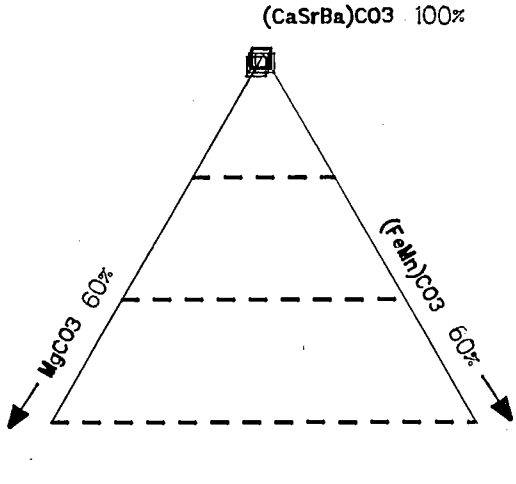

Sample 9: ☐ Massive carbonates

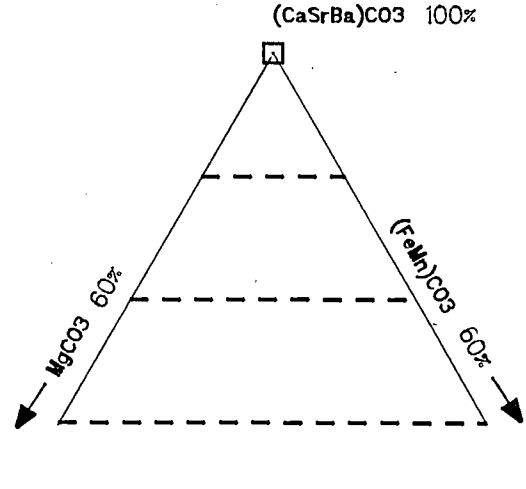

Figure 10: Massive carbonate compositions - Group ia) high-Ca carbonates.

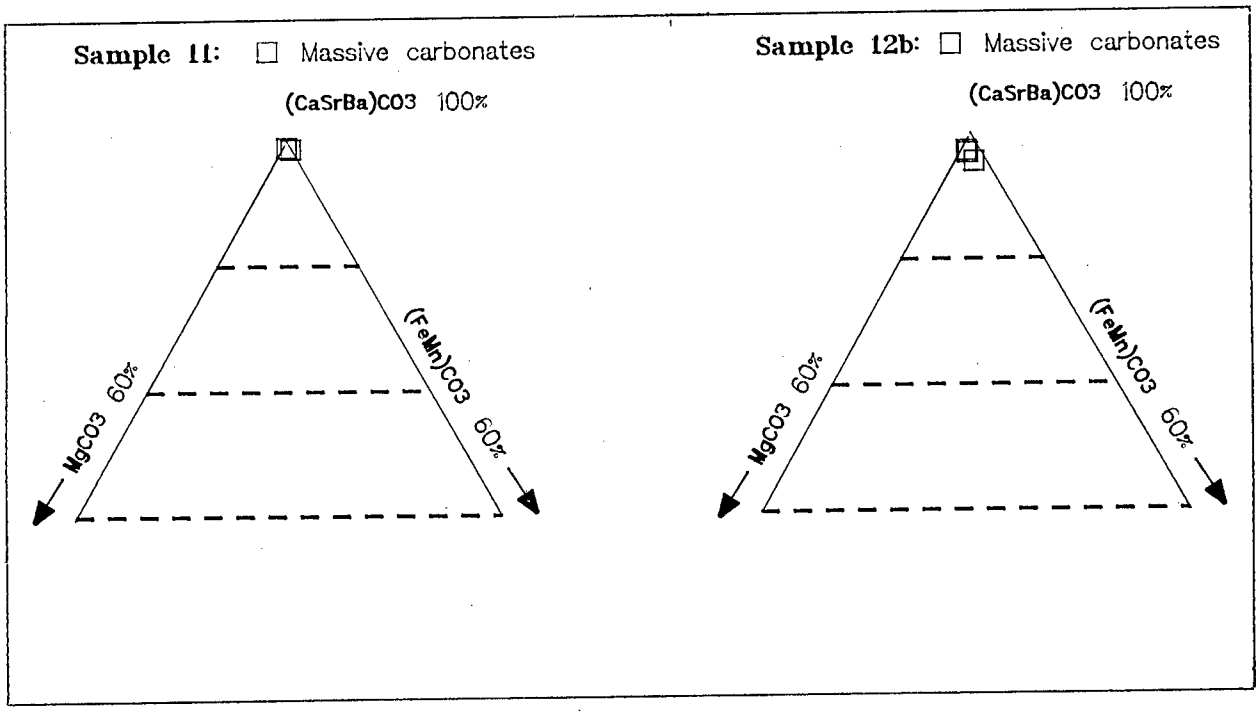

Figure 10 (cont.): Massive carbonate compositions - Group ia)

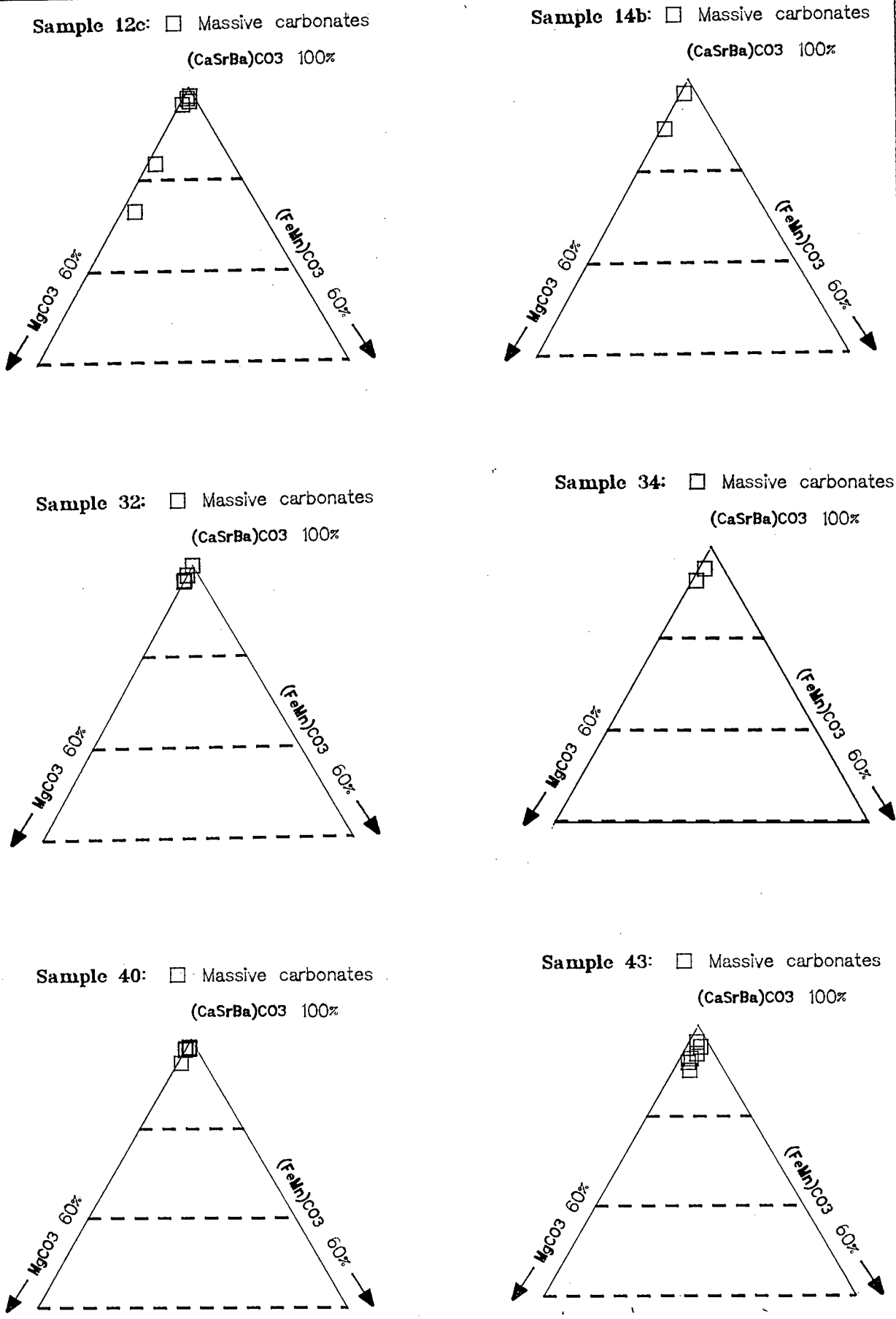

Figure 11: Massive carbonate compositions - Group ib) high-Ca carbonates with significant Mg content.

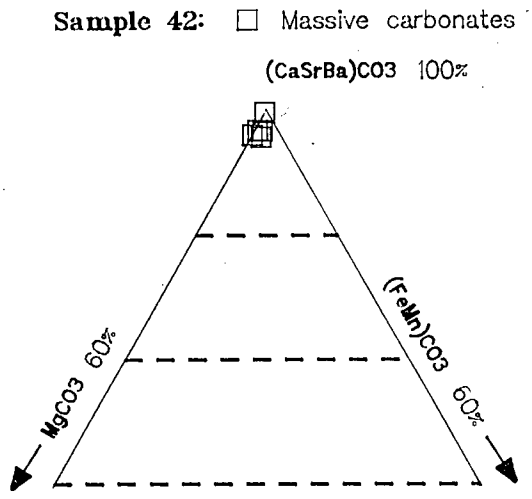

Figure 11 (cont.): Massive carbonate compositions - Group ib).

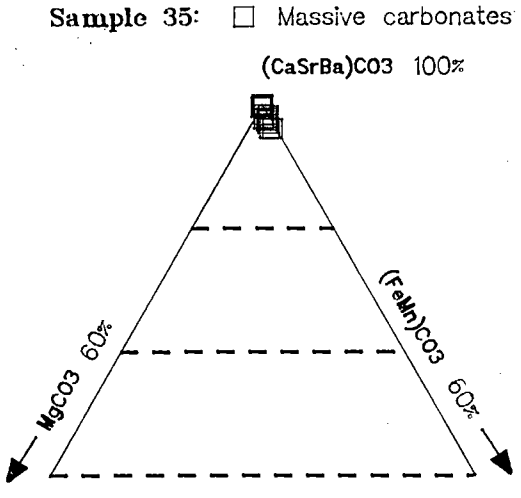

Figure 12: Massive carbonate compositions - Group ic) high-Ca carbonates with significant Fe+Mn content.

ii) siderites. These include samples 15, 1a, 1b and 2. No pure $(FeMn)CO_3$ siderites were found. All contain between five and ten percent Mg and Ca. They may show strong compositional differentiation, and are either intergrown siderite and dolomite (sample 2), or siderite and low-Mg Ca carbonate (sample 15). Siderite is more common towards the centre of each spherical body, while intergrowths become more common towards the pyrite rims. These intergrown siderites and calcites or dolomites all belong to textural group (iv), as described above, and are rimmed with pyrite. Compositions of these siderites and the intergrowths are plotted on carbonate triangles in Figure 13. Textural groups are (iii), (iv) and in one case (sample 15), (ii) and (iv).

iii) dolomites. Compositions of samples 39 and 44 are plotted on Figure 14. Sample 39 shows variation from high-Mg Ca carbonate to dolomite, while sample 44 shows compositional variation from dolomite to ankerite. These samples both fall into textural groups (i) and (ii).

Figure 15 shows the distribution of the different groups, described above, across the study area. Pure Ca carbonates occur in the south west and centre, whereas low FeMn calcites, siderites and dolomites occur in the centre. Low Mg calcites occur both in the centre and in the north east of the study area.

Sample 15: □ Massive carbonates

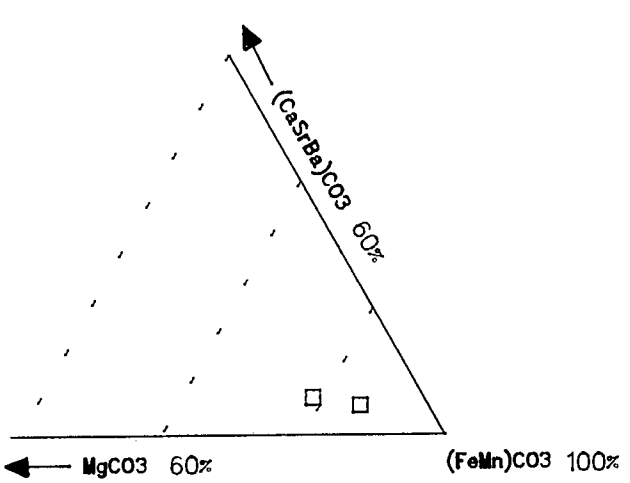

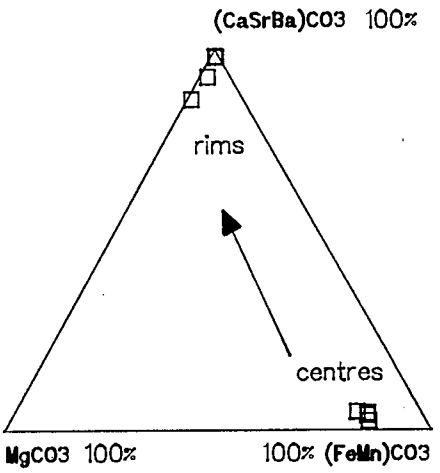

Sample 15: □ Massive carbonate centres

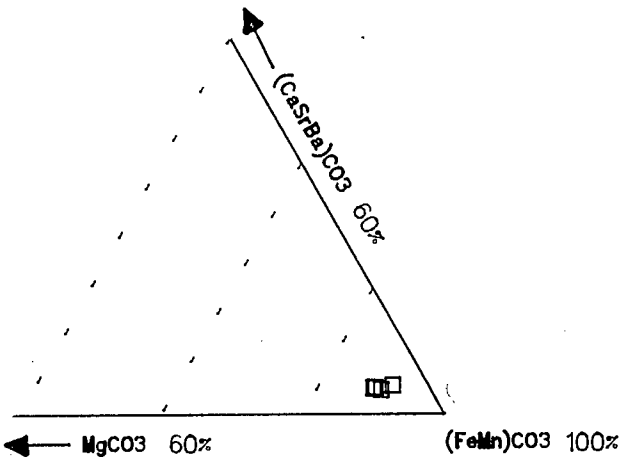

Sample 1a: □ Massive carbonates

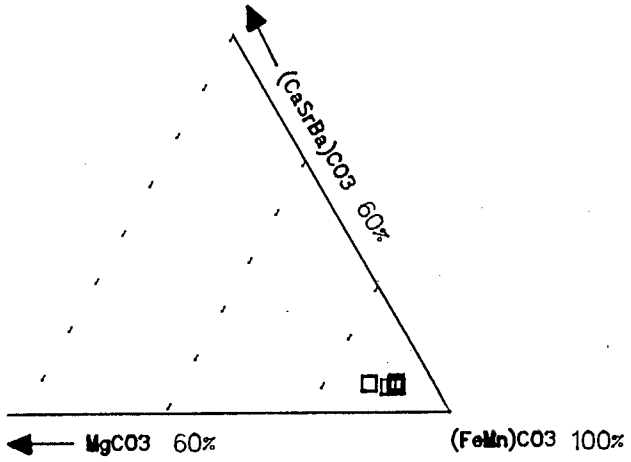

Sample 1b: □ Massive carbonates

Sample 2: □ Massive carbonates

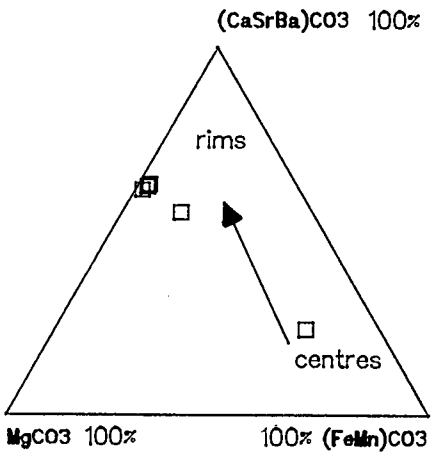

Figure 13: Massive carbonate compositions:

Group ii) siderite.

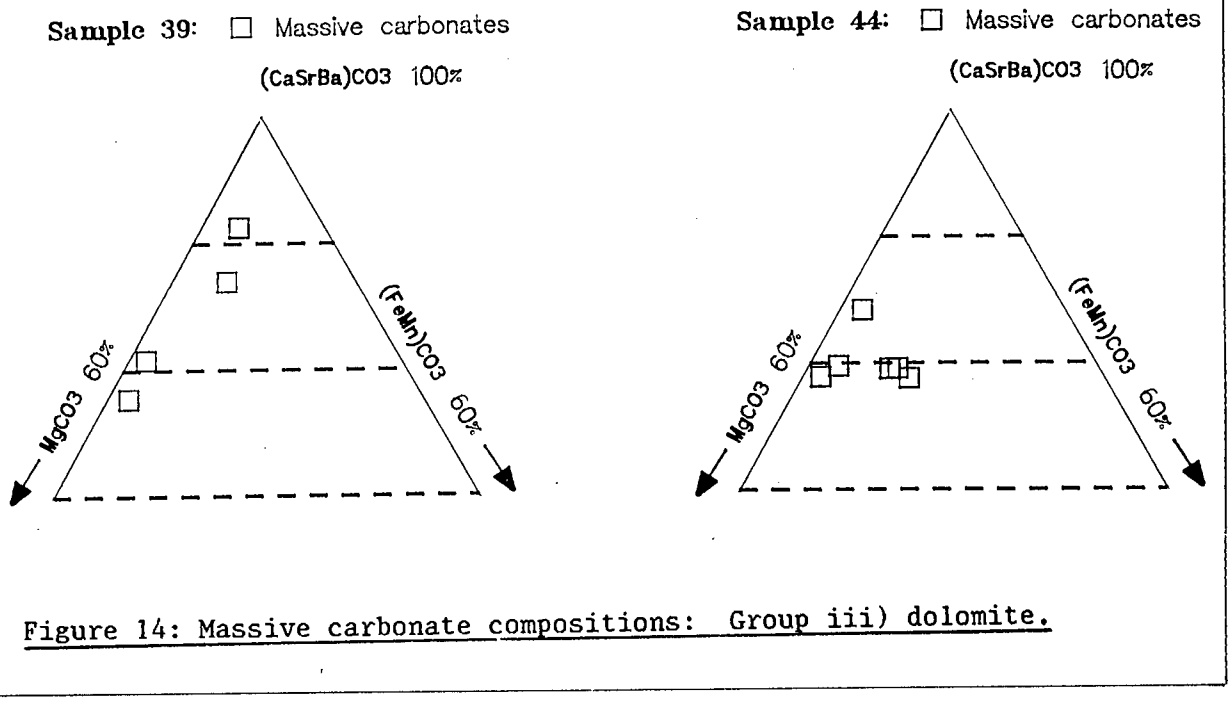

Figure 14: Massive carbonate compositions: Group iii) dolomite.

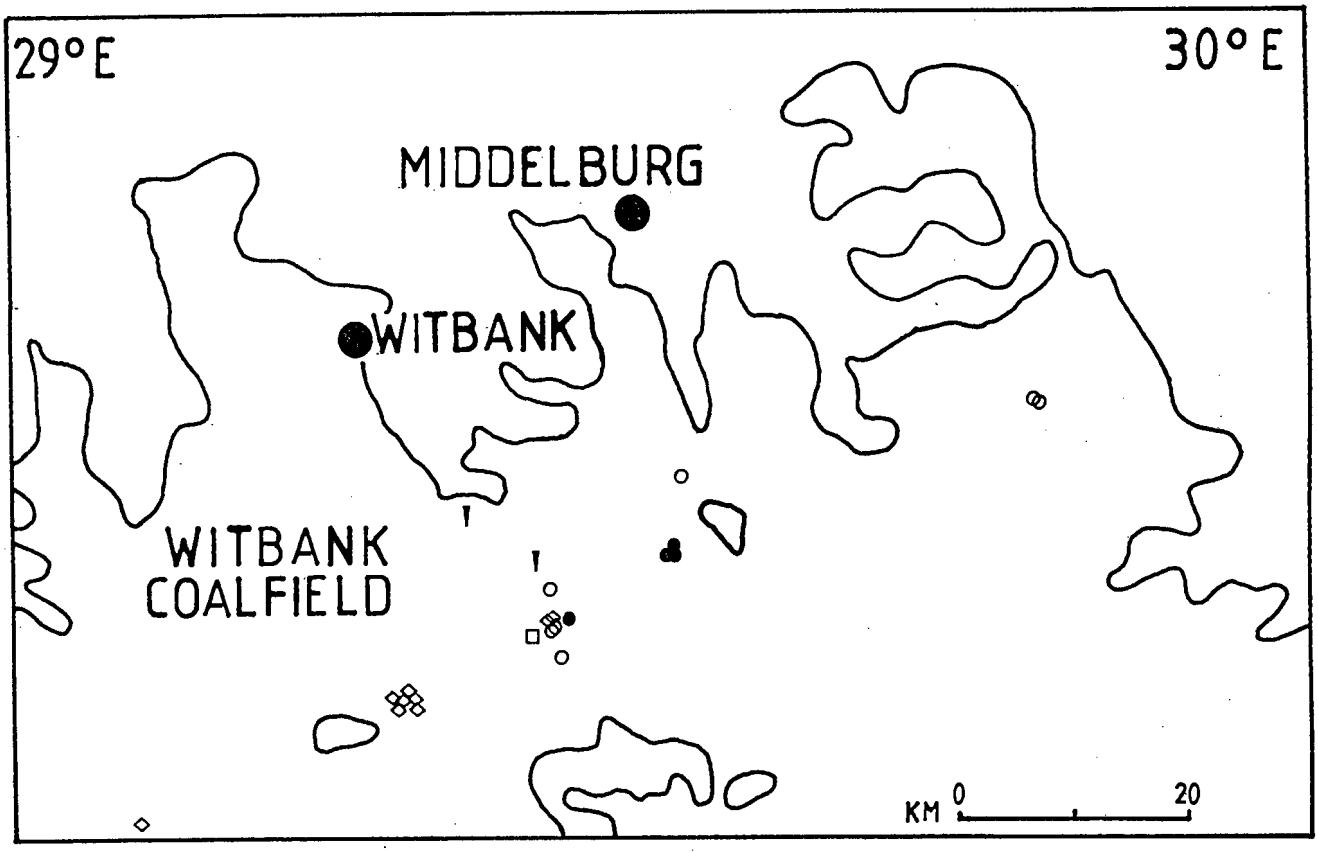

◇ ia) calcites
○ ib) calcites with Mg content
□ ic) calcites with FeMn content
● ii) siderites.
! iii) dolomites

Figure 15: Compositional distribution of massive carbonates across the study area.

3.3.3.c Relationship to macerals

The massive carbonate bodies are large, and thus never occur within a single maceral type as is the case for the smaller authigenic carbonates already described. Their relationships to macerals are best described through those included within their structure, and these include fusinite, semi-fusinite and vitrinite. Exinitic macerals have not been identified within massive carbonate bodies. In some of the massive carbonates, the texture of the included organic matter appears to suggest chemical destruction by the carbonate-bearing fluids or alternatively this texture may be due to bacterial degradation (Plate 16).

3.3.3.d Relationship to other minerals

XRD results show that these massive carbonate bodies are not mono-mineralic, the Ca carbonates usually having dolomite and pyrite as secondary minerals while Fe carbonates are always associated with pyrite. Where aragonite is the major Ca carbonate, it is always associated with calcite.

Staining with Alizarin-red demonstrates that dolomite and calcite relationships are complex. The dolomite has precipitated either between the calcite and the organic matter or is entirely enclosed in calcite (Plate 17).

Plate 18 shows the relationship of aragonite to calcite. While there is no evidence of inversion of aragonite to calcite within the major aragonite body, calcite occurs as cleat-fill in vitrinite bands included within the structure of the larger carbonate.

Pyrite occurs as rims to most of the sideritic carbonate bodies, and extensive pyrite development may entirely enclose small carbonate grains. Pyrite also occurs as a replacement mineral in almost all the massive carbonate bodies and as a fracture and cleat filling mineral within them.

Other minerals commonly occurring within the Ca carbonates are tiny apatite grains and in some cases, gorceixite.

One sample, 35, shows the development of Sr-rich "exsolution lamellae" (Plate 19), containing up to nearly 3% Sr while the greater carbonate body contains about 1%. The $SrCO_3$-$(Fe+Mn)CO_3$-$BaCO_3$ ratios of these Sr-rich zones are plotted on Figure 16. Two distinct compositional groups emerge, viz. high-Ca carbonate where Sr is the only impurity, and high-Ca carbonate with constant, very low Ba contents and similar Sr and Fe+Mn contents.

Sample 35

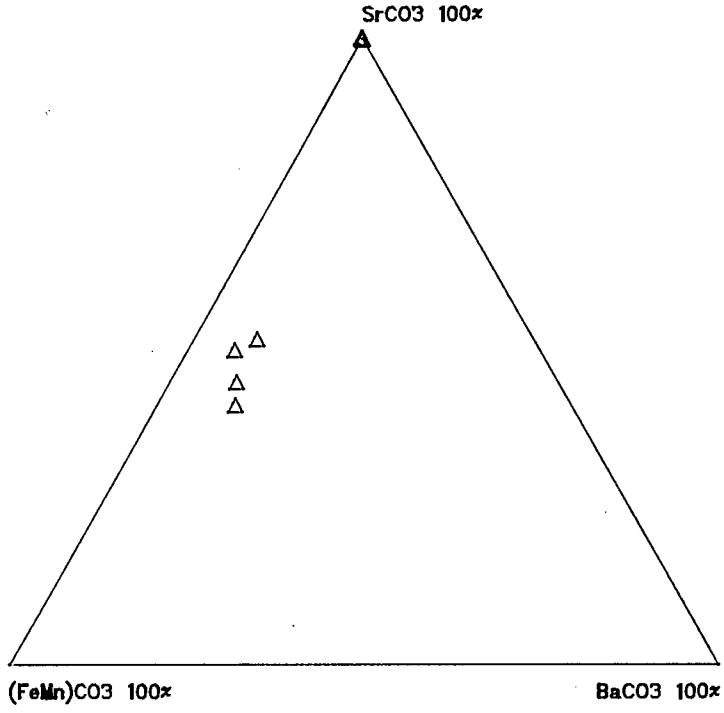

Figure 16: $SrCO_3$-(FeMn)CO_3-$BaCO_3$ plot of the Sr-rich "exsolution lamellae" in sample 35.

3.3.4 Cleat carbonates

Cleat-filling carbonates occur in all samples studied. Obviously, they are most common in vitrinite although some cleats are relatively large and intersect many layers of different macerals.

3.3.4.a Mineral compositions

Cleat-filling carbonate compositions fall into four groups:-

i) high-Ca carbonates, usually containing small percentages Mg and/or Fe. This group include samples 4, 5, 6a, 8 (vertical and horizontal cleats), 9 and 11 (horizontal cleats). Their compositions are shown in Figure 17.

ii) high-Ca carbonates with large variations in Mg content. This group includes samples 11, 12d, 14a + b, 15 (vertical and horizontal cleats), 30, 35 and 44. Three of these, 14a, 35 and 44, also have relatively large variations in Fe content. One analysis of a horizontal cleat in sample 15, however, deviates from this group and has a composition of about 60% Ca, 10% Mg and 30% FeMn. The compositions are shown in Figure 18.

iii) dolomites. This group includes samples 1b, 2, 7, 12b, 37, 38 and 42. The compositions are shown in Figure 19.

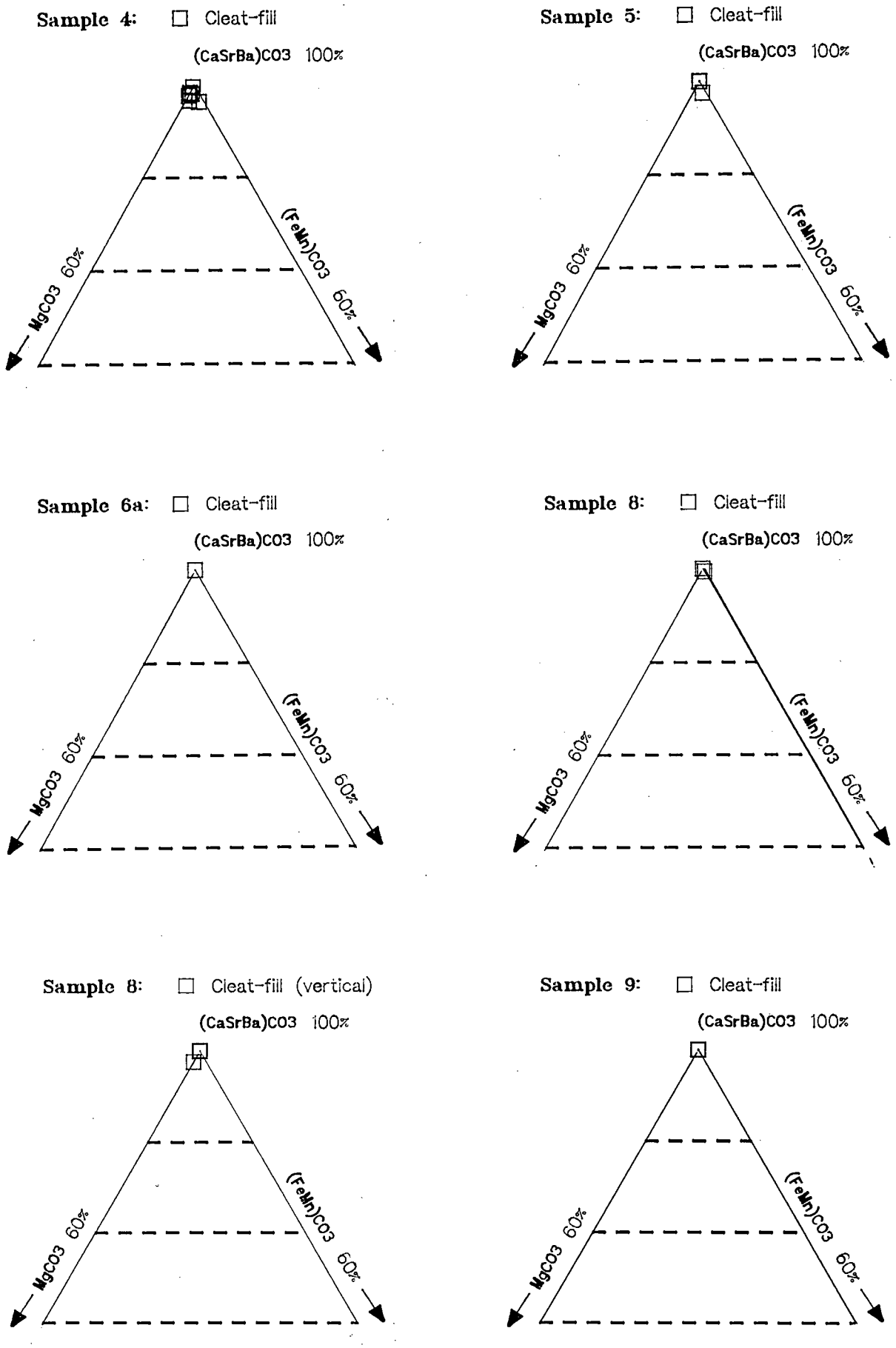

Figure 17: Cleat-fill carbonate compositions: Group i) high-Ca carbonates.

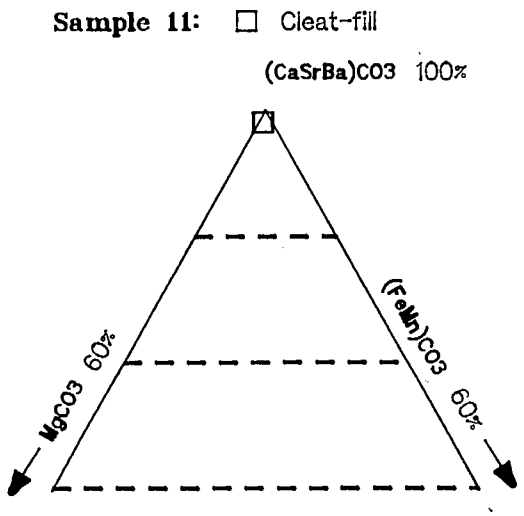

Figure 17 (cont.): Cleat-fill carbonate compositions: Group i).

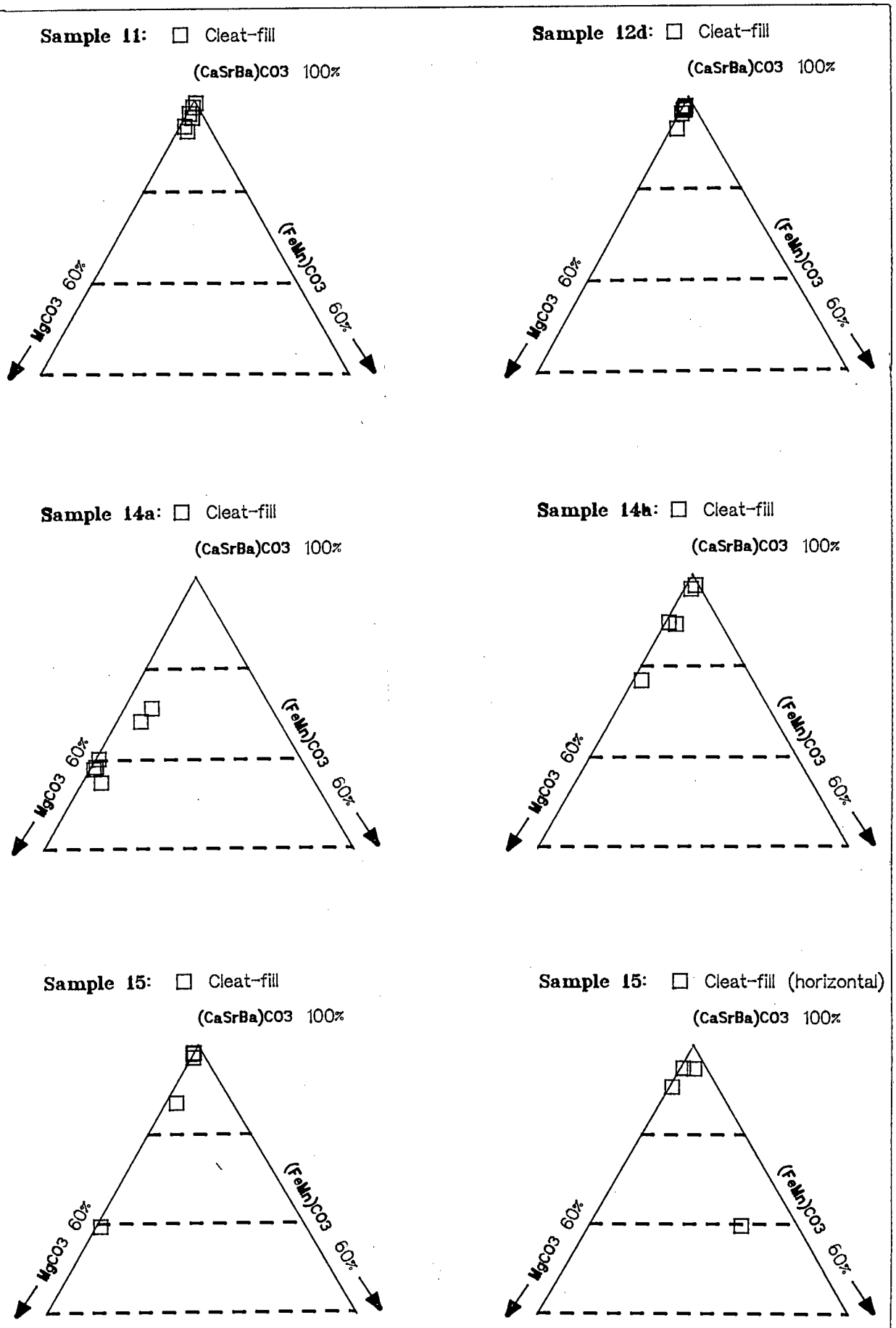

Figure 18: Cleat-fill carbonate compositions: Group ii) high-Ca carbonates with significant Mg content.

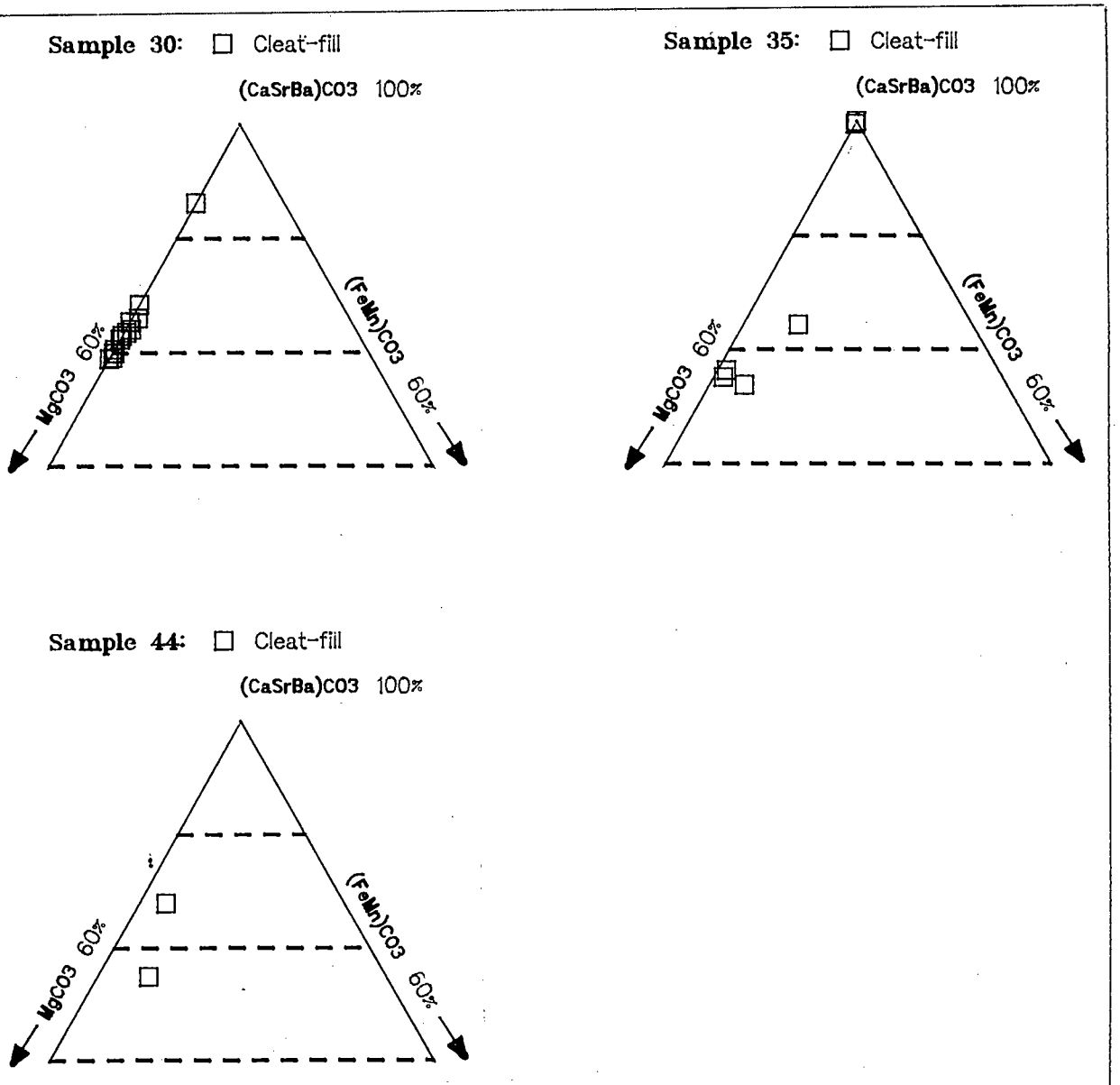

Figure 18 (cont.): Cleat-fill carbonate compositions: Group ii).

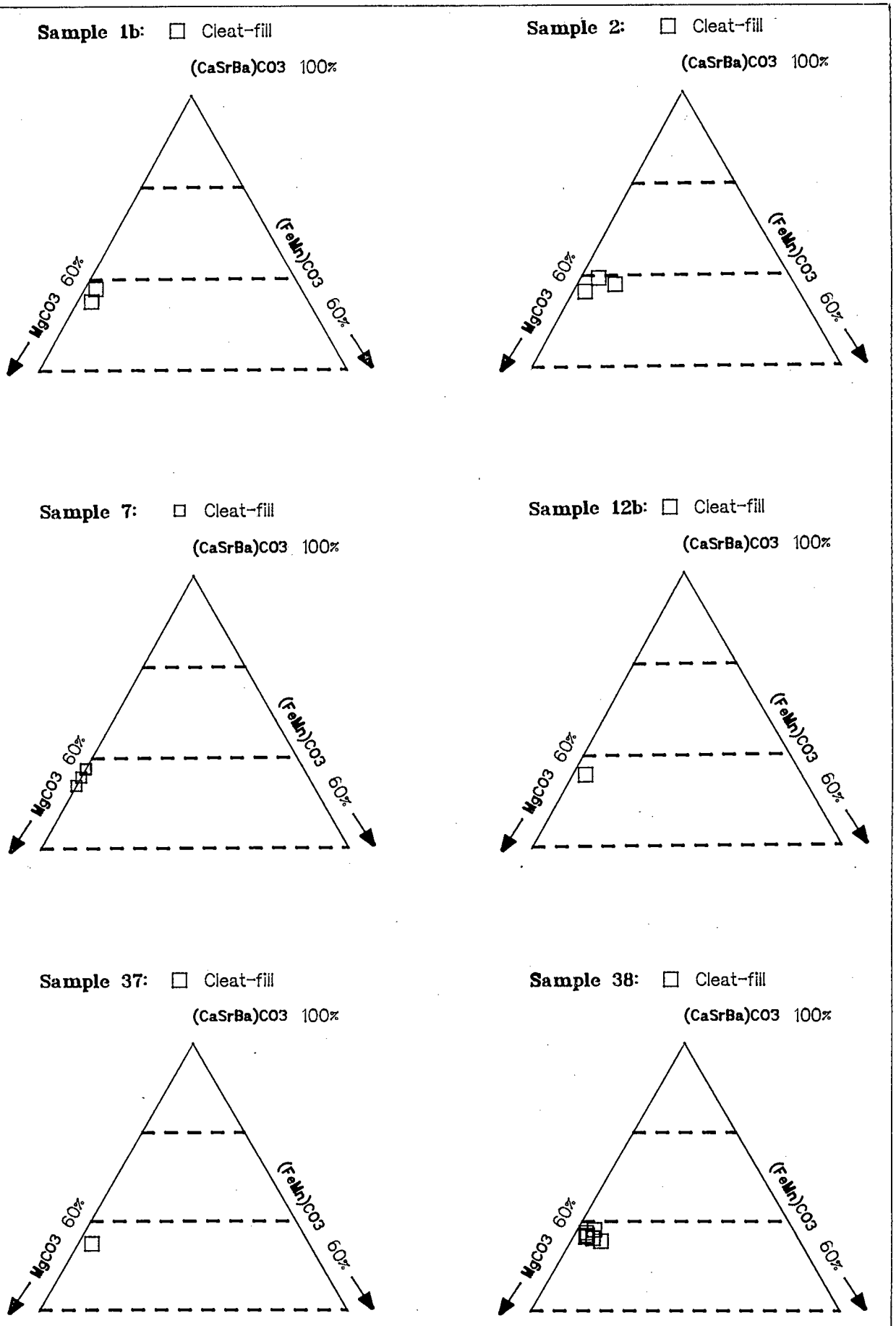

Figure 19: Cleat-fill carbonate compositions: Group iii) dolomite.

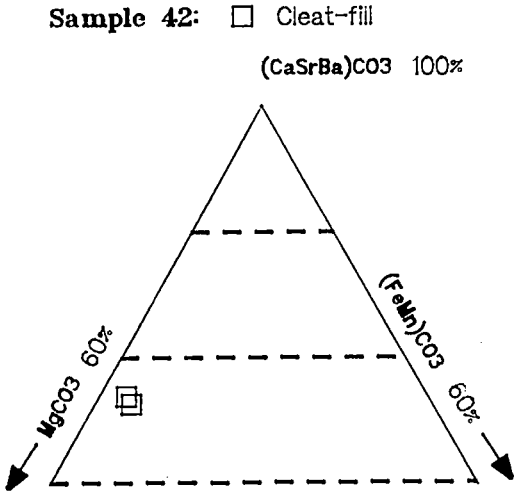

Figure 19 (cont.): Cleat-fill carbonate compositions: Group iii).

iv) ankerites. Only two samples showed cleat-fill with ankeritic compositions, viz. 1a and 43. The compositions are shown in Figure 20.

3.3.4.b Relationships to macerals

Almost all cleats occur in vitrinite layers, either in thin bands between other macerals or included within larger massive carbonates.

3.3.4.c Relationships to other minerals

Alizarin-red staining has demonstrated that some cleat-fills are at least two phase, with earlier calcite followed by dolomite emplacement. Calcite may show textures suggesting shrinkage, these voids being filled at a later stage by dolomite (Plate 20). Other two-phase emplacements consist of an initial pure Ca carbonate followed by Ca carbonate riddled with inclusions of almost sub-microscopic apatites (Plate 21).

Other minerals occurring as cleat-fill include kaolinite, either separate or together with carbonate, and pyrite, often replacing carbonate.

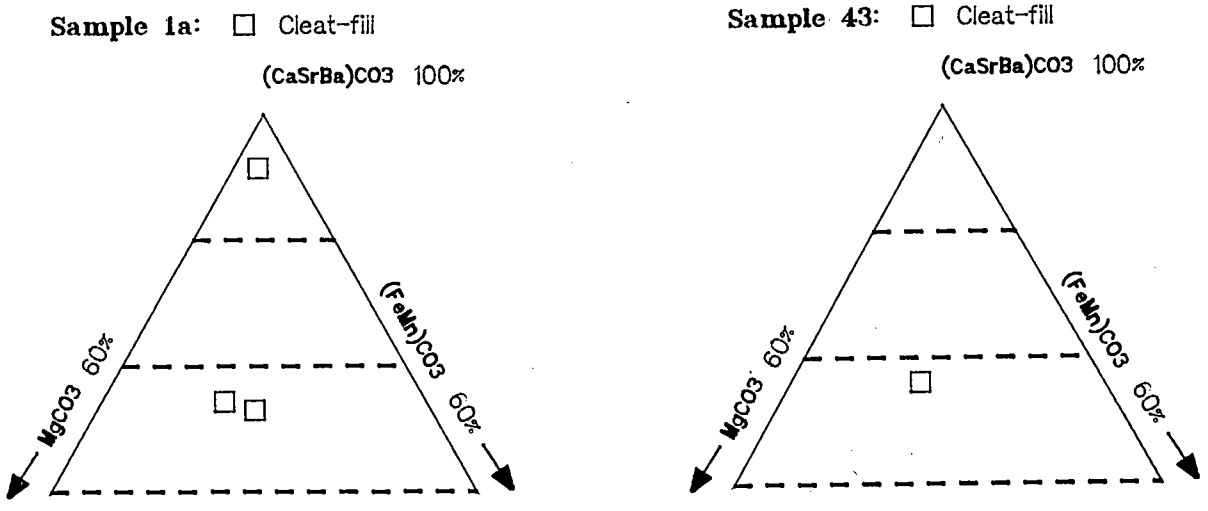

Figure 20: Cleat-fill carbonate compositions: Group iv) ankerite.

3.3.5 Vein and fracture fill

Veins and fractures are obviously associated with all macerals and minerals which they intersect although they bear no genetic relationship to these. In some cases, veins form sub-parallel networks around the larger carbonate bodies. They are generally dolomitic or high-Ca carbonates, although fractures in sample 1a were sideritic. Their compositions are plotted in Figure 21. Plate 22 shows how exinitic and other macerals may be stretched across the veins during crystalisation. A number of fracture-filling carbonates were emplaced in two or more phases, with the later phases containing myriads of almost sub-microscopic apatite inclusions.

3.3.6 Capping sandstone cement

Sample 10 is a capping sandstone directly overlying the no.2 seam. The sandstone is cemented by ankerite, as shown in Figure 22.

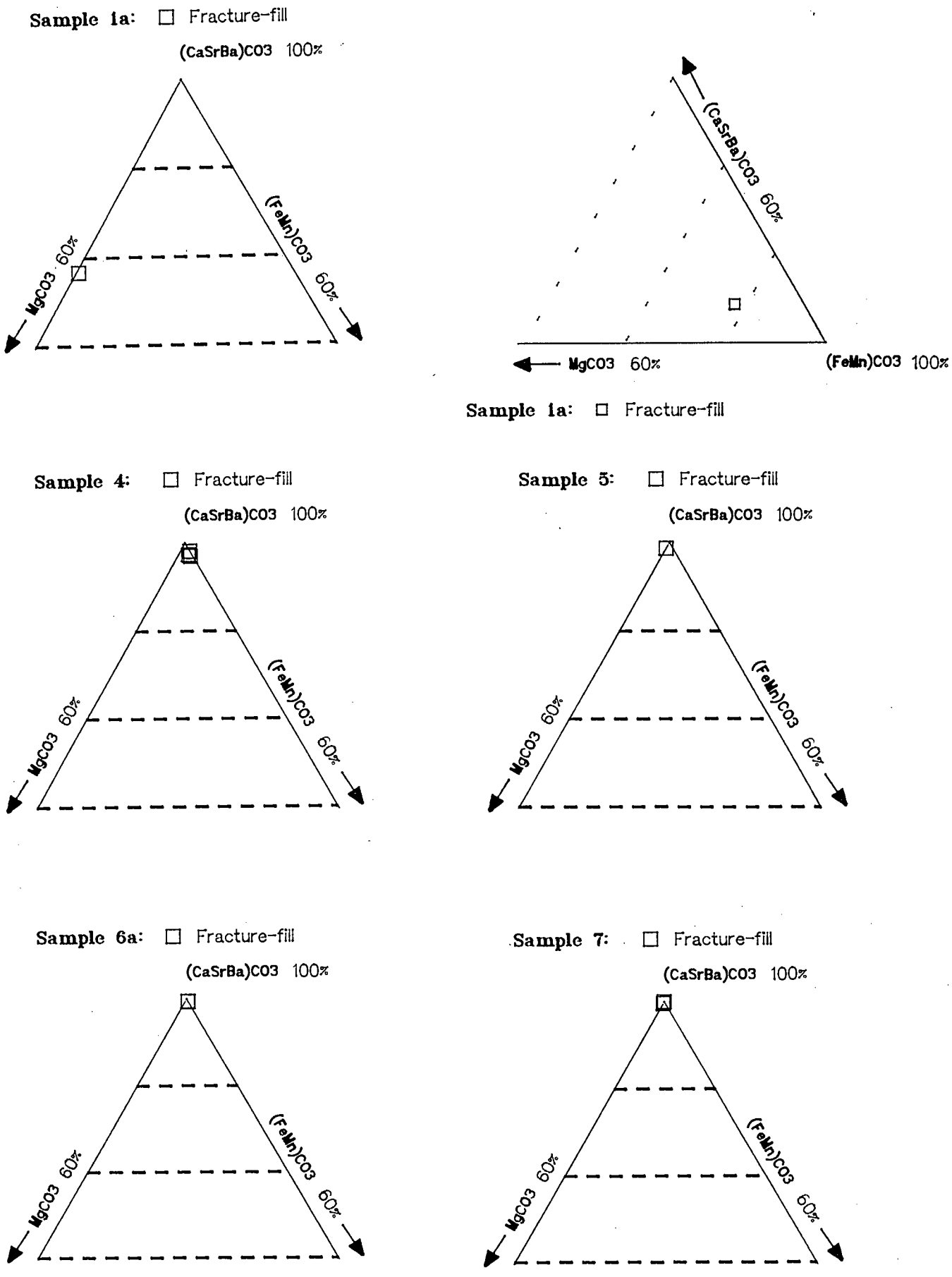

Figure 21: Fracture-fill carbonate compositions.

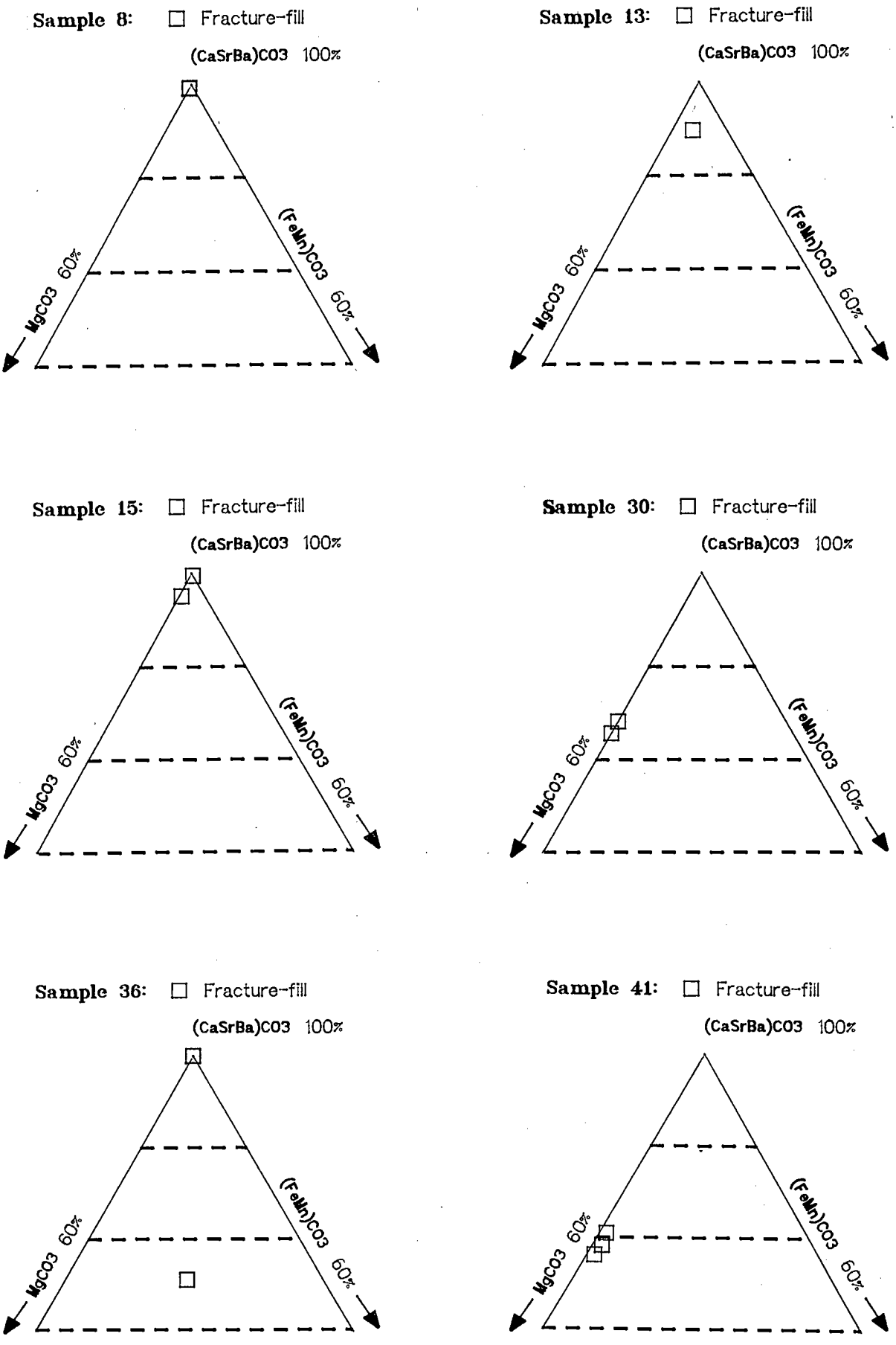

Figure 21 (cont.): Fracture-fill carbonate compositions.

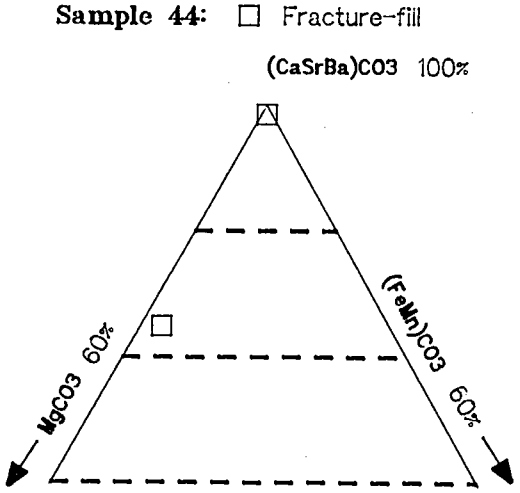

Figure 21 (cont.): Fracture-fill carbonate compositions.

Sample 10: ☐ Carbonate cement

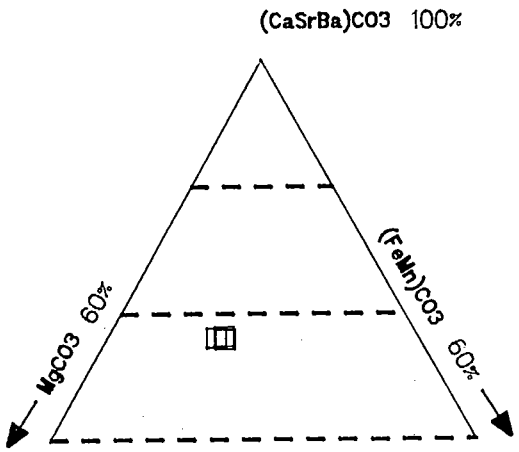

Figure 22: Capping sandstone carbonate cement composition.

3.3.7 Isotope data

$^{13}C/^{12}C$ and $^{18}O/^{16}O$ isotope ratios were determined for a number of the massive carbonate samples at the Schonland Research Centre, University of the Witwatersrand, under the direction of Professor B.Th. Verhagen (Falcon and Verhagen, 1990). Block samples of 2-3cm thickness were analysed from samples 11, 12, 13 and 14. The results of these analyses are presented in Table 3, adapted from Table 1 of Falcon and Verhagen (1990). The isotopic abundances are expressed as fractional deviations permille, d, from those of the Cretaceous belemnite from the Peedee Formation. This standard is referred to as PDB. Very little variation occurs within particular carbonate bodies, as well as between carbonate bodies. The $d^{13}C$ values range from -6.3 to -9.1 relative to PDB, while $d^{18}O$ values cover a range of -11 to -15.7 relative to PDB.

More detailed isotope analyses for sample 6 were also published and are presented in Figure 23, adapted from Figure 1 of Falcon and Verhagen (1990). $d^{18}O$ values are fairly constant within the massive carbonate and in smaller carbonates occurring in the coal above the massive carbonate. They range between about -12 to -14 relative to PDB, a range that is similar to that of the bulk samples of massive carbonates discussed above. $d^{13}C$ values, however, show greater variation. They range from -10 to -15 in the lower massive carbonate, but become positive for carbonates in the coal above the massive carbonate. In the higher coal layers, there is a zone where carbonates again show larger negative values. More specific data regarding the type of carbonate occurrences (cleats, fracture fill or early authigenic carbonate blebs) are not available from the authors.

Table 3 Bulk sample isotope values across some massive carbonates From Falcon and Verhagen (1990).

Sample	Position	d13 C(°/oo)PDB	d18 O(°/oo)PDB
11	top	-8.9	-14.6
11	base	-6.2	-14.8
12	top	-6.7	-14.4
12	middle	-9.3	-15.7
12	base	-7.6	-14.8
13	top	-8.6	-13.0
13	middle	-8.7	-14.1
13	base	-9.1	-13.9
14	top	-7.9	-12.3
14	base	-8.0	-11.3

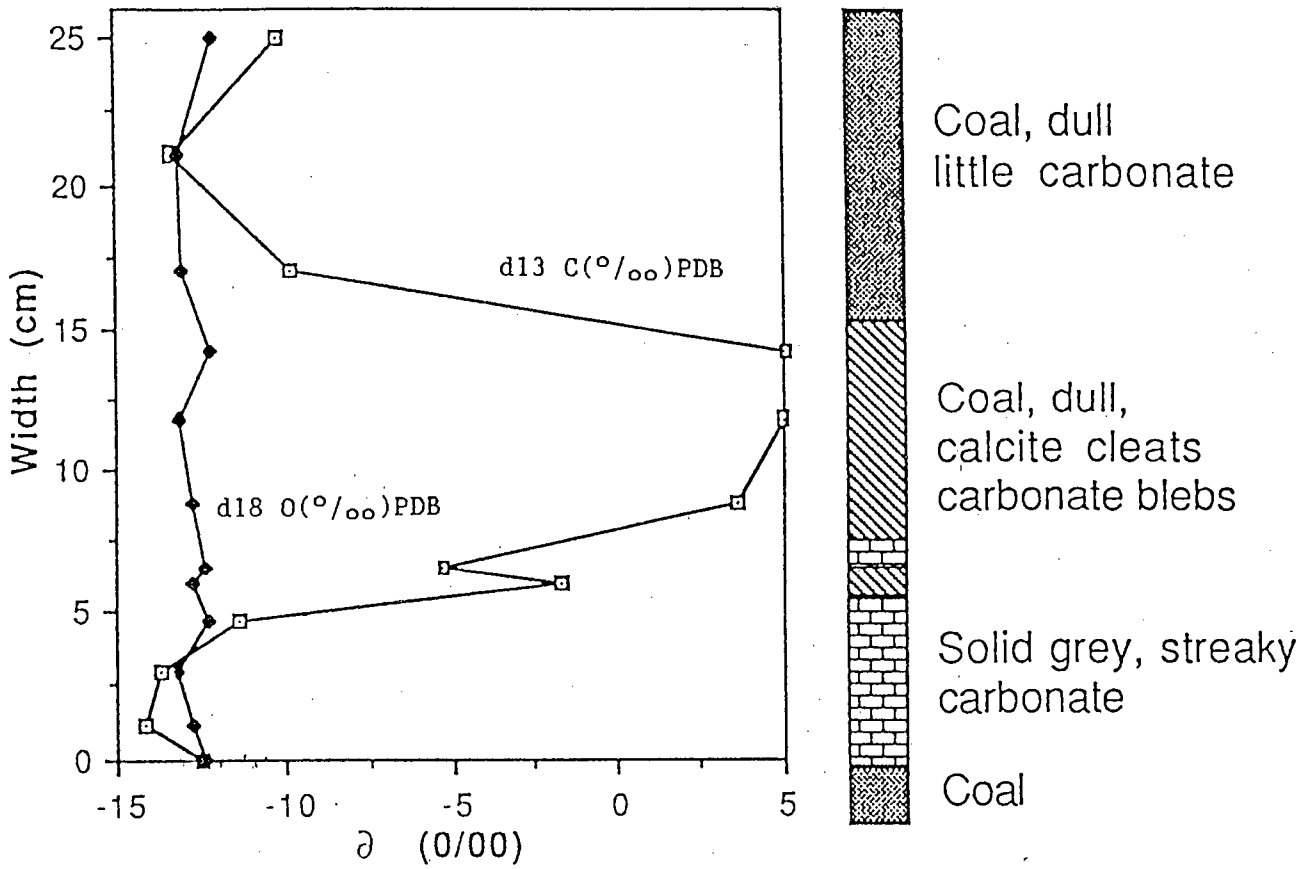

Figure 23:$d^{13}C$ and $d^{18}O$ values from detailed sampling across sample 6, from figure 7, Falcon and Verhagen (1990).

3.3.8 Summary

The above results are tabulated according to sample in Table 4. The major points are summarised below:-

a) six different types of carbonate occurrence were identified, viz:

i) cell-fill

ii) small, early authigenic bodies (spherulites)

iii) massive carbonates

iv) cleat-fill

v) fracture-fill

vi) cement in the capping sandstone

b) cell-filling carbonates were found to be relatively pure Ca carbonates with small percentages of Mg and Fe. Some were found to contain small amounts of Sr. Associated minerals were kaolinite, gorceixite and pyrite. Tiny, euhedral pyrites occurred included in some samples.

c) early, small authigenic carbonates were found to be spherical or weakly elongate in the plane of bedding, often draped by macerals. They were divided into three groups on the basis of composition, viz:

i) low-Mg Ca carbonates

ii) Ca-Mg siderites

iii) dolomite

Table 4: Summary of results.

SAMPLE NUMBER	CELL-INFILLING MINERALS			EARLY AUTHIGENIC CARBONATES					MASSIVE CARBONATES											CLEAT CARBONATES									FRACTURE FILL	
	COMPOSITION	ASSOCIATED MINERALS	ASSOCIATED MACERALS	SIZE IN MM	COMPOSITION		ASSOCIATED MINERALS	ASSOCIATED MACERALS	SIZE IN MM	TEXTURAL GROUP				COMPOSITION						ASSOCIATED MINERALS	ASSOCIATED MACERALS	SIZE IN MM	COMPOSITION				ASSOCIATED MINERALS	ASSOCIATED MACERALS	ONE PHASE	TWO OR MORE PHASES	COMPOSITION	
					i low Mg Ca-Carbs	ii Siderites				i	ii	iii	iv	ia	ib	ic	ii	iii					i	ii	iii	iv					Calcite	Dolomite
1a	not found	not found		1mm < 1mm		• EDS	pyrite apatite (EDS)	vitrinite	80 thick x 300			•		• EDS	intergrown ⟷ •				pyrite-rims	vitrinite	1-2 mm	•			•	none	vitrinite		/	low Mg Fe (EDS)	
1b	not found	not found		1mm to < 1m		•	pyrite apatite	vitrinite	80 x 300			•		•	intergrown		•			pyrite-rims	vitrinite	1-2 mm			•		none	vitrinite	?		low Mg Fe	
2	detrital kaolinite		fusinite rich bands			•	pyrite apatite	vitrinite					•				•			pyrite-rims	vitrinite				•		pyrite kaolinite			/		
3	calcite (EDS)	none	fusinite	2mm and less		•	pyrite apatite	vitrinite sporinite							none												ND				none	none
4	ND	detrital quartz kaolinite	fusinite		•		kaolinite dissemi-nated	vitrinite	see sample descriptions	•	•			•					none	semi-fusinite/ vitrinite			•				none	intersects all	/		none	none
5	low Mg calcite	detrital kaolinite feldspars	fusinite bogen-structure sclero-tinite	1-2 mm or less	•		pyrite in vitrinite TiO2	vitrinite tri-macerite layers			none											1-4 mm	•				none	intersects all	/		none	none
6a		none found		1-2 mm	•		apatite pyrite	vitrinite		•	•			•						gorceixite	semi-fusinite		•				apatite	vitrinite		/	none	
6b		none found		3mm or less	•		apatite pyrite	vitrinite		•	•			•						gorceixite	semi-fusinite		•				apatite	vitrinite		/	none	
7	Ca-carbonate		fusinite	2mm or less	• EDS		apatite kaolinite pyrite	vitrinite		•	•			•						apatite pyrite	semi-fusinite					•		vitrinite	/		/	
8		none			• EDS		apatite kaolinite TiO2	vitrinite		•	•			•						kaolinite TiO2	vitrinite => others		•								/ EDS	
9		none			• EDS		none	mixed layer coal		•	•			•						pyrite	vitrinite		•				within massive carb	vitrinite			/	

Table 4 (cont.): Summary of results.

SAMPLE NUMBER	CELL-INFILLING MINERALS			EARLY AUTHIGENIC CARBONATES					MASSIVE CARBONATES											CLEAT CARBONATES									FRACTURE FILL	
	COMPOSITION	ASSOCIATED MINERALS	ASSOCIATED MACERALS	SIZE IN MM	COMPOSITION		ASSOCIATED MINERALS	ASSOCIATED MACERALS	SIZE IN MM	TEXTURAL GROUP				COMPOSITION					ASSOCIATED MINERALS	ASSOCIATED MACERALS	SIZE IN MM	COMPOSITION				ASSOCIATED MINERALS	ASSOCIATED MACERALS	ONE PHASE	TWO OR MORE PHASES	COMPOSITION	
					i low Mg Ca-Carbs	ii Siderites				i	ii	iii	iv	ia	ib	ic	ii	iii				i	ii	iii	iv					Calcite	Dolomite
11	none found	none found		2mm or less	• (EDS)		illite kaolinite pyrite	vitrinite		•	•			•					none	vitrinite		• H	• V			pyrite	vitrinite		/	/ (EDS) apatite p	
12a	low Mg Ca-carbonate	none	semi-fusinite and fusinite	3 x 2m or less	• EDS		none	semi-fusinite														•				pyrite	vitrinite		/	none	
12b				4 x 2mm or less	•		apatite pyrite	vitrinite		•	•			•					apatite gorceixite pyrite	vitrinite			•			kaolinite	vitrinite				
12c									see sample descriptions	•	•				•				apatite gorceixite pyrite	vitrinite			•	•		kaolinite	vitrinite		/		
12d																				semi-		•				kaolinite pyrite	vitrinite		/	/ (EDS)	
13				2mm or less	• (EDS)	apatite kaolinite	vitrinite										•				• EDS				illite kaolinite gypsum	vitrinite	/		/ (EDS) p	
14a				1-2 mm	•		pyrite some incl. in massive c	vitrinite		•	•				•				pyrite dolomite	vitrinite semi-fusinite			•		•	none	vitrinite		/	/ (EDS)	
14b																						•			•	none	vitrinite		/	/ (EDS)	
15												•		•	•	intergrown		•	pyrite rims	vitrinite					•		vitrinite	/		/	
30	Ca-carbonate	kaolinite in adjacent cells pyrite	fusinite	4 t < mm	iii dolomite		apatite pyrite	semi-fusinite														•				apatite kaolinite	vitrinite		/		/
31	Ca-carbonate	kaolinite in adjacent cells pyrite	fusinite	5 t < mm	•		apatite	semi-fusinite														•				apatite kaolinite	vitrinite		/		/

Table 4 (cont.): Summary of results.

SAMPLE NUMBER	CELL-INFILLING MINERALS			EARLY AUTHIGENIC CARBONATES					MASSIVE CARBONATES												CLEAT CARBONATES									FRACTURE FILL	
	COMPOSITION	ASSOCIATED MINERALS	ASSOCIATED MACERALS	SIZE IN MM	COMPOSITION i low Mg Ca-Carbs	COMPOSITION ii Siderites	ASSOCIATED MINERALS	ASSOCIATED MACERALS	SIZE IN MM	TEXTURAL GROUP i	TEXTURAL GROUP ii	TEXTURAL GROUP iii	TEXTURAL GROUP iv	COMPOSITION ia	COMPOSITION ib	COMPOSITION ic	COMPOSITION ii	COMPOSITION iii	ASSOCIATED MINERALS	ASSOCIATED MACERALS	SIZE IN MM	COMPOSITION i	COMPOSITION ii	COMPOSITION iii	COMPOSITION iv	ASSOCIATED MINERALS	ASSOCIATED MACERALS	ONE PHASE	TWO OR MORE PHASES	COMPOSITION Calcite	COMPOSITION Dolomite
32	detrital kaolinite	apatite pyrite	semi-fusin. fusinite sclerot.-inite		none found					•	•				•				pyrite-replace + tiny euhedral	vitrinite	1-2 mm	•	•			kaolinite apatite	vitrinite larger cleats others		/	low Mg /	/
33	detrital kaolinite	apatite pyrite	semi-fusinite and fusinite		none found					•	•				•					vitrinite	1-2 mm	•	•			kaolinite apatite	vitrinite		/	/	/
34	calcite	detrital kaolinite quartz monazite	fusinite		none		TiO2 chalco-pyrite	vitrinite		•	•			•						trimac-erite						none found				low Mg + pure Ca	
35	low Mg Fe calcite (EDS)	none	fusinite			• (EDS)	TiO2 pyrite	vitrinite	see sample descriptions		•					•			strontia-nite (exsolved)	non-specific			•			vitrinite	/		none	
36	low Mg FE calcite	none	fusinite			• (EDS)	TiO2 pyrite	vitrinite			•					•			strontia-nite				•			vitrinite	/		none	
37	high Mg low Fe calcite	kaolinite in adjacent cells	fusinite		none		apatite pyrite	vitrinite				none found							kaolinite barite					•	apatite kaolinite	intersects all		/	none	
38	high Mg low Fe calcite	kaolinite in adjacent cells	fusinite		none		pyrite apatite	vitrinite				none found							kaolinite barite					•	apatite kaolinite	intersects all		/	none	
39			composite			•	dolomite rims	unknown		•	•							•	none	semi-fusinite						none found			none found	
40			"		none					•	•				•				none	semi-fusinite										
41			"		none							none														none				/
42			"		none					•	•				•				none	semi- fus				•		vitrinite				
43			"		none			semi-		•	•				•				none	semi-fus					•		all				
44			"		none					•	•							•	none	semi-fusinite			•	•			vitrinite			/	/

One sample showed zoning from siderite to dolomite. These bodies were found to have a strong association with vitrinite. Other minerals associated with vitrinite were apatite, kaolinite, TiO_2 (rutile or anatase), pyrite and, in one case, chalcopyrite.

d) massive carbonates occur as large, elongate bodies. Four textural groups were described, viz:

i) non-destructive cell-fill

ii) destructive cell-fill

iii) massed aggregates of smaller elongate bodies

iv) numerous, small spherical carbonates joined by pyrite rims.

The massive carbonates were divided into three groups on the basis of their compositions, viz:

i) high-Ca carbonates with a) small Mg and/or Fe contents
b) large variations in Mg content
c) variation in FeMn content

ii) siderites

iii) dolomites

Textural groups (i) and (ii) corresponded to compositional groups (i) and (ii), while textural groups (iii) and (iv) corresponded to compositional group (ii). Massive carbonates were found to be associated with fusinite, semi-fusinite and vitrinite.

XRD analyses showed the high-Ca carbonates to be associated with dolomite and pyrite as secondary minerals, and, in the case of aragonites, with calcite. Staining showed these secondary minerals to be cleat-fills in vitrinite included within the massive carbonates. Siderites were often

found to be rimmed with pyrite. Other minerals found included in massive carbonates were apatite, pyrite and gorceixite. One sample showed the development of Sr-rich lamellae within a high-Ca carbonate.

e) Cleat carbonates were found in all samples. Four compositional groups were identified, viz:

i) high-Ca carbonates with small Mg and Fe contents

ii) high-Ca carbonates with large Mg variations

iii) dolomites

iv) ankerites

Cleat carbonates were found to show a strong affinity to vitrinite. Other cleat-filling minerals are kaolinite and pyrite. Some cleats showed two-phase emplacements, either of Ca carbonate followed by dolomite, or clear Ca carbonate followed by carbonate rich in apatite inclusions.

f) Fracture-fill carbonates were found to be high-Ca carbonates or dolomite. They often formed horizontal networks around massive carbonates.

g) A capping sandstone was found to have ankerite cement.

h) Vitrinite reflectance suggests a maximum burial of between 1400m and 3000m for these coals.

i) Early authigenic carbonates show the following areal distribution:- low-Mg Ca carbonate or dolomite occurs in the south west and centre of the study area and siderite in the north east, closer to large basement highs.

j) Massive carbonates show the following compositional distributions. High-Ca carbonates occur in the south west, while dolomite, siderite and low-Mg Ca carbonates occur in the centre of the area. Samples from the north east are only low-Mg Ca carbonates.

k) d13C values for bulk samples of massive carbonates are negative relative to PDB and range from -6.2 to -9.3. d18O values are also negative relative to PDB and range from -11.3 to -15.7. More detailed isotope analyses across a massive carbonate and associated coal yielded fairly constant negative d18O values relative to PDB while d13C values ranged from strongly negative across the massive carbonate to positive in the coal above it, returning to strongly negative above that.

4 DISCUSSION

4.1 Textural relationships and relative timing of carbonate formation

Six types of carbonate occurrence have been described. Of these, five occur directly associated with coal while the sixth form of occurrence is as a cementing mineral in a capping sandstone. To describe the changes in depositional environment and later diagenetic environment in terms of carbonate chemistry, it is essential to identify the relative timing of the formation of the various forms. Consideration of the entire mineral assemblage representative of a particular stage in the coal's formation will give a clearer picture of events, since carbonate chemistry cannot be described in isolation. A discussion of the evidence for timing of formation of each of the types of carbonate occurrence and accompanying mineral assemblages follows.

4.1.1 Cell-filling carbonate

Mineral matter filling relatively undeformed cells should represent the earliest stage of authigenic mineral precipitation in close association with the organic material collecting in the peat bog. If this is not the case, then it must represent a replacement of either the original organic cell contents or early formed minerals

that were able to support the structure of the plant cells during later burial. To have replaced original organic cell contents, the minerals must have precipitated within the cell lumens before any major degradation, either bacterial, mechanical or chemical/diagenetic, could destroy these structures. This implies that the minerals filling these lumens are an expression of the original fluids within the cells at the time of organic matter accumulation, i.e. the original fluids present within the circulatory system of the plant, if any, and their reaction with the fluids and available ions in the swamp under the pH and Eh conditions present during the earliest stage of peat formation. The composition of the fluids within the early swamp are in turn an expression of the original water supply to the swamp together with the detrital material brought into the swamp by this water.

4.1.2 Small, spherical bodies (spherulites) associated with vitrinite

While these bodies occur in what is now a relatively brittle material, this would not always have been the case. The near spherical shape of the majority of these carbonate bodies implies that they must have grown under relatively little directional pressure, and that chemical species required for their formation must have been in equally ready supply over the entire surface of the growing spheres. This means that the medium into which they grew was soft and flexible and allowed for great mobility of fluids. It is thus suggested that these spherical carbonates and the mineral assemblages

accompanying them within vitrinite microlithotypes grew at a stage of shallow burial while the organic matter was in a fluid, colloidal state generally described as the precursor to vitrinite formation (Stach, et al., 1975). This is supported by the intimate inclusion of structureless organic material within individual carbonate growths. For the formation of vitrinite, the organic material must have been quickly submerged into an anaerobic or relatively reducing environment (Falcon and Snyman, 1986), and it is in such an environment that these carbonates are thought to have precipitated.

4.1.3 Massive carbonate bodies

Overall, these bodies are generally elongate in the plane of coal bedding and may be large discoid structures with long dimensions of greater than a metre. However, up to four different internal textures have been described, with more than one texture occurring within any single carbonate-rich body. These textures are indicative of both early and late formation of the carbonate.

Masses of small, spherical bodies, with inclusions of organic material within their structure, making up larger bodies suggest formation under conditions as described in section 4.1.2 while the non-destructive filling of cell lumens suggests precipitation of the carbonate at a very early stage as is described in section 4.1.1.

The overall elongate form, tapering towards the edges and often markedly draped by organic material, suggests formation under some overburden pressure, confirmed by obvious preferential growth of the carbonate in planes parallel to coal bedding. However, the overall shape may also be due to initial precipitation in small, restricted "pans", as suggested by Falcon (1989), with draping being the result of later differential compaction.

The later preferential growth directions exhibited by carbonate in some of these bodies suggests that even if initial precipitation was at the sediment-water interface, further growth continued under some burial pressure. The inclusion of organic matter within the carbonate as previously described, suggests later continued growth, at a stage when gellification of vitrinite precursors was taking place.

A number of the carbonate bodies exhibit textures possibly representing some form of destructive emplacement into the organic matter, suggesting that semi-fusinite and fusinite were fairly rigid at the time, as these textures are more commensurate with fracturing and splintering than with deformation of soft material. Others show evidence of more than one phase of carbonate precipitation, the second phase definitely fracturing rigid macerals.

It is suggested that while the formation of these structures may have begun in shallow, restricted pans within the peat swamp, further growth and possible remobilisation occurred with increasing burial,

so that their chemistry and mineralogy must be regarded as the product of the sum of these stages in peat formation, rather than representative only of an early, shallow burial phase.

4.1.4 Cleats

Cleat formation in vitrinite has been documented as a fairly late occurrence in the process of coalification, when vitrinite begins to shrink, leaving characteristic cleats at ninety degrees to bedding (Ting, 1977). From observation of carbonate mineralisation filling cleats in the Witbank coals, it is clear that the organic material was brittle and non-plastic, as any organic matter included within the mineralisation is in the form of angular blocks and shards.

The multiple episodes of carbonate and other mineralisation observed in cleats are thus regarded as the product of fluids moving through the coal at a late stage in its history, possibly containing ions released during diagenesis of detrital minerals and remobilisation of earlier precipitated minerals. At these depths (a few kilometres, as suggested by reflectance modelling) it could be expected that the pore waters would have a very different composition to the original water flowing into the early peat bog.

middle to late burial - cleat-fill, massive carbonates, cleat-fill replaces cell fill.

Late burial - fracture-fill, multi-phase, possibly affecting all earlier formed carbonates.

4.2 Carbonate geochemistry

4.2.1 Cell-filling carbonate

During the first stages of peat formation, the climate was cold; water entering the swamp would probably have been from glacial runoff, therefore fresh and possibly carrying fine detritus in the form of glaciogenic rock flour. It could thus be expected to have a low ionic concentration, to be acidic and to be low in sulphate content (Curtis and Coleman, 1986).

However, all early cell-filling carbonates analysed have been shown to be high-Ca calcites with low Mg and/or Fe content and often with inclusions of tiny euhedral pyrite crystals. They commonly occur in inertinite, while other cell infilling minerals include pyrite, illite and gorceixite. Cells are also commonly filled with kaolinite, although the more deformed appearance of the cell walls suggests that this mineralisation could have taken place at a later stage. The absence of siderite and a mineral assemblage consisting of pyrite, Ca-carbonate and illite is generally suggestive of a more

alkaline depositional environment for these early carbonates (Curtis and Coleman, 1986; Matsumoto and Iijima, 1981 and Renton, 1982).

In an alkaline environment, bacterial action is not inhibited (Berner, 1971) and any sulphate present would be reduced to sulphide, as long as organic materials were available, enabling the precipitation of pyrite (Curtis and Coleman, 1986). Bacterial sulphate reduction would also increase the pore water concentration of carbonate, and Fe-poor calcite together with pyrite, would precipitate. Sulphate reduction and pyrite precipitation increase the saturation with respect to Fe-poor carbonates by generating both bicarbonate and hydroxyls, while maintaining Fe activity at low levels:

$15CH_2O+2Fe_2O_3+8SO_4^{2-} \rightarrow 4FeS_2+7H_2O+15HCO_3^-+OH^-$

(Curtis and Coleman, 1986).

Dolomite would precipitate only if the sulphate levels were low enough (Matstumoto and Iijima, 1981). The inclusions of pyrite within calcite support the availability of sulphur as sulphide during the precipitation of the calcite, as described by Curtis and Coleman in a study of carbonates in coals influenced by marine transgression (Curtis and Coleman, 1986). Illite's common occurrence as the cell-filling clay mineral also lends support to the hypothesis of neutral to alkaline depositional waters (Renton, 1982).

The above suggests an early brackish influence on the peat swamp (high sulphate supply, alkaline pH). However, this is not necessarily the case. Renton (1982) describes a freshwater basin rich in fossils and freshwater limestones with precisely this mineral

assemblage, deposited in fresh but alkaline waters. Altschuler et al.,(1983), describe pyrite formation in early peat from the Everglades, in fresh water with alkaline pH.

Cell-filling carbonate shows an association with inertinite suggesting an oxidising environment. While some anaerobic conditions must have existed locally (pyrite cell-fills), degradation under oxidizing or suboxic conditions must have occurred, inhibiting formation of sulphide. Under such conditions, Fe could be removed as oxides and the siderite typical of initially fresh depositional waters would not have precipitated (Curtis and Coleman, 1986). It is also possible that the cold climate would not have been conducive to earlier formation of Fe-rich soils, usually considered as the most important detrital supply of Fe to many swamps.

Kaolinite commonly occurs in cells adjacent to calcite with pyrite inclusions, indicating the existence of acid environments adjacent to more alkaline environments. This may be indicative of fairly closed micro-environments with different pHs from cell to cell. The diverse mineral assemblage does, however, support evidence for mobility of ions at this time.

As noted by Curtis and Coleman (1986), the possibility also exists of a marine transgression completely obscuring the chemical imprint of earlier fresh depositional water. Alternatively, cyclothemic conditions resulting in a seasonally oscillating water table, as suggested by Falcon (1989), may have prevented the reduction of Fe, thus preventing precipitation of siderite.

4.2.2 Early spherulites

Except for those now entirely enclosed by massive carbonates, all the spherulites occur in vitrinite. Vitrinite represents the survival of that portion of the organic material most difficult to preserve (Renton, 1982). The process of vitrinite formation generally requires low pH and low Eh to inhibit bacterial degradation, although it is possible that low temperatures could have produced this effect at a somewhat higher pH. Inhibited reduction of sulphate and availability of reduced Fe should result in the precipitation of siderite, as long as oxygen is excluded (Garrels and Christ, 1965).

It is reasonable to assume the earliest depositional waters were fresh, carrying rock flour, fine detritus and little sulphate. Low temperatures could have inhibited bacterial activity, as would the release of acids during organic material degradation, resulting in a low pH. This would have prevented the reduction of sulphate to sulphide. Fe from sesquixides and soil hydroxides would be reduced in the acid environment, and combine with carbonate produced by organic degradation to precipitate siderite.

The analysis of spherulites revealed three groups:-

(i) low-Mg calcite,
(ii) siderites (with varying Mg and Ca contents); and
(iii) one dolomite sample.

The siderite group represents the expected carbonate precipitated during vitrinite formation, under conditions of stagnation, low ionic strength and acidic pH. Fe is in the reduced state and mobile, and easily combines with carbonate from organic material degradation

resulting in siderite precipitation, while oxygen is excluded (Curtis and Coleman, 1986; Renton, 1982; Matsumoto and Iijima, 1981).

The intimate association of siderite with vermicular kaolinite, as observed in sample D3, has been noted by various authors (Matsumoto and Iijima, 1981; Renton, 1982) and may be explained when the source of Fe into the swamp is considered. Fe oxides and hydroxides form in the surrounding soils and these and kaolinitic clays would be brought into swamps as colloidal particles. Carroll (1958) suggested that Fe entered the swamp as soil hydroxides coating kaolin micelles. These conditions, favouring siderite formation and kaolinite survival, would also explain the common occurrence of kaolinite and apatite in the vitrinite layers. Anaerobic organic degradation releases ammonia and supplies phosphate for the formation of apatite (Nathan and Sass, 1981). Not all kaolinite is necessarily detrital, as that within cell lumens must have formed from the amorphous Si and Al contained within plant cellular structure (Renton, 1982). See Plate 3b.

Analyses of the carbonate spherulites showed most to belong to group (i), low-Mg Ca carbonates, and associated vitrinite was often riddled with pyrite, and in some cases chalcopyrite and TiO_2. As in the case of cell infill, these carbonates and the accompanying mineral suite are indicative of an alkaline, possibly marine influence duringthe formation of the spherulites (Curtis and Coleman, 1986, and Matsumoto and Iijima, 1981). The single dolomite may represent an isolated and/or local occurrence where sulphate levels were lowered sufficiently to allow the precipitation of Mg-calcite (Matsumoto and Iijima, 1981).

The areal distribution of the groups shows the siderite occurrences

to be very localised, and relatively close to basement highs (palaeohighs). Here the runoff of fresh water (meteoric and glacial melt) might be expected to be higher, carrying Fe-rich soil and detritus into the peat. The rest of the swamp was isolated from these effects and may have retained an overall, more alkaline character. Proximity to channels would probably find expression in similar Fe-rich carbonate mineralogy.

4.2.3 Massive carbonates

The internal textures of some of these bodies suggest that they were initially aggregates of small, massed spherulites which underwent modification during later burial with exposure to higher temperatures and possible remobilization of ions.

4.2.3.a High-Ca carbonates

While these bodies now show the most massive textures (textural groups i and ii), it is possible that initial precipitation began as small spherulites. The earliest conditions of formation would besimilar to those described for Fe-poor spherulites in the previous section. Group ib, with varying Mg content may represent further precipitation as sulphate levels became progressively decreased (Matsumoto and Iijima, 1981; Curtis and Coleman, 1986). The single location showing higher Fe content (group ic) could correspond to the calcites observed by Matsumoto and Iijima (1981) which precipitate from fresher water in their stages I and II, or simply to local variation in the supply of Ca^{2+}, Mg^{2+} and Fe^{2+} ions. The destruction of early spherulitic textures may have occurred with further burial and remobilisation.

Cleat-shaped contraction cracks filled with relatively organic-free carbonate of identical composition to the main bodies are common, as are elongate growths of large sparry calcite parallel to coal bedding. This attests to continued growth under pressure (Irwin, 1980), while the pore fluid composition remained fairly constant.

The mode of formation of such agglomerations of Ca-rich carbonates is difficult to envisage. The supply of Ca to the peat swamp is problematic. Matsumoto and Iijima (1981) noted that Ca- and Mg-rich bodies occurred preferentially in fossil-rich beds, and pointed out that Mg and Ca concentrations in sea water are too low to precipitate significant carbonate. Ions must be supplied by "primary" marine carbonates, i.e., carbonates of biogenic origin. Carbonate precipitation can usually be demonstrated to have begun around decaying soft body parts (Matsumoto and Iijima, 1981). Berner (1971) has described alkaline decay at such sites and the early precipitation of the Ca cation as metallic soaps, regarded as a carbonate precursor. The biogenic source of Ca is also considered as the most likely by others (Curtis and Coleman, 1986). Renton (1982), however, described calcitic bodies as fairly common in freshwater coal, citing dissolution of freshwater mollusc shells as a suitable supply of the Ca ions required to form such bodies. Although the massive carbonates in the no.2 seam occur preferentially at particular stratigraphic levels, no fossil remains have been found associated with them, and none of these bodies shows any obvious fossil or other nuclei.

A number of the high-Ca carbonates have been shown by XRD analysis to be aragonite. Careful examination of Plate 23 reveals an ovoid, spherultic shape within the massive aragonite of sample 9. Suess and

Futterer (1972) demonstrated that aragonite precipitates at 25 °C from sea water within a period of a few hours, in the presence of humic acid and carbonate. Their experiment involved agitation and was aimed at the study of oolite formation. However, semi-spherical, ovoid bodies were found to form on the bottom of non-agitated beakers. The necessary conditions of humic acid and carbonate supply would be met easily in a peat swamp during early coal formation, and a similar mode of formation to that from seawater is suggested for these bodies, i.e., the aragonite is primary and has precipitated in parts of the swamp where marine influence was strong. However, aragonite is generally regarded as the high temperature form of $CaCO_3$ (Deer, Howie and Zussman, 1966). At surface temperatures and pressures low-Mg calcite or dolomite are the stable carbonate phases that could be expected to precipitate from solutions supersaturated with the Mg^{2+} ion (Bathurst 1981). However, carbonate precipitation under laboratory conditions from artificial preparations of "seawater" (i.e., solutions with $Mg^{2+}/Ca^{2+} = 5$) has always produced aragonite (Bathurst, 1981; Morse, 1983 and Berner, 1975). This phenomenon is attributed to the interfering effect of the Mg^{2+} cation on the growth of calcite. Berner (1975) has shown that the Mg^{2+} cation adsorbs itself onto the calcite crystal structure, which he described as crystal "poisoning". This adsorption prevents the growth of calcite beyond a subcritical size whereas the Mg^{2+} ion is not adsorbed on aragonite and has no retarding effect on its growth. Bathurst (1981) has suggested that the difference between the Gibbs free energy involved in the dehydration of the Mg^{2+} ion to allow the precipitation of low-Mg calcite from seawater and that involved in the precipitation of aragonite from seawater favours the latter. The Sr contents of the aragonites are lower than those in the artificially precipitated

aragonites of Suess and Futterer (1972) and may indicate mixing and dilution of sea water or a lower temperature control of Sr fractionation or a lack of available Sr in solution.

The Sr-rich "exsolution lamellae" described in sample 35 (Plate 19) may have formed during the reversion of such an aragonite body to calcite. The large Sr ion does not fit easily into the calcite structure and may have been concentrated in these lamellae during calcite formation.

$d^{13}C$ and $d^{18}O$ values are available for a number of massive carbonate bodies. The $d^{13}C$ values for massive carbonates are all negative with respect to PDB. They are commensurate with carbonate supplied for the formation of these bodies during organic degradation (Falcon and Verhagen, 1990; Curtis and Coleman, 1986; Pye et al., 1990) by the activity of either aerobic or sulphate-reducing bacteria, and perhaps a later continued supply from thermal decarboxylation. The heavy values, suggested as indicative of evaporative deposits by Falcon and Verhagen (1990) occur in carbonates other than the massive bodies.

The $d^{18}O$ values, however, may suggest a fresh water influence. Falcon and Verhagen (1990) state that they indicate "isotopically light, low alkalinity diagenetic fluids ... the most probable source being glacial meltwater." $d^{18}O$ values for snow and ice may be extremely negative with respect to PDB (Hudson, 1978). Thus the effects of glacial meltwaters could account for the low $d^{18}O$ values of these carbonates. However, the values are more negative than those for fresh water carbonates given by Curtis and Coleman (1986) and occur at the most negative end of the range given by Hudson (1977).

They are similar to those found by Gould and Smith (1979) for Australian Permian coal carbonates. The extremely low values in this case are thought to represent the effects of high temperature groundwater at depth. This decreasing trend of $d^{18}O$ with increasing burial temperature has also been noted by Hoefs (1987). Thus the $d^{18}O$ values of the carbonates from the present study have probably resulted from the combined effects of glacial meltwater and higher temperature groundwaters with burial. Hoefs (1987) has also noted that there is a strong argument for lower oceanic $d^{18}O$ values with increasing geological age and this factor may also have had some influence.

4.2.3.b Siderites

All the massive siderites display clear textural evidence of initial formation as separate, small spherulites forming large agglomerations. Their early conditions of formation are thus considered to be identical to those of the single siderite spherulites discussed in the previous section. The megascopic "concretions" are thought to be the result of the concentrated, heterogenous distribution of detrital Fe brought into the swamp. This contrasts with the more even distribution of these nuclei throughout the peat which resulted in individual spherulite formation, as suggested by Matsumoto and Iijima (1981). The major difference between the massive aggregates and the individual spherulites is the chemical zonation and rimming observed in spherulites making up the massive aggregates. While the smaller, individual spherulites generally ceased to grow before pore waters

changed in composition (only one sample shows zonation), the supply of Fe to the larger aggregates continued as conditions favouring siderite precipitation changed to those favouring Fe-poor carbonate and pyrite precipitation.

Siderites rimmed with pyrite have been previously described by Smyth (1965) in Australian coals. She successfully grew pyrite rims on siderites by bubbling hydrogen sulphide over siderite in distilled water of moderate temperature. This led to the conclusion that pyrite was epigenetic. Garrels and Christ (1965), have shown that to eliminate the field of pyrrhotite (in terms of pH and eH) in a system containing Fe, S and CO_2, the concentration of carbonate must be very high relative to that of sulphur. The siderite stability field then ranges across very strong to moderately strong reducing conditions (see Figure 24). If pH changed sufficiently for bacterial activity to begin sulphate reduction, and the supply of sulphate, carbonate and Fe continued, it is to be expected that precipitation would change from siderite to Fe-poor carbonates and pyrite. The formation of Fe-poor carbonates and pyrite some distance into the siderite is similar to the formation of pyrite in previously precipitated siderite observed by Smyth in her experiments. It is not unlikely that dissolution of siderite occurred to some extent with later precipitation of Fe-poor carbonates and pyrite.

Thus, these pyrite- and Fe-poor carbonate-rimmed siderites reflect changes in the composition of pore water. Early stages of formation took place in an acid, sulphide-free environment which abruptly changed to an alkaline, sulphide-rich environment. A marine

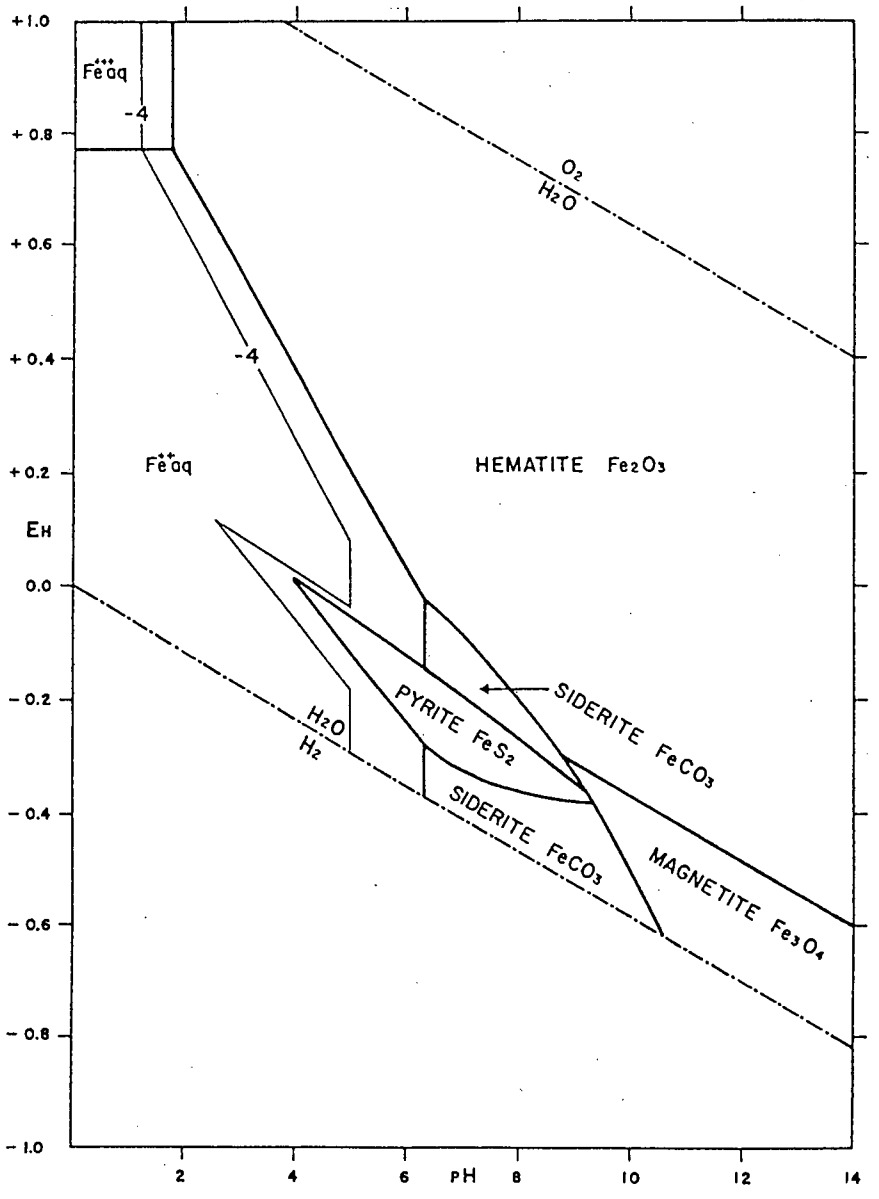

Figure 24: Stability relations of Fe-oxides, sulphides and carbonate in water at 25°C and 1 atmosphere pressure. Total dissolved sulphur = 10^{-6}. Total dissolved carbonate = 10^{0}. From figure 7.21, Garrels and Christ (1965).

transgression would result in just such a change, as described by Curtis and Coleman (1986). Alkaline, high ionic strength depositional water charged with sulphate, Ca and Mg ions would then directly overlie the coal and these ions could migrate down into zones of weak ionic strength. Sulphate reduction would begin immediately (plentiful supply of non-degraded organic material) and pyrite precipitation would result as long as the Fe supply held out.

4.2.3.c Dolomite

These massive carbonates probably represent the result of a marine transgression where the Fe supply had been depleted. One of the two dolomitic samples contained small spherulites with sideritic cores and dolomitic rims, lending support to this hypothesis. Tiny euhedral pyrite crystals within the dolomite attest to the availability of sulphide but low Fe concentrations. The sulphate levels must have been sufficiently low to allow the precipitation of dolomite rather than calcite from depositional water with a strong marine influence (Curtis and Coleman, 1986; Matsumoto and Iijima, 1981).

4.2.4 Cleat mineralisation

The time of cleat formation in coal diagenesis is unresolved. Renton (1982) considers it to be late syngenetic and to continue into the epigenetic phase. Price (1966) argued that cleat formation is due to

stress differentials during uplift. The decrease in lateral stress would proceed at a different rate to the reduction in gravitational loading, resulting in the formation of lateral extension fractures. Ting (1977) attributes cleat formation to the volume change associated with the change from peat to high rank coal. At low ranks, this would mainly be accommodated by compaction, while at higher ranks volumetric changes occur in the horizontal direction. This implies cleat formation as a late stage event at depth.

The association of cleats with vitrinite observed in this study is common and is attributed to vitrinite being the weakest microlithotype (Stach et al., 1982). Spears and Caswell (1986) consider mineralisation in small cleats to be earlier than that in cleats cutting across several coal types because vitrinite would form cleats first.

Carbonate cleat mineralisation in this study falls into four groups:-

i) high-Ca calcites with low Mg and/or Fe content;

ii) high-Ca calcites with variations in Mg content;

iii) dolomites;

iv) ankerites.

Other minerals commonly observed in cleats include pyrite, kaolinite and euhedral apatites within the calcites. This assemblage is fairly typical and is described from many coals by various authors, including Spears and Caswell (1986).

The ankerite and calcites (groups (i) and (ii)) are the anticipated later stage carbonates as described by Matsumoto and Iijima (1981) and correspond respectively to the later part of their stage II and their stage III observed in freshwater coal.

However, no mention is made of dolomite occurring in these stages. Renton (1982) states that calcite is the most common cleat-filling carbonate but that dolomite is not uncommon, but he does not elaborate.

Dolomite is a fairly common cleat-filling mineral in the samples of this study, often following an original calcite precipitation or vice versa. By the stage of cleat mineralisation, it is possible that sulphate diffusion from above (marine transgression - sulphate rich water) may be used up sufficiently no longer to inhibit dolomite precipitation from marine-influenced pore water. This may explain the initial stage of calcite mineralisation (sulphate levels still too high)commonly preceding dolomite. With further diagenesis Spears and Caswell (1986) suggest that some mobile reduced sulphur may be liberated from the organic material, raising concentrations sufficiently to allow pyrite precipitation. Fe^{2+} could still be circulating in pore waters from detrital sources or may be liberated during diagenetic alteration of primary silicates. The precipitation of pyrite locally would aid in lowering sulphate levels and so encourage dolomite precipitation.

If pH levels remained relatively low, the diagenesis of detrital clays and degraded illite would release mobile Al, which together with Si would precipitate as kaolinite in cleats (Spears and Caswell, 1986). Another possible source for Al and Si is the amorphous material within the organic matter itself, although Renton (1982) is of the opinion that these ions are released at an early stage.

In a study of carbonates in Permian Australian coals, Gould and Smith (1979) found cleat-filling calcites to represent a late stage mineralisation event. $d^{13}C$ values were up to +25‰ relative to PDB. This was explained as the carbonate having precipitated from heavy CO_2 enriched during isotopic exchange with CH_4 from methanogenesis in the coal. As the heavy CO_2 escaped along joints and cleats, reaction occurred with metallic ions in pore waters and "heavy" calcite precipitated.

The $d^{13}C$ values in the cleat-rich coal above the massive carbonate in sample 6 were also positive. Falcon and Verhagen (1990) explain this as possibly due to enrichment by evaporation or the effect of oxidised organic carbon enriched through bacterial methane loss. However, no diagnostic evaporitic minerals were observed in association with these carbonates. It is suggested that the $d^{13}C$ enrichment observed is at least partially due to the mechanism as described by Gould and Smith (1979).

4.2.5 Fracture-filling carbonates

The final stage of all Matsumoto and Iijima's (1981) carbonate progressions is vein calcite. This calcite is deposited in fractures once the coal has undergone uplift and groundwaters can freely percolate through the fractured coal (Matsumoto and Iijima, 1981). The vein calcites identified in this study are thought to have formed at this stage. The mineralisation often shows more than one phase, which is not surprising considering the length of time after uplift. The tiny apatite crystals included within the calcite are possibly indicative of a lowered pH during precipitation (Nathan and Sass, 1981).

A number of fractures were found to contain dolomite. Most fractures form along natural weaknesses within the coal and frequently follow cleats in which other minerals have previously precipitated. The dolomite analysed from some fractures is thought to be that deposited during the stage of cleat mineralisation. Some percentage of fractures must have formed at depth as solutions suitable for pyrite precipitation used these as access routes to massive carbonates where replacement by later pyrite is common.

4.2.6 Capping sandstone cement

The carbonate occurring in the capping sandstones is a fairly late stage cement, partly replacing feldspathic grains. Ankerite is commonly described as a late diagenetic stage cement in lithic sandstones (Larson and Chilingar, 1983). Mg^{2+} and Fe^{2+} cations

are strongly hydrated at surface temperatures or do not occur in sufficient concentrations to precipitate ankerite. With increasing temperatures, they become increasingly less hydrated and late diagenetic carbonates in sandstones are most commonly Fe and Mg rich, and dolomite, ankerite or siderite may form. Fe and Mg cation concentrations may be limited and a possible source is the release from silicates such as biotite and chlorite as diagenesis proceeds (Parker and Sellwood, 1983).

4.3 Chemical evolution of the Witbank carbonates

4.3.1 Siderite chemistry

Both Matsumoto and Iijima (1981) and Curtis and Coleman (1986) noted trends involving Mg/Fe and Mn/Fe ratios within siderites precipitated in coal.

Matsumoto and Iijima (1981) noted that siderites in kaolinite clay within the coal measures (freshest water environment) have characteristically low Ca and Mg contents, while in brackish-marine sediments combined Ca and Mg contents range from 28 to 48 mol %. The siderites in Japanese coal were found to occupy a field intermediate to these and to overlap both. The Japanese siderites also showed increases in combined Ca and Mg contents from the centre to margins of composite bands. Figure 25 shows a comparison of the Japanese siderites with those from this study. The Witbank siderites all show fairly high Mg/(Ca + Mg) ratios, defining a parallel but higher trend

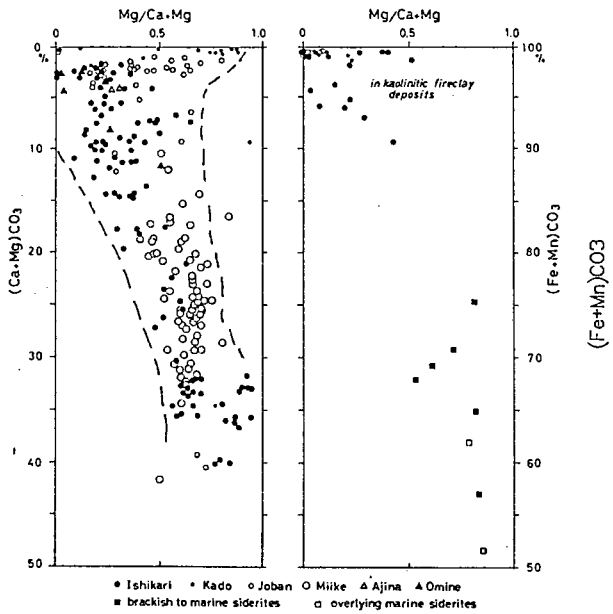

(Ca+Mg)CO_3 versus Mg/(Ca+Mg) variation diagrams of siderite in various facies. The diagram on the left shows freshwater siderite, excluding siderite in kaolinitic fireclay deposits which are plotted on the diagram on the right with brackish-marine siderite.

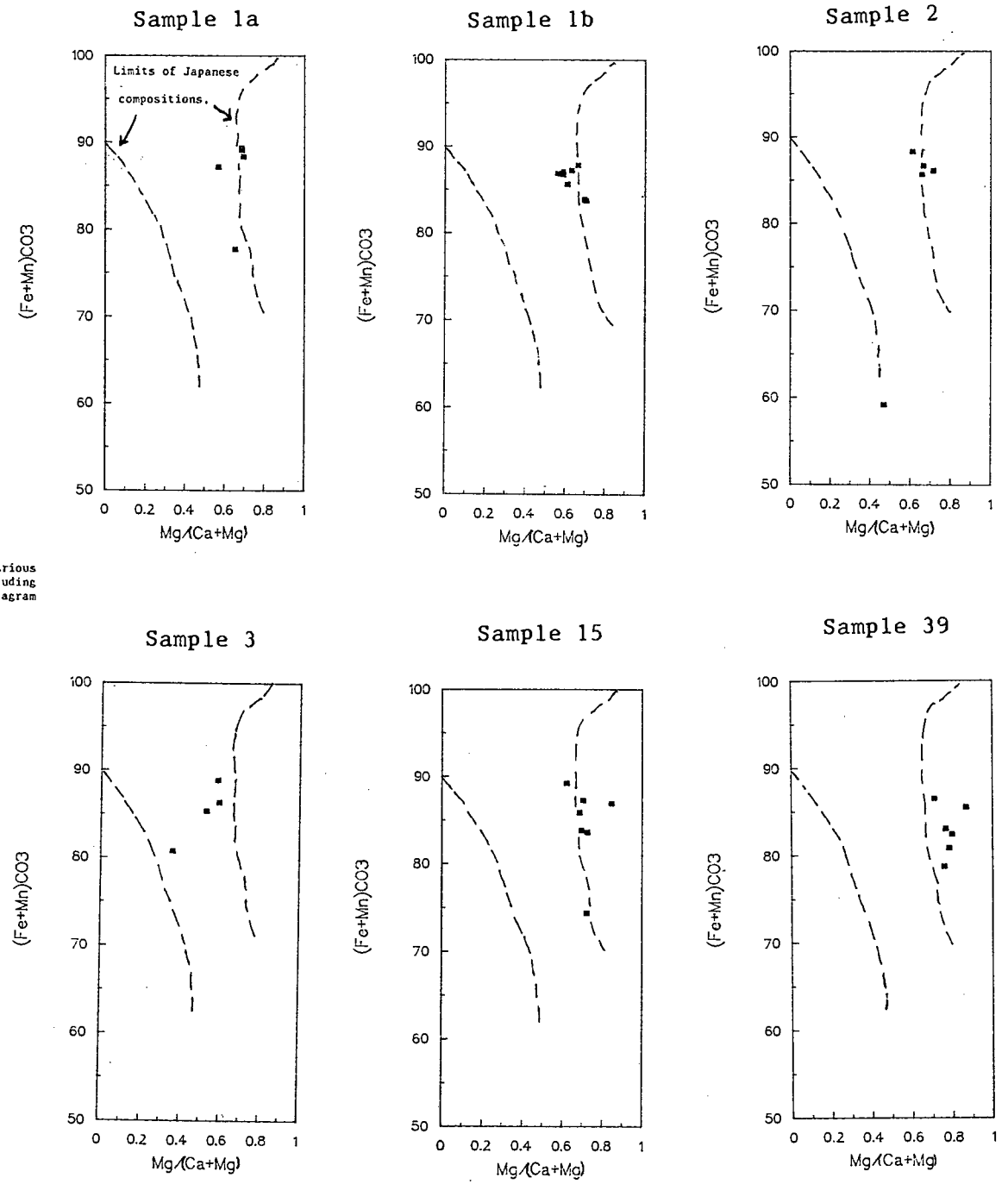

Figure 25: Comparison of Japanese siderites with Witbank no.2 seam siderites.

than the Japanese siderites, which suggests greater availability of the Mg ion in the Witbank coals, i.e. a greater brackish influence.

Figure 26 shows variation diagrams of Mg/Fe against Mn/Fe for early sideritic spherulites from samples 2 and 39, as well as for all siderites analysed. A weak, but discernable trend (low-Mg, high-Mn centres and high-Mg, low-Mn edges) is shown for the spherulites. This same trend can be seen between the early spherulites and the later formed massive carbonates.

The trend of increasing Mg content in siderites with depth was interpreted by Matsumoto and Iijima (1981) to represent mixing of fresh and marine pore waters with depth. However, Curtis and Coleman (1986) disagree, and although they concede that this mixing may have some role to play, they consider detrital source controls more important. They explain the increase in Mg content as follows. As detrital Fe becomes depleted during burial and continuing siderite precipitation, less reactive sources of cations would increase in importance. Mg present in interlayer hydroxide sheets would be the most likely source.

In the case of the Witbank siderites, supply of Fe remained high throughout siderite precipitation (pyrite rims occur on most of the massive siderite bodies) so that the explanation of Matsumoto and Iijima (1981), i.e. increasing marine influence, seems most applicable in this case.

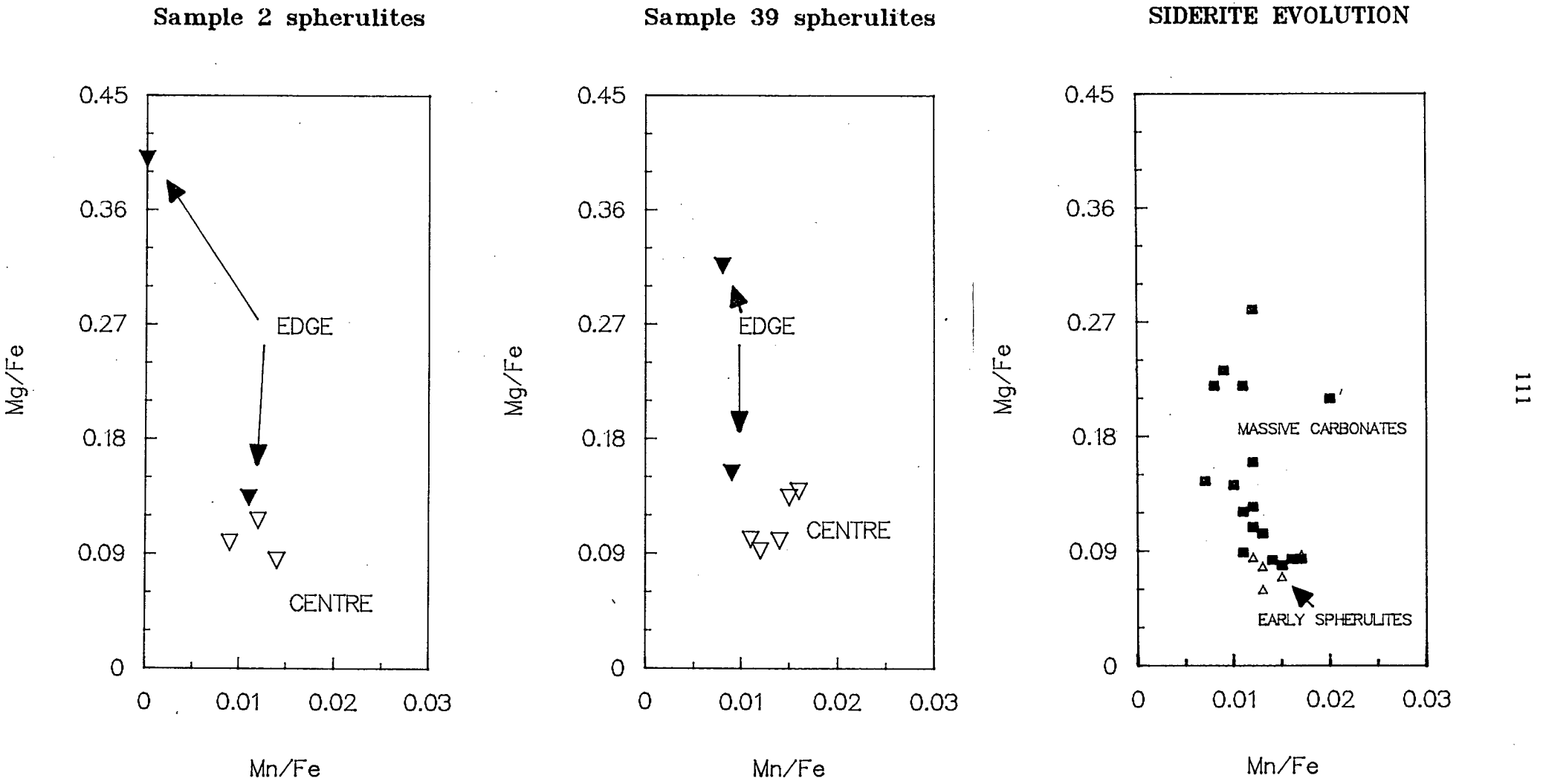

Figure 26: Mg/Fe - Mn/Fe variation diagrams for 2 early spherulites and all siderites analysed.

The decrease of Mn/Fe ratio with continuing precipitation was also observed by Curtis and Coleman (1986). The earliest precipitated siderite had high Mn contents, while later-formed siderite showed lower, more constant Mn/Fe ratios. This can be explained if the differential redox behaviour and mobility of these two metals is considered. Mn^{4+} oxides concentrate at the redoxcline and Mn^{2+} concentrations are enhanced below it. The continuation of this trend observed in the Witbank massive siderites lends support to the hypothesis that massive siderites formed as aggregates of early spherulites, but with siderite precipitation continuing to a later stage in coal diagenesis.

4.3.2 Calcite chemistry

The calcites described by Matsumoto and Iijima (1981) were grouped into Mg, Fe-Mg and Fe varieties, according to the ratio of Mg/(Mg+Fe+Mn). This was related to diagenetic stage as well as sedimentary facies. As a whole, the ratio decreased with increasing depth of burial and precipitation (Figure 27a). Mg calcite is characteristic of stage I (brackish and marine) corresponding to shallow burial where the Mg^{2+}/Ca^{2+} ratio is high in interstitial water of marine terriginous sediments (Sayles et al., 1972 and Manheim et al., 1974). Fe- and Fe-Mg calcites characterise stage II and precipitate from mixed pore waters. According to Curtis and Coleman (1986), compaction may drive fresh water upwards or brackish or marine water may move downwards into the sediment. Light $d^{18}O_{PDB}$ values of -17 to -13.5 in calcites from the Joban coals are attributed to the mixing of fresh and brackish

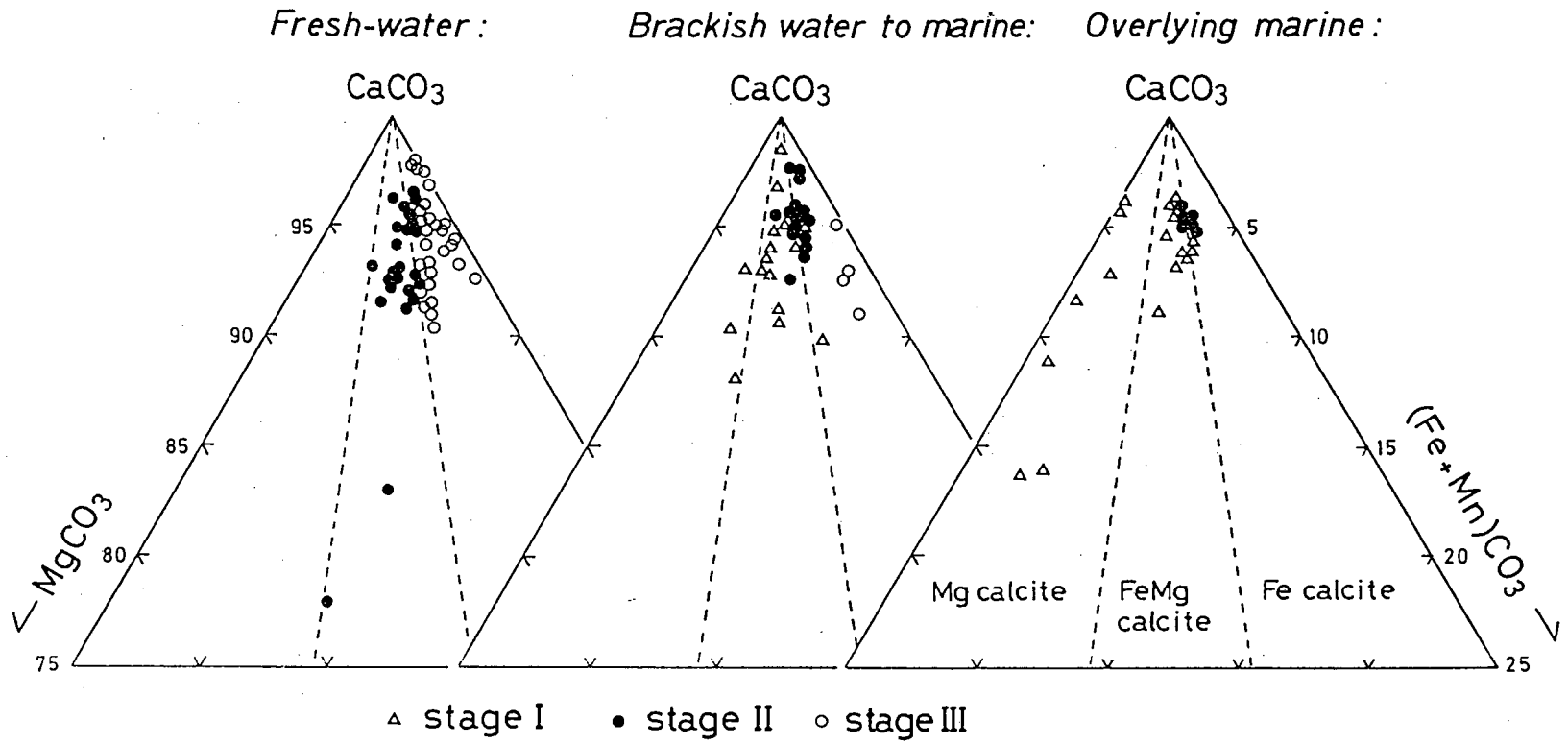

Figure 27a: Diagenetic stages and the chemical composition of Japanese calcites in various sedimentary facies. From figure 10, Matsumoto and Iijima (1981).

water. Stage III is characterised by Fe calcite. The Ca for these late calcites is thought to have been partly derived from the dissolution of Ca-bearing primary silicates.

Figure 27b is a plot of the Mg/(Mg+Fe+Mn) ratios of some calcites from this study. On the basis of the classification of Matsumoto and Iijima (1981), all the early Witbank spherulite calcites analysed in this study are Mg calcites with Mg/(Mg+Fe+Mn) ratios $\geq$ 0.6. These include samples 4, 5, 6a, 6b, 14a and 12.

The massive carbonates, although mostly Mg calcites, also comprise some Fe-Mg calcites (samples 12b and 43) and Fe calcites (samples 35 and 36).

The group (i) cleat-fills (high-Ca carbonates) show examples of all three of Matsumoto and Iijima's (1981) groups, although Fe-Mg and Fe calcites are represented (samples 4 and 5). Fracture-filling calcites also show examples of all three groups with Fe calcites being represented by samples 4 and 6a.

Thus, although the expected progression is not rigidly adhered to by the Witbank no.2 seam calcites, there is some evidence that the Japanese progression is valid for these coals, particularly in samples 4, 5 and 12b. It is noteworthy that the earliest spherulitic calcites only fall into the Mg-group while examples of the other groups occur in the later-formed massive, cleat and fracture calcites. This lends further support to the order of precipitation suggested for these various carbonates.

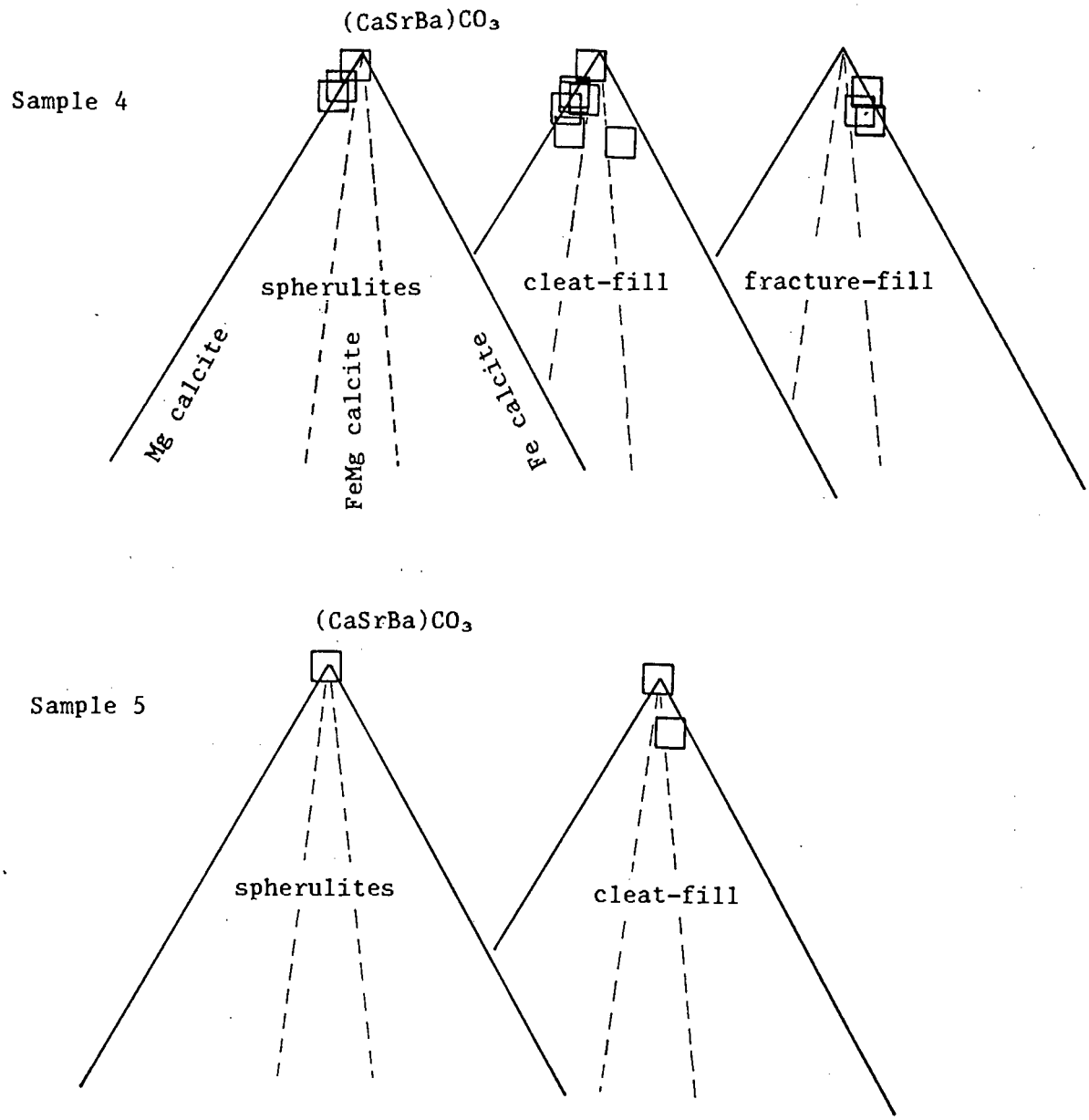

Figure 27b: Chemical evolution of some Witbank calcites.

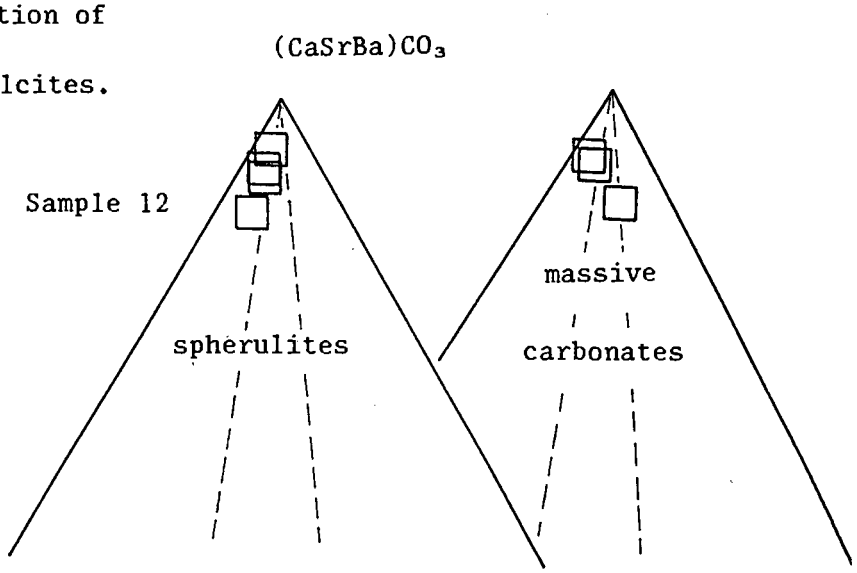

The high proportion of Mg calcites at all stages must be an expression of the continued supply of the Mg^{2+} cation throughout coalification. While Mg was depleted in the example of Matsumoto and Iijima (1981), and other sources of cations became more important, this was not usually the case for the Witbank calcites. This is possibly due to the Mg content being repeatedly supplemented by numerous transgressions or large amounts of brackish water being trapped in the original sediment or source rock.

4.3.3 Chemical evolution of carbonates

Matsumoto and Iijima (1981) described three sequences of authigenic carbonate precipitation in Japanese coals. While these are described in detail in the introduction, they are summarised here in Table 5 for convenience. Similar carbonate chemistries, controlled by early depositional waters and later obscured and complicated by marine transgressions, have been described by Curtis and Coleman (1986). Various shorter sequences within these progressions have been described (Smyth, 1965; Gould and Smith, 1979; Spears and Caswell, 1986; Pye et al., 1990).

While certain elements of these environment-specific progressions are clearly represented in the evolution of the Witbank no.2 seam carbonates, the overall evolutionary paths are generally more complicated. Figure 28 is a representation of the various paths observed.

Table 5. Sequence of precipitation of authigenic carbonates in Japanese Coalfields, from table 1, Matsumoto and Iijima (1981).

Freshwater sediments	Brackish water to marine sediments	Overlying marine deposits
Low Ca-Mg siderite	Mg calcite	Mg calcite
↓	↓	↓
High Ca-Mg siderite	dolomite	dolomite
↓	↓	↓
ankerite	Fe-Mg calcite	Fe-Mg calcite
↓	↓	↓
Fe dolomite	Fe dolomite	↓
↓	↓	↓
Fe magnesite	ankerite	↓
↓	↓	↓
Fe calcite	↓	↓
↓	Extremely high Ca-Mg siderite	Extremely high Ca-Mg siderite
↓	↓	↓
Vein calcite	Vein calcite	Vein calcite

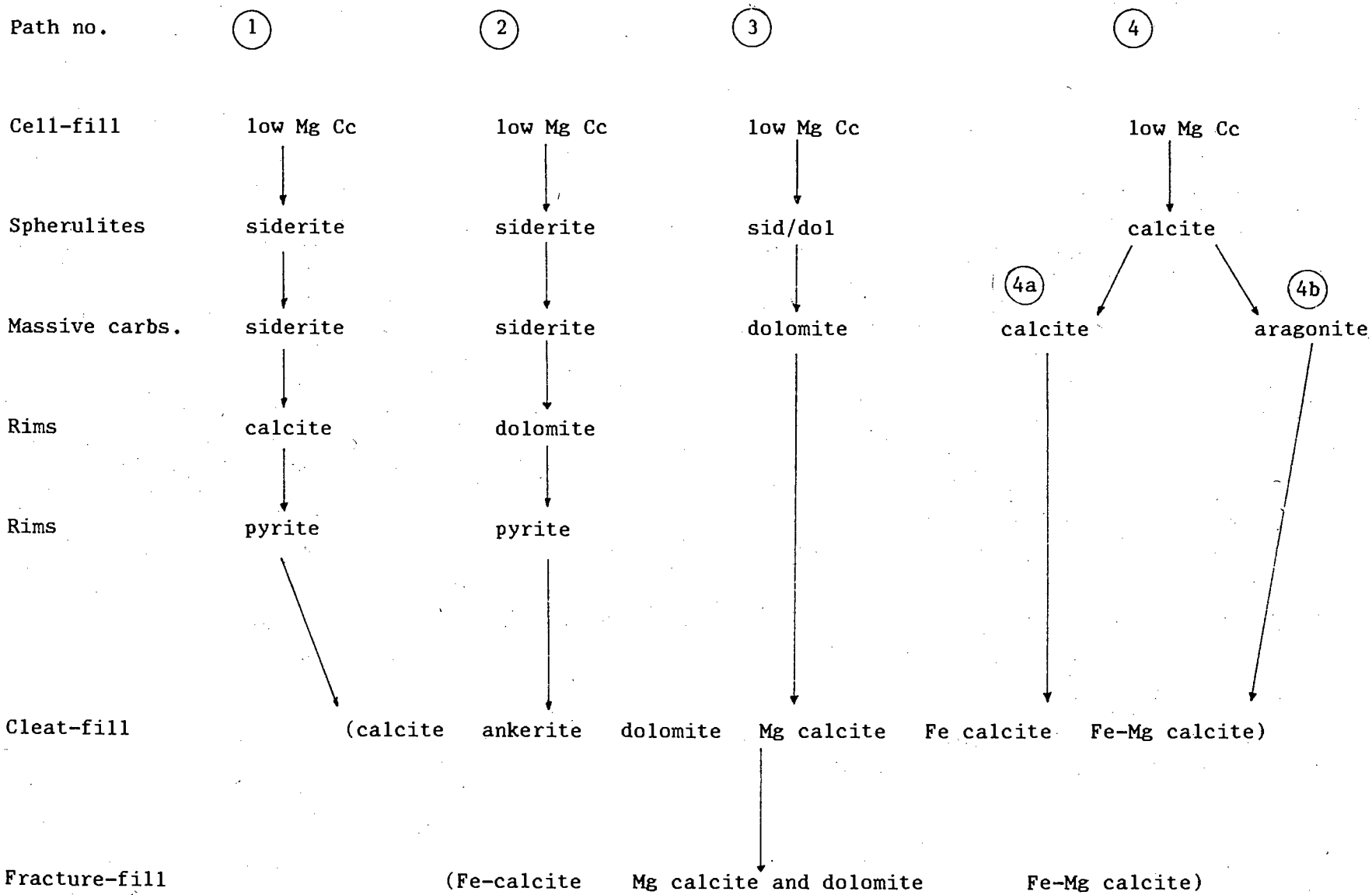

Figure 28: Carbonate evolution paths identified in the Witbank no.2 coal seam. (Cc-calcite, dol-dolomite, sid-siderite).

Low Mg calcite is the only carbonate precipitated at the very earliest stage.

The paths from low Mg calcite to low Ca-Mg siderite (1, 2 and 3) progressing to higher Ca-Mg siderite (Matsumoto and Iijima's (1981) fresh water progression) soon deviate towards the brackish to marine progression, with calcite (path 1) and dolomite (paths 2 and 3) precipitated together with pyrite.

At the cleat-fill and fracture-fill stages, the carbonates precipitated are similar to those precipitated at a similar stage in all three facies considered by Matsumoto and Iijima (1981). This indicates the mixing of pore waters at depth and diagenetic reorganisation of primary silicates.

The path (4) showing continuing calcite precipitation splits only to calcite (4a) or aragonite (4b), later showing the mixed carbonate assemblage of all progressions before returning to the final vein calcite common to all.

The initial calcite precipitation could represent alkaline conditions (marine?) or high O_2 levels, preventing early siderite formation, as discussed earlier.

The deviations from the freshwater progression as described by Matsumoto and Iijima (1981) are interpreted as the disruption of this environment by the influx of more alkaline, possibly marine water.

Sulphate levels, and therefore sulphide levels, must have risen, causing siderite precipitation to cease and Fe-poor carbonates and pyrite to precipitate (Berner, 1971; Garrels and Christ, 1965).

The paths exhibiting continual calcite precipitation in the early stages are similar to those identified by Matsumoto and Iijima (1981) in their progression for brackish to marine sediments.

Figures 29a to d are annotated diagrammatic summaries of the various evolutionary paths followed by the Witbank No. 2 seam carbonates. Comparison with carbonate evolution described in the literature suggests a strong influence of alkaline water with high sulphate levels in the early stages for most samples, or alternatively of oxic or suboxic conditions commensurate with Falcon's (1989) hypothesis of a seasonal variation in the water table. While a small number of samples may have initially experienced a reducing acidic environment, their later evolution points to a disruption of the initial pH conditions and relative ionic availabilities, possibly through marine influence.

This influence remained strong, until its signature was masked by the carbonate assemblage of deeper burial which was no longer affected by the composition of the initial depositional water.

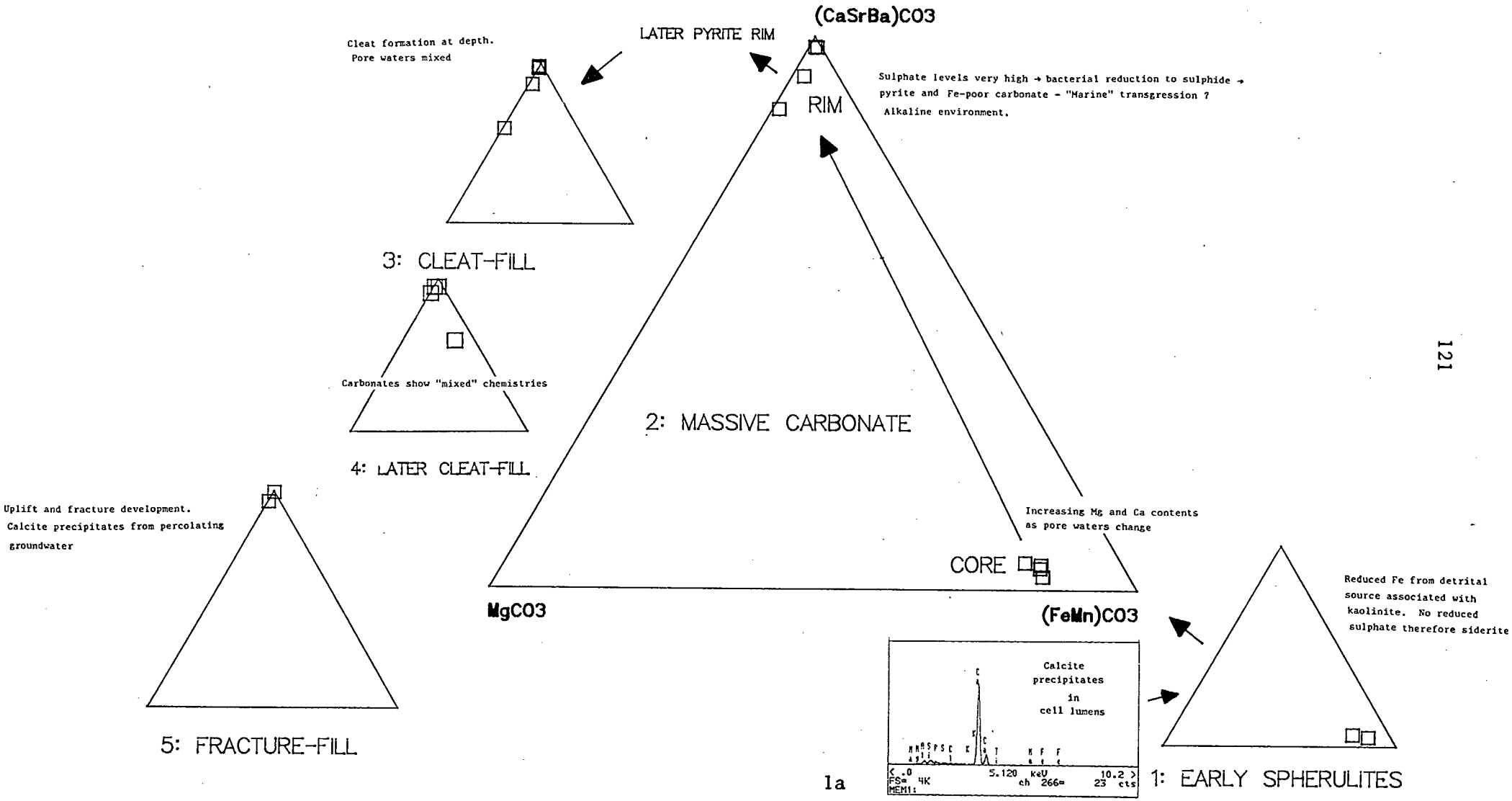

Figure 29a: Annotated diagrammatic summary of evolutionary path 1.e.g. Sample 15 All triangles full carbonate triangles

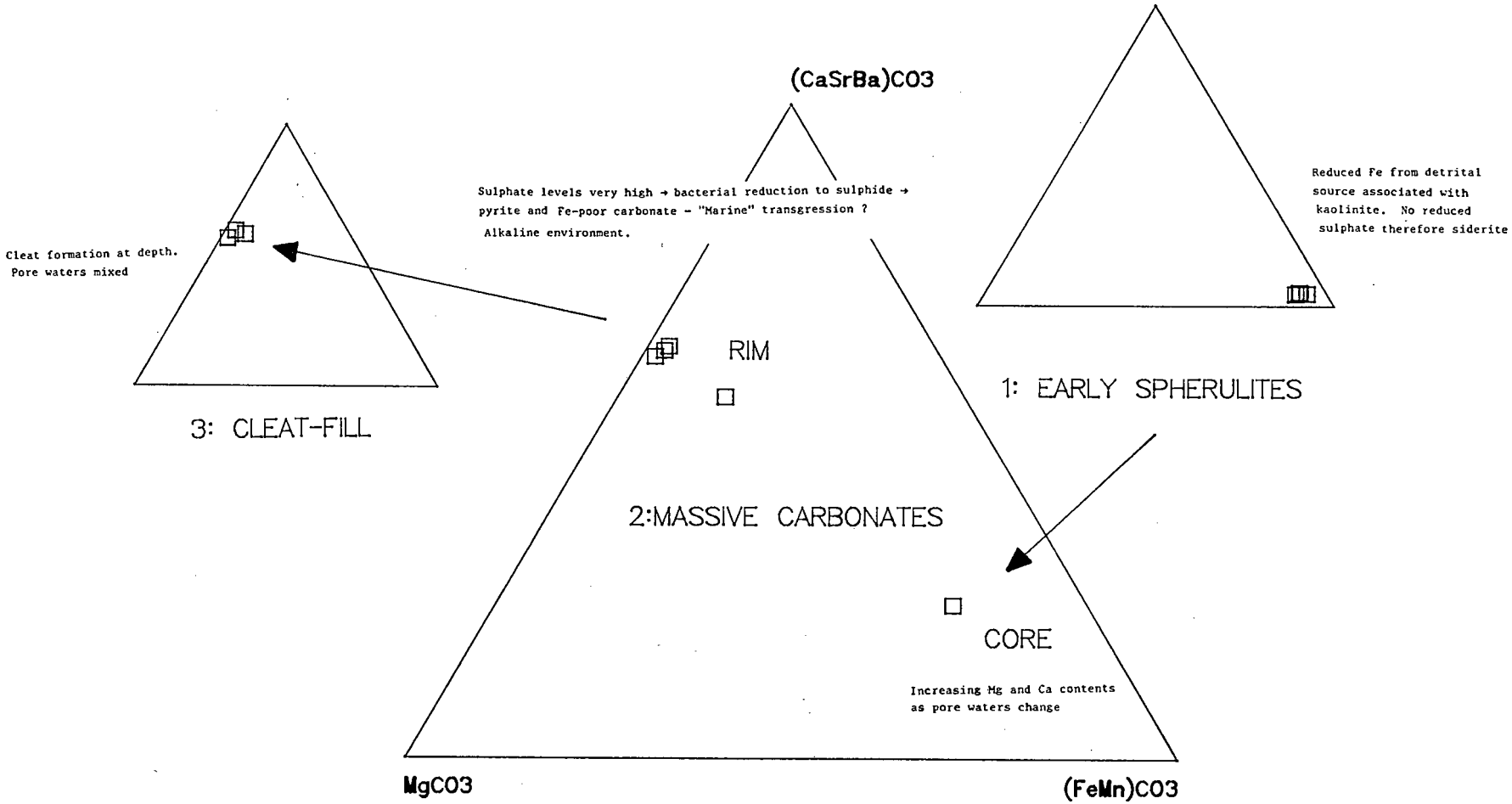

Figure 29b: Annotated diagrammatic summary of evolutionary path 2. e.g Sample 2 All triangles full carbonate triangles

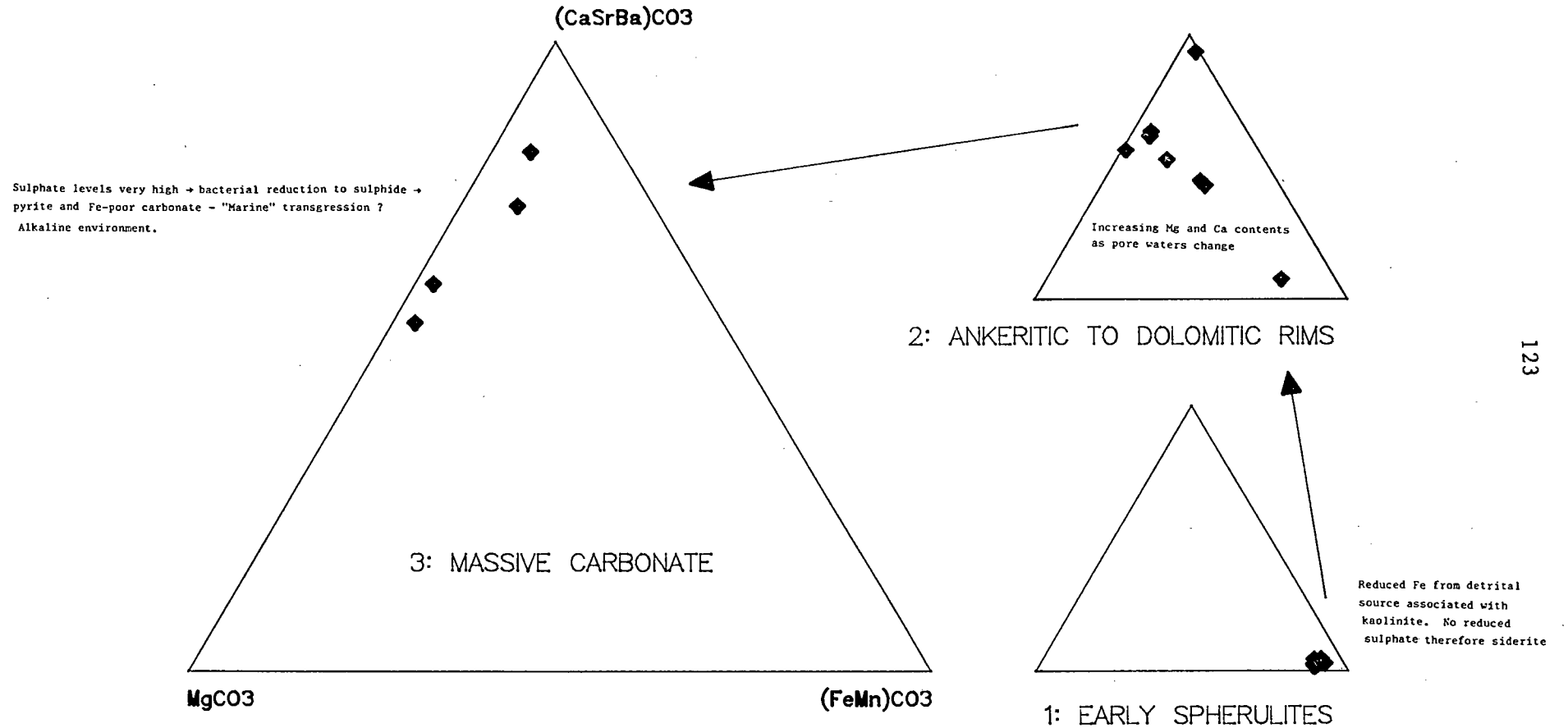

All triangles full carbonate triangles

Figure 29c: Annotated diagrammatic summary of evolutionary path 3. e.g. Sample 39

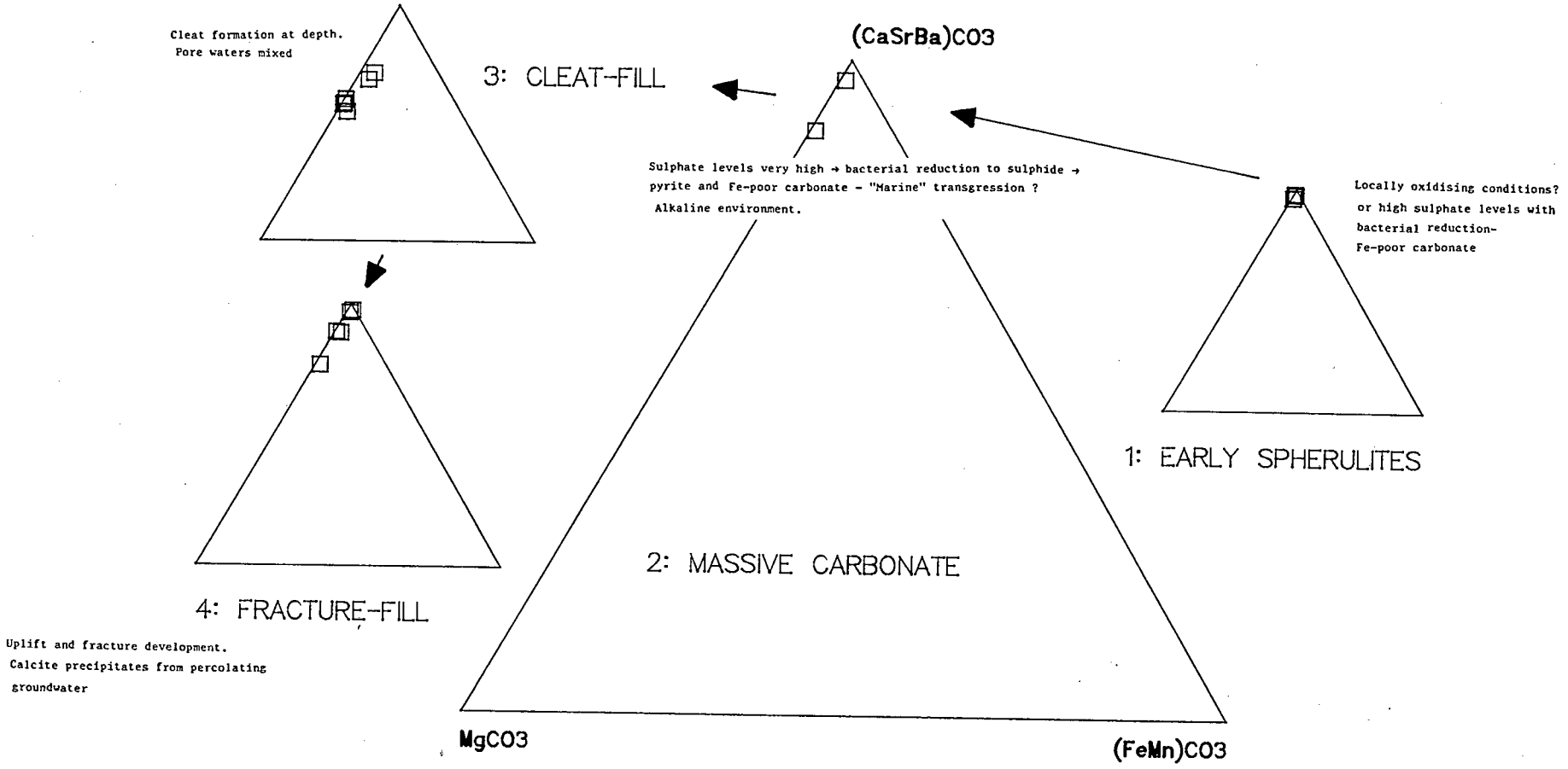

Figure 29d: Annotated diagrammatic summary of evolutionary path 4. e.g. Sample 14 All triangles full carbonate triangles

5 CONCLUSIONS AND RECOMMENDATIONS

5.1 Conclusions

a) Six different types of authigenic carbonate are associated with coals of the no.2 seam in the Witbank basin, with precipitation occurring in the following order: cell-fill, spherulites, massive carbonates, cleat-fill and fracture-fill. Ankerite occurs as a late stage cement in a capping sandstone above the coal seam.

b) The chemistry of the earliest cell-filling carbonates is indicative of an early brackish, alkaline environment with high sulphate levels, or, alternatively of locally oxidising conditions prevailing during their precipitation. The latter would have effectively prevented the reduction of Fe which would have remained in a mobile, oxidised state, thus escaping precipitation as siderite.

c) Spherulite chemistry is largely representative of the continuing alkaline, sulphate-rich nature of depositional waters. Calcite chemistries match those of the shallowest burial stages described for brackish and marine sediments by Matsumoto and Iijima (1981).

d) Those spherulites with sideritic compositions indicate the existence of locally acidic conditions, often close to palaeohighs which probably acted as a source of fresh run-off water. The rest of the basin probably retained an overall alkaline pH.

e) Fe-oxides were transported into the swamp in close association with kaolinite, as evidenced by the occurrence of vermicular kaolinite with siderite.

f) Siderites show higher Ca and Mg contents than those from Japanese coals, indicating more alkaline, possibly brackish initial conditions for the Witbank no.2 seam coals. The observed evolution of Mn/Fe ratios with depth confirms the relative stages of formation postulated for the spherulites and more massive carbonates, while the changes observed in Ca and Mg contents support later mixing of brackish and fresher water. A diminishing iron supply with depth is not a suitable explanation as pyrite precipitation is greatest at this stage.

g) One of the major findings of this study was the occurrence of aragonite. This mineral has not been described in previous studies of fossil-free carbonate bodies associated with coal. It is suggested that the aragonite precipitated from "near seawater" reacting with humic acids and bicarbonate. Although the precipitation of both these and the large calcite bodies may have begun at the sediment/water interface, textures and isotope data (available for calcite only) indicate continued growth at depth.

h) The overall chemical evolution of the carbonates in the no.2 seam of the Witbank basin is in accordance with that expected from brackish water or from oxidising conditions, or both. However, acidic, fresh water conditions prevailed in certain localities and low $d^{18}O$ values suggest that the influence of glacial meltwater was significant. Nevertheless, a strong brackish or marine imprint over even these early "freshwater" chemistries can be seen in later stages, while the effects of mixing, primary silicate dissolution and eventual uplift are evidenced by the carbonates of later stages. Thus, the evolution of authigenic carbonates in Witbank no.2 seam coals, in agreement with other studies and with depositional models in the literature, leads to the interpretation that the early swamp was only locally "fresh", and provides strong evidence for a "marine" influence at both early and late stages of deposition and diagenesis.

The low $d^{18}O$ values determined by Falcon and Verhagen (1991) provide some evidence against this interpretation. However, these values occur in association with values of $d^{13}C$ suggestive of a marine environment. Falcon and Verhagen suggest glacial meltwater as the most probable source of isotopically light (with respect to $d^{18}O$), low alkalinity diagenetic fluids affecting the swamp at an early stage. This is in accordance with the presence of localized fresh water conditions, as noted above.

(i) Mineralogical and chemical studies of carbonates in coal seams can reveal the effects of the depositional environment and later diagenetic history of the coal. An understanding of the palaeo-environmental

implications of these mineral chemistries should aid beneficiation of coal (Falcon and Verhagen, 1990).

Carbonates act as fluxing agents and those occurring as discrete minerals in commercial coal supplies can cause slagging problems in pulverised fuel boilers. Different carbonates have different hardnesses (Deer, Howie and Zussman, 1966) and fluxing abilities. Thus an understanding of their distribution within a coalfield can improve the efficiency of coal exploitation with respect to requirements regarding ash fushion temperatures and the Hardgrove grindability index (Ward, 1984).

5.2 Recommendations for further research

A number of problems remain unresolved, including the following:-

a) The source of Ca and Mg cations to the swamp in sufficient quantity to allow the formation of large carbonate bodies is problematic, as Matsumoto and Iijima (1981) have shown that concentrations of these elements in sea water are too low for substantial carbonate precipitation. No fossil remains or nuclei have been found in association with these bodies. However, a possible source for these ions is suggested by the evidence that the source of mineral detritus for the no.1 and early part of the no.2 seams was from rocks of predominantly basic composition (pers. comm. J.P. Willis, 1991).

b) There is no explanation for the carbonate bodies occurring preferentially at particular stratigraphic levels as there is no remaining evidence of any fossil-rich precursor layers (assuming a fossil source). The dissolution of bones could, however, also account for the high P_2O_5 content of these coals (pers. comm. J.P. Willis, 1991).

c) It is suggested that a strong marine influence has resulted in aragonite occurring as the major carbonate making up a massive carbonate body. Although Matsumoto and Iijima (1981) carried out XRD analyses on their samples, none of the Japanese carbonates was identified as aragonite. It is possible that the Witbank no.2 seam coals experienced a greater marine influence than did the Japanese coals, with relatively high strontium concentrations and crystal "poisoning" by Mg^{2+} ion encouraging the precipitation of aragonite. Quantitative XRD analyses should be performed to establish aragonite/calcite ratios.

Further work should be carried out on a detailed, regular grid to determine more accurately the effect of channels and other detritus and freshwater sources on the carbonate mineralogy.

The effects of initial depositional waters on other minerals, particularly clays such as illite and kaolinite, should be investigated. The occurrence of apatite and gorceixite, and their relationship to carbonates also merits further study.

Further research should be expanded to include comparisons between other seams in the Witbank coal field, and between seams from other basins in southern Africa. Other Gondwana coals, from Australia, India and South America, could also be included.

ACKNOWLEDGEMENTS

I am greatly indebted to Prof. J. P. Willis, my supervisor, for originally suggesting this study and for the interest he has shown in this work. He provided many useful suggestions and much encouragement and it was a privilege to study under him. I am also indebted to Dr. D. van Wyk of Rand Mines (Pty.) Ltd. for arranging the opportunity to collect samples from a number of mines and for his continued interest in this study. I am also indebted to Rand Mines (Pty.) Ltd. for permission to publish this work.

Dick Rickard and Gordon Bosch are thanked for help with microprobe work and XRD respectively and I am grateful to Jenny Marot for the assistance and tuition she provided while I was familiarizing myself with the techniques of SEM observation, EDS analyses and BSE photography. I am also indebted to SOEKOR (Pty) Ltd. for permission to use various analytical instruments.

I would also like to thank Brian Matjan and Gary Stevens for help with sample preparation and Dave Wilson for the expertly made polished thin sections

Lastly, I would like to thank my wife, Patricia, for the moral support she has provided.

REFERENCES

Altschuler, Z.S., Schnepfe, M.M., Silber, C.C. and Simon, F.O. (1983). Sulphur diagenesis in Everglades peat and origin of pyrites in coal. Science, 221, 4607, 221-227.

Bathurst, R.G.C. (1981). Early diagenesis of carbonate sediments. In: Parker, A and Sellwood, B.W. Eds. Sediment diagenesis. Reading, U.K., 427 pp.

Berner, R.A. (1971). Principles of Chemical Sedimentology. McGraw-Hill, New York.

Bouma, A.H.(1969). Methods for the study of sedimentary structures. Wiley and Sons, New York.

Brown, G., Ed. (1961). The X-ray identification and crystal structures of clay minerals. Mineralogical Society, London, 544pp.

Cairncross, B. and Cadle, A.B. (1988). Palaeoenvironmental control coal formation, distribution and quality in the Permian Vryheid Formation, East Witbank Coalfield, South Africa. Int. J. Coal Geol., 9, 343-370.

Cairncross, B. and Hart, R.J. (1988). Coal black but neutron clear. Nuclear Active 39, 8-12 July.

Cairncross, B. (1989). Palaeoenvironmental environments and tectono-sedimentary controls of the postglacial Permian coals, Karoo Basin, South Africa. Int. J. Coal Geol., 12, 365-380.

Carroll, D. (1958). Role of clay minerals in the transportation of Iron. Geochim. Cosmochim. Acta, 14, 1-27.

Curtis, C.D. and Coleman, M.L. (1986). Controls on the precipitation of early diagenetic calcite, dolomite and siderite concretions in complex depositional sequences. Roles of organic material in sediment diagenesis SEPM special publication 38.

Deer, W.A., Howie, R.A. and Zussman, J. (1966). An introduction to the rock-forming minerals. Longman, London. 528 pp.

Falcon, R.M.S., Pinheiro, H.J. and Shephard, P. (1984). The palynobiostratigraphy of the major coal seams in the Witbank basin with lithostratographic, chronostratigraphic and palaeoclimatic implications. Geol. Soc. S. Afr., Quarterly News Bulletin 28, 1, 36-38.

Falcon, R.M.S. and Snyman, C.P. (1986). An introduction to coal petrography: atlas of petrographic constituents in the bituminous coals of southern Africa. Geol. Soc. S. Afr. Review Paper 2.

Falcon, R.M.S. (1987). The origin and formation of southern African coals with comments on their classification. Unpubl. Report.

Falcon, R.M.S. (1989). Macro- and micro-factors affecting coal-seam quality and distribution in southern Africa with particular reference to the no.2 seam, Witbank coalfield, South Africa. Int. J. Coal Geo. 12, 681-731.

Falcon, R.M.S. and Verhagen, B.Th. (1990). Isotopes of carbon and oxygen in the carbonate impurities of coal have potential as palaeoenvironmental indicators. Abstracts Geocongress '90, Geol. Soc. S. Afr., Cape Town, July 1990.

Garrels, R.M. and Christ, C.L. (1965). Solutions, Minerals and Equilibra. Cooper and Freeman, San Francisco.

Goff, J.C. (1983). Hydrocarbons generation and migration from Jurassic Source rocks in East Shetland basin and Viking graben of the northern North Sea. J. Geol. Soc. London, 140, 445-474.

Gould, K.W. and Smith, J.W. (1979). The genesis and isotopic composition of carbonates associated with some Permian Australian coals. Chem. Geol., 24, 137-150.

Hagelskamp, H.H.B., Eriksson, P.G.and Snyman, C.P. (1988). The effect of depositional environment on coal distribution and quality in a portion of the Highveld coalfield, South Africa. Int. J. Coal Geol. 10, 51-77.

Henoc J., Heinrich K.F. and Myklebust R.L. (1973). A rigorous correction procedure for quantitave electron probe analysis microanalysis (COR2) U.S. Bureau of Standards Technical Note, 769. U.S. Govt. Printing Office, Washington D.C.

Hobday, D.K. (1987). Gondwana coal basins of Australia and South Africa: tectonic setting, depositional systems and resources. Coal and coal bearing strata: recent advances, Scott (ed)., (1987) Geol. Soc. South Africa Spec. Pub. 32, 219-233.

Hoefs, J. (1987). Stable isotope geochemistry. Springer Verlag, Berlin, 241 pp.

Holland, M.J., Cadle, A.B., Pinheiro, R. and Falcon, R.M.S. (1989). Depositional environments and coal petrography of the Permian Karoo sequence: Witbank coalfield, South Africa. Int. J. Coal Geol. 11, 143-169.

Hood, A., Gutjahr, C.C.M. ahd Heacock, R.L. (1975). Organic metamorphism and the generation of petroleum. AAPG Bull. 59, 986-996.

Hudson, J.D. (1977). Stable isotopes and limestone lithification. J.Geol.Soc.Lond. 133, 637-660.

Hudson, J.D. (1978). Concretions, isotopes, and diagenetic history of the Oxford Clay (Jurassic) of central England. Sedimentology 25, 339-369.

Irwin, H. (1980). Early diagenetic carbonate precipitation and pore fluid migration in the Kimmeridge clay of Dorset, England. Sedimentology 27, 577-591.

Issler, D.R. (1984). Calculation of organic maturation levels for offshore eastern Canada - implications for general application of Lopatin's method. Can. J. Earth Sci. 21, 477-488.

Keller, W.D. (1958). Glauconitic mica in the Morrison Formation in Colorado. Clays Clay Miner. 5 Nat. Conf., 120-128.

Larson, G. and Chilingar, G.V. (eds) (1983). Developments in sedimentology 25B: diagenesis in sediments and sedimentary rocks, 2. Elsevier, New York.

Le Blanc Smith, G. and Eriksson, K.A. (1979). A fluvioglacial and glaciolacustrine deltaic depositional model for Permo-Carboniferous coals of the Northern Karoo basin, South Africa. Palaeogeography, Palaeoclimatology, Palaeoecology, 27, 67-84.

Le Blanc Smith, G. (1980). Genetic stratigraphy for the Witbank coalfield. Trans. geol. Soc. S. Afr. 83, 313-326.

Manheim, F.T., Waterman, L.S. and Sayles, F.L. (1974). Interstitial water studies on small core samples, Leg 22. In: C.C. von der Borch, J. E. Sclater et al. (eds), Initial Reports of the Deep Sea Drilling Project, 22, U.S. Government Printing Office, 657-662.

Matsumoto, R. and Iijima, A. (1981). Origin and diagenetic evolution of Ca-Mg-Fe carbonates in some coal fields of Japan. Sedimentology 28, 239-259.

Morse, J.W. (1983). The kinetics of calcium carbonate dissolution and precipitation. In: Reeder, R.J. Ed. Carbonates: mineralogy and chemistry. Reviews in mineralogy VII. Min. Soc. Am. 394 pp.

Nathan, Y. and Sass, E. (1981). Stability relations of apatites and calcium carbonates. Chemical Geol. 34,1030111.

Parker, A. and Sellwood, B.W. (eds.) (1983). Proceedings of the NATO ASI-Sediment Diagenesis. D. Reidel.

Price, N.J. (1966). Fault and joing development in brittle and semi-brittle rock. Pergamon Press, New York.

Pye, K., Dickson, J.A.D., Schiavon, N., Coleman, M.L. and Cox, M. (1990). Formation of siderite-Mg-calcite-iron sulphide concretions in intertidal marsh sandflat sediments, north Norfolk, England. Sedimentology 37, 325-343.

Renton, J.J. (1982). Mineral matter in coal. Coal Structure. London. Academic Press.

Roberts, D.L. (1988). The relationship between macerals and sulphur content of some South African Permian coals. Int. J. Coal Geol. 10, 399-410.

Royden, L.C., Sclater, J.G. and von Herzen, R.P. (1980). Continental margin subsidence and heat flow: important parameters in formation of petroleum hydrocarbons. AAPG Bull. 64, 173-187.

Sayles, F.L., Mannheim, F.T. and Waterman, L.S. (1972). Interstitial water studies on small core samples, Leg II. In: Hollister, C.D. and Ewing, J.I. et al. (eds). Initial Reports of the Deep Sea Drilling Project, 11. U.S. Government Printing Office, Washington, 791-799.

Smyth, M. (1965). A siderite-pyrite association in Australian coals. Fuel, 45, London. 221-231.

Spears, D.A. and Caswell, S.A. (1986). Mineral matter in coals: cleat minerals and their origin in some coals from the Englsih midlands. Int. J. Coal Geol. 6, 107-125.

Stach, E. (1975). Stach's textbook of coal petrology. 2nd ed. Gebruder Borntraeger, Berlin.

Stach, E. (1982). Stach's textbook of coal petrology. 3rd ed. Gebruder Borntraeger, Berlin.

Suess, E. and Futterer, D. (1972). Aragonite ooids: experimental precipitation from seawater in the presence of humic acid. Sedimentology 19 1/2.

Taylor, G.H., Liu, S.Y. and Diessel, C.F.K. (1989). The cold-climate origin of inertinite-rich Gondwana coals. Int. J. Coal Geol. 11, 1-22.

Ting, F.T.C. (1977). Origin and spacing of cleats in coal beds. J. Pressure Vessel Technology. Trans. AME 99, 624-626.

van der Spuy, D. and Willis, J.P. (1991). The occurrence of aragonite in carbonate lenses in coals from the Witbank area. Trans. geol. S. Afr. (in press).

Waples, D.W. (1980). Time and temperature in petroleum formation: application of Lopatin's method to petroleum exploration. AAPG Bull. 64, 916-926.

Waples, D.W.. (1985). Geochemistry in petroleum exploration. IHRDC, Boston.

Ward, C.R. (ed). (1984). Coal Geology and Coal Technology. Blackwell Scientific Publications, Melbourne. 345 pp.

APPENDIX A

Sample 1a 8 cm thick, brownish bronze, mineral-rich layer, draped by coal, some zones pyrite rich. Small, elongate pyrite bodies 2 x 0,5 cm, giving a dotted appearance to large mineralized zone. Bright coal contained in small pockets within mineral-rich zone. Smaller, elongate mineral-rich zone below the larger structure. 2 cm thick and thinning to edges over 5 cm.

Sample 1b & 2 12 cm x 3 cm at thickest point, elongate, thinning to edges pyrite body, frog's egg texture, obviously draped. Set in alternating bands of bright and dull coal, about 0,5 cm thick, mostly bright coal. Whitish cleat mineralisation. Pyrite-rich 0.5 x 3cm high "vein" below elongate body, weathers orange to sulphur-yellow.

Sample 3 Large coal sample, alternating bright and dull coal. Frog's egg texture 0.5 mm spherical bodies in bright coal, larger elongate mineral blebs in dull coal, white cleats in bright coal.

Sample 4 8 cm thick, brownish grey carbonate body with common organic inclusions less than 1 mm across and whitish mineral-enriched veins. Topped by alternating bright and dull coal on a mm scale, with a 3 cm x 1 cm draped, spidery pyrite body.

Sample 5 Coal 15 cm thick, mostly dull, one or two bright bands up to 0.5 cm thick. Elongate 3 x 1 cm pyrite bodies. Whitish cleat fill in bright coal.

Samples 6a & 6b 33 cm thick coal sample dull and bright. Small pyrite blebs 1 cm x 1.5 cm , 7 mm x 9 mm. Large, whitish cleats 90° to

bedding up to 4 cm long. Small carbonate bodies in bright coal mm scale, slightly elongate, draped.

Sample 7 4 cm x 9 cm brownish carbonate body made up of a number of spherical bodies, draped by coal and enclosed by a thin network of whitish carbonate veins, star-like pyrite a few mm in cross-section below this body and growing into it. Some elongate, some semi-circular carbonate bodies below major structure. Light coloured "veins" can be seen within these.

Sample 8 Alternating bright and dull coal, draped, semi-elongate pyrite bodies less than 1 cm in size, no spidery pyrite. Whitish cleats in bright coal and up to 3 cm long cleats crossing multiple coal bands.

Sample 9 7 cm thick brownish carbonate body, made up of a number of smaller, spherical bodies, enclosed by horizontal whitish veins up to 1 mm thick. Some smaller spherical carbonate bodies occur in coal above the larger structure. Pyrite bodies, 1 cm x 3 cm also occur in this zone. 4 cm thick layer of dull coal occurs below the large carbonate body. 8 cm thick alternating dull and bright coal above. Small pyrite bodies common.

Sample 10 Capping sandstone, medium to fine reddish to grey sandstone, low porosity, well cemented, high organic matter content. About 20cm thick.

Sample 11 Draped pyrite bodies, 1 cm x 1.5 cm in dull coal. Cleats at 90° to bedding filled with whitish carbonate in 5 mm thick

bright coal bands.

Samples 12 a-d Elongate, brownish carbonate body, inclusions of bright coal with cleat fill. Overlain by alternating dull and bright coal showing drape over the carbonate structure. Coal below is similar, but contains an "invasive" pyrite body, at 30° to coal bedding, the progress of which has been halted by the impermeable carbonate body. Some carbonate has been replaced by this pyrite "intrusion".

Sample 13 3.5 cm x 9 cm pyrite body, draped by coal. Solid pyrite in centre, containing many inclusions of organic matter towards edges. Pyrite has feathery extensions, giving it a spidery appearance. Whole structure is "enclosed" by a network of sub-parallel whitish veins. The central area is solid pyrite, with thick "feeder" veins branching outwards.

Samples 14 a & b 14 cm thick carbonate body, an aggregate of roundish, smaller bodies. Topped by 10 cm x 4 cm feathery pyrite and white vein fill. Smaller spidery pyrite occurs below the main structure together with white cleat fill mineral in bright coal bands.

Sample 15 Feathery and speckled pyrite occurring together with elongate carbonate and pyrite body. The massive carbonate/pyrite body is 6 cm thick at its thickest point. Enclosed by thick, sub-parallel veins.

Sample 16 Shale, rich in organic matter.

Samples 30 & 31 Alternating bright and dull coal in mm thick bands. 1 cm diameter pyrite body, spidery ends, draped. Smaller, elongate 3 mm x 1 mm dark brownish mineral bodies and whitish to clear mineral bodies, 1cm x 0.5 cm.

Samples 32 & 33 An elongate, brownish carbonate body 4cm at its greatest thickness. Length unknown. Not obviously draped from macroscopic observation of sample provided. Set in mostly dull coal with mm thick lenses of bright coal containing cleats at 90° to bedding. Some pyrite replacement of carbonate while pyrite bodies also occur away from carbonate. Network of lighter veins relatively organic-free carbonate within main body.

Sample 34 Dull coal with whitish mineral blebs > 1 mm in size, evenly distributed throughout. Thick calcite vein 4 mm thick with inclusions of organic matter.

Samples 35 & 36 7 cm thick organic-rich, fine grained sandstone to silt, overlain by alternating mm thick bands of bright and dull coal. Spidery "stars" of carbonate within coal up to 1 cm in diameter, some not obviously draped, some elongate parallel to bedding. Lighter coloured "veins" commonly occur within "star" nodes.

Sample 37 Dull coal, obviously draping buff to pinkish brown clay bodies showing slight elongation parallel to bedding, commonly up to 2 x 1 cm in size. White cleat-fill apparent in vitrinite bands.

Sample 38 As above, very strongly draped, flattish mineral bodies, 1,5 cm x 2 cm thinning to edges. Whitish cleat fill in bright coal bands. Pyrite bodies also draped, very irregular in form, - spider-like, with extensions out into coal at both low and high angles to bedding. Pyrite is thin and disseminated.

APPENDIX B

MICROPROBE ANALYSES

Analyses were undertaken on a Cameca Camebax Microbeam electron microprobe in the Geochemostry Department, U.C.T. Operating conditions were as follows:

Beam current:	40nA
Beam focus:	Defocussed to 10-20 microns
Accelerating voltage:	15 kV
Analysing crystals:	TLAP for Mg, Sr, Si
	PET for Ca, Ba
	LiF for Fe, Mn, Zn
Detection:	Flow counters with Ar/CO_2 gas mixture

Standards for carbonate analyses.

Oxide	Standard
Si	Diopside
Mg	Diopside
Ca	Diopside
Mn	Rhodonite
Fe	Ilmenite
Sr	Synthetic Sr-silicate
Ba	Synthetic Ba-silicate
Zn	Gahnite

Counting times were 10 seconds for peaks and 5 seconds for backgrounds either side. For $SrCO_3$, $BaCO_3$ and $ZnCO_3$, counting times were increased to 30 seconds for increased precision. All counts were corrected for dead time. Nominal concentrations were calculated online from cps/%oxide using net (background corrected) peak intensities. The concentration data were then corrected using the Cameca ZAF online program (modified after Henoc et. al., 1973).

XRD Analyses

All XRD analyses were carried out on a Philips PW1130/90 X-ray diffractometer housed in the Department of Geology at U.C.T. Specifications were as follows:

Cu K-alpha radiation

45kV, 40mA

Divergence slit: 1°

Pre-slit (fixed): 2mm

Receiving slit: 1° or 1/2°

anti-scatter slit: none

Curved graphite crystal monochromator

PHS set to pass 95% pulse amplitude peak

Scintillation counter

Vitrinite Reflectance: raw data, mean, random, measured in oil, 50 readings per sample. Numbers at head of columns are sample numbers.

	32	37	38	17	18	19
1.	0.61	0.48	0.58	0.53	0.80	0.60
2.	0.50	0.52	0.62	0.50	0.66	0.55
3.	0.66	0.55	0.48	0.55	0.63	0.57
4.	0.64	0.53	0.54	0.63	0.59	0.53
5.	0.64	0.44	0.50	0.49	0.79	0.54
6.	0.61	0.58	0.56	0.61	0.78	0.50
7.	0.54	0.50	0.40	0.60	0.63	0.64
8.	0.60	0.59	0.57	0.55	0.54	0.58
9.	0.75	0.50	0.40	0.54	0.68	0.63
10.	0.64	0.51	0.48	0.54	0.59	0.54
11.	0.63	0.60	0.61	0.59	0.63	0.56
12.	0.56	0.56	0.49	0.51	0.66	0.59
13.	0.61	0.53	0.57	0.59	0.66	0.66
14.	0.48	0.49	0.46	0.65	1.03	0.41
15.	0.61	0.62	0.53	0.55	0.83	0.62
16.	0.70	0.58	0.57	0.61	0.48	0.64
17.	0.63	0.51	0.54	0.58	0.44	0.55
18.	0.66	0.54	0.58	0.52	0.89	0.44
19.	0.50	0.54	0.64	0.58	0.90	0.56
20.	0.63	0.49	0.52	0.55	0.49	0.57
21.	0.65	0.46	0.56	0.54	0.93	0.50
22.	0.74	0.59	0.46	0.52	0.98	0.53
23.	0.71	0.53	0.57	0.64	0.86	0.69
24.	0.65	0.49	0.47	0.59	0.55	0.56
25.	0.64	0.49	0.53	0.57	0.61	0.44
26.	0.59	0.53	0.45	0.56	1.28	0.65
27.	0.62	0.47	0.53	0.52	1.00	0.52
28.	0.94	0.50	0.50	0.65	0.99	0.54
29.	0.78	0.58	0.50	0.50	0.88	0.52
30.	0.58	0.57	0.48	0.54	0.84	0.58
31.	0.50	0.57	0.64	0.68	0.81	0.59
32.	0.66	0.57	0.61	0.58	0.82	0.61
33.	0.61	0.49	0.54	0.61	0.91	0.57
34.	0.71	0.53	0.59	0.61	0.77	0.43
35.	0.63	0.50	0.51	0.57	0.53	0.54
36.	0.56	0.53	0.57	0.56	0.58	0.59
37.	0.64	0.49	0.53	0.60	0.60	0.46
38.	0.63	0.49	0.47	0.56	0.54	0.48
39.	0.59	0.56	0.41	0.54	0.93	0.51
40.	0.66	0.58	0.59	0.50	0.87	0.59
41.	0.61	0.48	0.58	0.53	0.66	0.60
42.	0.64	0.57	0.48	0.54	0.59	0.54
43.	0.50	0.54	0.64	0.58	0.90	0.56
44.	0.91	0.50	0.50	0.65	0.49	0.54
45.	0.64	0.49	0.53	0.60	0.60	0.59
46.	0.61	0.50	0.56	0.61	0.61	0.59
47.	0.61	0.58	0.53	0.55	0.48	0.55
48.	0.65	0.49	0.47	0.59	0.61	0.56
49.	0.61	0.53	0.54	0.61	0.61	0.57
50.	0.50	0.55	0.62	0.50	0.53	0.54
x =	0.63	0.53	0.53	0.57	0.60	0.56
s	0.09	0.04	0.06	0.05	0.09	0.06

Vitrinite Reflectance: raw data, mean, random, measured in oil, 50 readings per sample. Numbers at head of columns are sample numbers.

	20	21	22	23	24
1.	0.70	0.78	0.51	0.74	0.66
2.	0.75	0.47	0.63	0.76	0.68
3.	0.66	0.52	0.54	0.82	0.73
4.	0.72	0.62	0.62	0.68	0.64
5.	0.85	0.59	0.51	0.70	0.73
6.	0.59	0.52	0.57	0.71	0.59
7.	0.70	0.63	0.52	0.59	0.79
8.	0.73	0.64	0.53	0.91	0.67
9.	0.65	0.64	0.54	0.67	0.60
10.	0.59	0.62	0.70	0.69	0.68
11.	0.59	0.65	0.68	0.80	0.75
12.	0.67	0.60	0.52	0.88	0.74
13.	0.63	0.58	0.57	0.77	0.76
14.	0.67	0.49	0.43	0.74	0.61
15.	0.64	0.69	0.62	0.89	0.65
16.	0.71	0.54	0.56	0.88	0.67
17.	0.67	0.62	0.64	0.70	0.70
18.	0.70	0.83	0.67	0.76	0.67
19.	0.82	0.53	0.62	0.78	0.73
20.	0.72	0.53	0.67	0.69	0.70
21.	0.73	0.48	0.66	0.58	0.71
22.	0.81	0.51	0.69	0.69	0.64
23.	0.70	0.48	0.67	0.56	0.74
24.	0.76	0.52	0.60	0.74	0.65
25.	0.70	0.57	0.61	0.64	0.70
26.	0.74	0.61	0.60	0.81	0.67
27.	0.72	0.53	0.68	0.95	0.71
28.	0.64	0.72	0.65	0.69	0.65
29.	0.66	0.54	0.62	0.64	0.49
30.	0.66	0.51	0.58	0.62	0.50
31.	0.81	0.78	0.51	0.69	0.54
32.	0.70	0.62	0.70	0.58	0.72
33.	0.67	0.53	0.62	0.75	0.72
34.	0.79	0.72	0.68	1.01	0.69
35.	0.71	0.63	0.57	0.71	0.67
36.	0.68	0.54	0.62	0.64	0.73
37.	0.78	0.57	0.67	0.61	0.61
38.	0.68	0.62	0.63	0.55	0.78
39.	0.69	0.60	0.70	0.61	0.61
40.	0.68	0.48	0.56	0.79	0.66
41.	0.70	0.51	0.61	0.74	0.66
42.	0.59	0.64	0.62	0.69	0.60
43.	0.82	0.83	0.52	0.76	0.70
44.	0.64	0.53	0.67	0.62	0.70
45.	0.68	0.52	0.62	0.64	0.72
46.	0.85	0.69	0.52	0.76	0.66
47.	0.67	0.52	0.56	0.80	0.67
48.	0.70	0.47	0.61	0.69	0.67
49.	0.70	0.65	0.62	0.69	0.70
50.	0.70	0.53	0.57	0.54	0.69
x =	0.70	0.59	0.60	0.72	0.67
s	0.06	0.09	0.06	0.10	0.06

Vitrinite Reflectance: raw data, mean, random, measured in oil, 50 readings per sample. Numbers at head of columns are sample numbers.

	25	26	27	28	29
1.	0.59	0.69	0.72	0.69	0.53
2.	0.75	0.65	0.83	0.72	0.58
3.	0.65	0.55	0.74	0.65	0.61
4.	0.69	0.61	0.71	0.70	0.80
5.	0.72	0.61	0.83	0.63	0.66
6.	0.55	0.77	0.60	0.63	0.49
7.	0.60	0.98	0.63	0.81	0.66
8.	0.65	0.76	0.78	0.68	0.57
9.	0.73	0.58	0.65	0.68	0.64
10.	0.77	0.63	0.72	0.65	0.61
11.	0.62	0.64	0.75	0.52	0.59
12.	0.71	1.41	0.67	0.80	0.65
13.	0.60	0.79	0.61	0.79	0.45
14.	0.66	0.67	0.80	0.79	0.54
15.	0.62	0.51	0.72	0.66	0.85
16.	0.71	0.96	0.68	0.78	0.60
17.	0.76	0.76	0.72	0.69	0.54
18.	0.78	0.80	0.62	0.61	0.62
19.	1.02	1.07	0.54	0.65	0.59
20.	0.63	0.98	0.67	0.59	0.55
21.	0.68	0.69	0.71	0.74	0.49
22.	0.68	0.82	0.72	0.67	0.45
23.	0.62	0.70	0.69	0.61	0.58
24.	0.73	0.67	0.51	0.70	0.75
25.	0.78	0.65	0.61	0.57	0.66
26.	0.58	0.74	0.70	0.65	0.62
27.	0.69	0.70	0.64	0.59	0.63
28.	0.72	0.63	0.76	0.54	0.60
29.	0.72	0.86	0.59	0.70	0.54
30.	0.65	0.66	0.66	0.58	0.58
31.	0.63	0.81	0.82	0.74	0.58
32.	0.60	0.71	0.83	0.75	0.46
33.	0.85	0.77	0.71	0.67	0.42
34.	0.60	0.73	0.72	0.67	0.50
35.	0.74	0.88	0.71	0.54	0.44
36.	0.64	0.77	0.69	0.65	0.66
37.	0.73	0.81	0.65	0.79	0.55
38.	0.70	0.73	0.67	0.67	0.61
39.	0.66	0.72	0.75	0.71	0.63
40.	0.66	0.72	0.53	0.70	0.50
41.	0.71	0.62	0.68	0.69	0.53
42.	0.78	0.67	0.58	0.65	0.64
43.	0.51	0.71	0.69	0.61	0.54
44.	0.59	0.71	0.62	0.59	0.66
45.	0.54	0.76	0.79	0.54	0.42
46.	0.65	0.68	0.70	0.65	0.53
47.	0.60	0.69	0.64	0.80	0.64
48.	0.73	0.73	0.71	0.59	0.54
49.	0.72	0.60	0.65	0.70	0.66
50.	0.65	0.69	0.63	0.67	0.42
x =	0.67	0.70	0.69	0.67	0.58
s	0.07	0.08	0.08	0.07	0.09

Vitrinite Reflectance: raw data, mean, random, measured in oil, 50 readings per sample. Numbers at head of columns are sample numbers.

	39	40	41	42	43	44
1.	0.60	0.55	0.53	0.55	0.53	0.69
2.	0.49	0.72	0.55	0.40	0.49	0.82
3.	0.47	0.64	0.51	0.42	0.55	0.61
4.	0.51	0.65	0.64	0.45	0.46	0.53
5.	0.54	0.69	0.44	0.56	0.51	0.50
6.	0.56	0.55	0.35	0.49	0.53	0.61
7.	0.50	0.56	0.43	0.50	0.42	0.71
8.	0.41	0.57	0.61	0.48	0.47	0.72
9.	0.43	0.65	0.60	0.45	0.63	0.56
10.	0.49	0.68	0.64	0.45	0.53	0.51
11.	0.61	0.61	0.55	0.68	0.57	0.53
12.	0.64	0.75	0.57	0.47	0.49	0.60
13.	0.53	0.63	0.81	0.31	0.45	0.70
14.	0.47	0.55	0.76	0.48	0.51	0.71
15.	0.51	0.57	0.61	0.52	0.46	0.55
16.	0.45	0.66	0.64	0.54	0.54	0.38
17.	0.67	0.45	0.55	0.57	0.46	0.51
18.	0.39	0.58	0.52	0.51	0.47	0.55
19.	0.48	0.57	0.52	0.59	0.54	0.55
20.	0.43	0.54	0.54	0.45	0.56	0.45
21.	0.52	0.69	0.57	0.56	0.55	0.61
22.	0.49	0.59	0.50	0.54	0.53	0.64
23.	0.51	0.55	0.56	0.57	0.66	0.63
24.	0.46	0.61	0.51	0.51	0.59	0.50
25.	0.47	0.65	0.59	0.49	0.41	0.61
26.	0.41	0.55	0.53	0.55	0.40	0.55
27.	0.48	0.68	0.64	0.45	0.53	0.56
28.	0.45	0.57	0.52	0.59	0.50	0.59
29.	0.51	0.64	0.51	0.42	0.51	0.61
30.	0.54	0.75	0.57	0.47	0.45	0.55
31.	0.60	0.63	0.53	0.55	0.53	0.69
32.	0.49	0.55	0.64	0.45	0.53	0.51
33.	0.48	0.68	0.52	0.52	0.46	0.55
34.	0.45	0.57	0.64	0.51	0.59	0.59
35.	0.50	0.57	0.35	0.42	0.49	0.71
36.	0.45	0.56	0.61	0.68	0.53	0.38
37.	0.47	0.66	0.51	0.45	0.47	0.61
38.	0.51	0.65	0.51	0.42	0.40	0.53
39.	0.53	0.65	0.57	0.48	0.46	0.70
40.	0.49	0.63	0.57	0.57	0.49	0.64
41.	0.60	0.59	0.57	0.55	0.55	0.82
42.	0.61	0.55	0.60	0.56	0.51	0.53
43.	0.43	0.61	0.52	0.48	0.47	0.45
44.	0.57	0.54	0.64	0.57	0.46	0.61
45.	0.41	0.64	0.35	0.40	0.40	0.72
46.	0.67	0.57	0.61	0.68	0.51	0.51
47.	0.41	0.45	0.56	0.45	0.51	0.55
48.	0.54	0.55	0.55	0.42	0.66	0.50
49.	0.47	0.69	0.55	0.50	0.49	0.71
50.	0.57	0.55	0.54	0.54	0.57	0.63
x	0.50	0.61	0.56	0.50	0.51	0.59
s	0.07	0.07	0.08	0.07	0.06	0.10

APPENDIX D

ND=not detected

All zero values printed as blanks

SAMPLE: 1A

	1	2	3	4	5	6	7	8
$CaCO_3$	4.41	3.86	4.20	4.11	54.94	90.57	53.07	8.68
$SrCO_3$	ND	ND	ND	ND	ND	0.65	ND	ND
$BaCO_3$	ND	ND	ND	ND	ND	0.35	ND	ND
$ZnCO_3$	ND	ND	ND	ND	ND	ND	ND	ND
$FeCO_3$	86.13	88.31	87.34	86.19	16.99	3.54	22.37	77.03
$MnCO_3$	1.08	1.07	1.05	0.97	0.52	ND	ND	0.72
$MgCO_3$	4.84	7.04	8.00	7.59	28.66	4.99	24.86	13.76
Total	96.46	100.28	100.59	98.86	101.11	100.10	100.30	100.19

Atomic proportions based on six oxygens.

Ca	0.103	0.086	0.093	0.093	1.057	1.814	1.038	0.189
Fe	1.744	1.708	1.678	1.687	0.282	0.061	0.384	1.446
Mn	0.022	0.021	0.020	0.019	0.009			0.014
Mg	0.135	0.187	0.211	0.204	0.655	0.119	0.581	0.355
Sr						0.009		
Ba						0.004		
Zn								
Sum	2.004	2.002	2.002	2.003	2.003	2.007	2.004	2.004

1 - 4 massive carbonate
5 - 7 cleat
8 horizontal vein

SAMPLE: 1B

	1	2	3	4	5	6	7	8
$CaCO_3$	3.84	4.35	4.59	4.22	3.93	3.85	4.26	4.56
$SrCO_3$	ND	ND	ND	ND	ND	ND	ND	ND
$BaCO_3$	ND	ND	ND	ND	ND	ND	ND	ND
$ZnCO_3$	ND	ND	ND	ND	ND	ND	ND	ND
$FeCO_3$	84.51	85.34	85.62	85.78	86.75	86.33	82.99	83.37
$MnCO_3$	1.16	1.45	1.29	1.35	1.12	0.95	0.81	0.56
$MgCO_3$	5.06	5.21	4.95	5.22	6.58	5.57	8.56	8.80
Total	94.57	96.35	96.45	96.57	98.38	96.70	96.62	97.28

Atomic proportions based on six oxygens.

Ca	0.092	0.102	0.107	0.099	0.090	0.090	0.098	0.105
Fe	1.744	1.724	1.730	1.730	1.710	1.738	1.652	1.651
Mn	0.024	0.029	0.026	0.028	0.022	0.019	0.016	0.011
Mg	0.144	0.145	0.137	0.145	0.178	0.154	0.234	0.239
Sr								
Ba								
Zn								
Sum	2.004	2.000	2.000	2.002	2.000	2.001	2.000	2.006

1 - 6 massive carbonate
7 - 8 massive carbonate, edge

SAMPLE: 1B

	9	10	11
$CaCO_3$	55.81	53.81	57.33
$SrCO_3$	0.56	0.32	0.22
$BaCO_3$	ND	ND	ND
$ZnCO_3$	ND	ND	ND
$FeCO_3$	2.27	2.73	0.52
$MnCO_3$	ND	ND	ND
$MgCO_3$	38.87	41.43	43.55
Total	97.51	98.29	101.62

Atomic proportions based on six oxygens.

Ca	1.074	1.021	1.047
Fe	0.038	0.045	0.008
Mn			
Mg	0.888	0.933	0.944
Sr	0.007	0.004	0.003
Ba			
Zn			
Sum	2.008	2.003	2.002

9 - 10 cleat
11 fracture fill

SAMPLE: 2

	1	2	3	4	5	6	7	8
$CaCO_3$	4.49	4.03	4.08	4.24	56.21	58.92	57.49	61.04
$SrCO_3$	ND	ND	ND	ND	ND	0.29	0.34	0.43
$BaCO_3$	ND	ND	ND	ND	ND	ND	ND	ND
$ZnCO_3$	ND	ND	ND	ND	ND	ND	ND	ND
$FeCO_3$	84.70	85.23	87.18	85.80	2.35	3.56	6.12	1.73
$MnCO_3$	1.02	0.93	1.19	0.93	ND	ND	1.35	ND
$MgCO_3$	7.18	8.51	5.38	7.18	41.03	36.94	34.50	36.91
Total	97.39	98.70	97.83	98.19	99.59	99.71	99.80	100.11

Atomic proportions based on six oxygens.

Ca	0.103	0.091	0.094	0.098	1.055	1.115	1.096	1.149
Fe	1.683	1.668	1.738	1.690	0.038	0.058	0.101	0.028
Mn	0.020	0.018	0.024	0.018			0.022	
Mg	0.196	0.229	0.147	0.194	0.914	0.830	0.780	0.825
Sr						0.004	0.004	0.005
Ba								
Zn								
Sum	2.002	2.006	2.003	2.000	2.007	2.007	2.003	2.007

1	small early carbonate
2	small early carbonate, edge
3 - 4	small early carbonate
5 - 7	cleat
8	massive carbonate with pyrite rims

SAMPLE: 2

	9	10	11	12
$CaCO_3$	23.26	61.87	54.50	62.29
$SrCO_3$	ND	0.77	0.52	0.63
$BaCO_3$	ND	ND	ND	ND
$ZnCO_3$	ND	ND	ND	ND
$FeCO_3$	59.20	2.74	13.56	2.54
$MnCO_3$	ND	ND	0.43	ND
$MgCO_3$	17.25	34.16	30.74	35.58
Total	99.71	99.54	99.75	101.04

Atomic proportions based on six oxygens.

Ca	0.493	1.179	1.056	1.167
Fe	1.082	0.045	0.227	0.041
Mn			0.007	
Mg	0.434	0.773	0.707	0.791
Sr		0.010	0.007	0.008
Ba				
Zn				
Sum	2.010	2.007	2.004	2.007

9 - 12 massive carbonate with pyrite rims

SAMPLE: 3

	1	2	3	4	5
$CaCO_3$	6.07	10.41	5.05	4.38	3.24
$SrCO_3$	ND	ND	ND	ND	ND
$BaCO_3$	ND	ND	ND	ND	ND
$ZnCO_3$	ND	ND	ND	ND	ND
$FeCO_3$	85.16	79.34	84.29	84.86	87.72
$MnCO_3$	1.29	0.92	1.07	1.46	1.18
$MgCO_3$	4.33	4.90	4.76	5.34	3.85
Total	96.85	95.57	95.17	96.04	95.99

Atomic proportions based on six oxygens.

Ca	0.142	0.243	0.124	0.103	0.077
Fe	1.714	1.604	1.727	1.719	1.793
Mn	0.026	0.019	0.022	0.030	0.024
Mg	0.120	0.136	0.134	0.149	0.108
Sr					
Ba					
Zn					
Sum	2.002	2.002	2.003	2.001	2.002

1 - 5 small early carbonate

SAMPLE: 4

	1	2	3	4	5	6	7	8
$CaCO_3$	98.84	99.54	99.22	99.75	101.57	98.95	97.88	99.28
$SrCO_3$	0.16	0.15	0.16	0.16	ND	0.19	0.20	0.21
$BaCO_3$	ND	ND	ND	ND	ND	ND	ND	ND
$ZnCO_3$	ND	ND	ND	ND	ND	ND	ND	ND
$FeCO_3$	ND	ND	ND	ND	ND	ND	ND	ND
$MnCO_3$	ND	ND	ND	ND	ND	ND	ND	ND
$MgCO_3$	1.24	1.29	1.41	1.18	0.51	1.66	2.28	1.79
Total	100.24	100.88	100.79	101.09	102.08	100.80	100.36	101.28

Atomic proportions based on six oxygens.

Ca	1.969	1.971	1.969	1.973	1.992	1.960	1.947	1.957
Fe								
Mn								
Mg	0.029	0.028	0.033	0.028	0.012	0.039	0.054	0.042
Sr	0.002	0.002	0.002	0.002		0.003	0.003	0.003
Ba								
Zn								
Sum	2.000	2.001	2.004	2.003	2.004	2.002	2.004	2.002

1 massive carbonate
2 massive carbonate
3 massive carbonate
4 massive carbonate
5 cleat
6 horizontal cleat
7 cleat
8 cleat

SAMPLE: 4

	9	10	11	12	13	14	15	16
$CaCO_3$	97.03	95.38	96.01	96.82	99.95	99.76	98.55	100.41
$SrCO_3$	ND	0.27	0.22	0.18	0.18	ND	ND	ND
$BaCO_3$	ND	ND	ND	ND	ND	ND	ND	ND
$ZnCO_3$	ND	ND	ND	ND	ND	ND	ND	ND
$FeCO_3$	1.36	ND	ND	ND	ND	ND	1.56	1.24
$MnCO_3$	1.34	0.69	0.48	ND	ND	ND	1.06	0.69
$MgCO_3$	0.95	2.59	1.39	1.94	1.43	0.48	0.43	ND
Total	100.68	98.93	98.10	98.94	101.56	100.24	101.60	102.34

Atomic proportions based on six oxygens.

Ca	1.934	1.929	1.961	1.947	1.967	1.993	1.947	1.969
Fe	0.023						0.027	0.021
Mn	0.023	0.012	0.009				0.018	0.012
Mg	0.022	0.062	0.034	0.046	0.033	0.011	0.010	
Sr		0.004	0.003	0.002	0.002			
Ba								
Zn								
Sum	2.002	2.007	2.007	1.995	2.002	2.004	2.002	2.002

9 cleat
10 cleat
11 cleat
12 small early carbonate
13 small early carbonate
14 small early carbonate
15 fracture fill
16 fracture fill

SAMPLE: 4

17

$CaCO_3$	98.71
$SrCO_3$	ND
$BaCO_3$	ND
$ZnCO_3$	ND
$FeCO_3$	1.32
$MnCO_3$	0.70
$MgCO_3$	0.62
Total	101.35

Atomic proportions based on six oxygens.

Ca	1.956
Fe	0.023
Mn	0.012
Mg	0.015
Sr	
Ba	
Zn	
Sum	2.006

17 fracture fill

SAMPLE: 5

	1	2	3	4	5	6	7	8
$CaCO_3$	101.29	101.02	100.42	99.91	99.93	99.43	99.11	95.91
$SrCO_3$	0.47	0.46	0.46	0.48	0.40	0.86	0.46	0.24
$BaCO_3$	ND	ND	ND	ND	ND	ND	ND	ND
$ZnCO_3$	ND	ND	ND	ND	ND	ND	ND	ND
$FeCO_3$	ND	ND	ND	ND	ND	ND	ND	0.85
$MnCO_3$	ND	ND	ND	ND	ND	ND	ND	0.92
$MgCO_3$	ND	ND	ND	1.33	ND	ND	ND	0.69
Total	101.76	101.48	100.88	101.72	100.33	100.29	99.57	98.61

Atomic proportions based on six oxygens.

Ca	1.996	1.994	1.998	1.964	1.996	1.991	1.997	1.949
Fe								0.015
Mn								0.006
Mg				0.031				0.017
Sr	0.006	0.006	0.006	0.006	0.005	0.012	0.006	0.003
Ba								
Zn								
Sum	2.002	2.000	2.004	2.001	2.001	2.003	2.003	2.000

1 small early carbonate
2 small early carbonate
3 small early carbonate, centre
4 vein
5 cleat
6 cleat
7 cleat
8 cleat

SAMPLE: 6A

	1	2	3	4	5	6	7	8
$CaCO_3$	96.13	97.03	100.63	101.38	92.18	93.44	100.96	100.00
$SrCO_3$	1.74	1.32	ND	0.32	ND	0.17	0.23	0.52
$BaCO_3$	0.23	ND	ND	ND	ND	ND	ND	ND
$ZnCO_3$	ND	ND	ND	ND	ND	ND	ND	ND
$FeCO_3$	ND	ND	ND	ND	ND	ND	0.62	0.52
$MnCO_3$	ND	ND	ND	ND	ND	ND	ND	ND
$MgCO_3$	1.44	1.48	1.17	ND	1.21	0.97	ND	ND
Total	99.54	99.83	101.80	101.70	93.39	94.58	101.81	101.04

Atomic proportions based on six oxygens.

Ca	1.943	1.955	1.978	1.996	1.974	1.974	1.991	1.990
Fe							0.011	0.009
Mn								
Mg	0.034	0.035	0.027		0.031	0.024		
Sr	0.024	0.018		0.004		0.002	0.003	0.007
Ba	0.002							
Zn								
Sum	2.003	2.008	2.005	2.000	2.005	2.000	2.005	2.006

1 massive carbonate
2 massive carbonate
3 massive carbonate
4 cleat
5 small early carbonate
6 small early carbonate
7 vein
8 vein

SAMPLE: 6B

	1	2	3	4	5	6	7	8
$CaCO_3$	96.31	99.22	102.78	101.49	99.03	98.68	96.02	96.16
$SrCO_3$	1.11	1.21	0.86	1.51	1.46	1.16	0.25	0.16
$BaCO_3$	ND	ND	ND	ND	ND	ND	ND	ND
$ZnCO_3$	ND	ND	ND	ND	ND	ND	ND	ND
$FeCO_3$	ND	ND	ND	ND	ND	ND	ND	ND
$MnCO_3$	0.56	ND	ND	ND	ND	ND	ND	ND
$MgCO_3$	ND	1.11	ND	0.88	1.24	0.44	0.93	1.23
Total	97.98	101.54	103.64	103.88	101.73	100.28	97.20	97.55

Atomic proportions based on six oxygens.

Ca	1.976	1.968	1.995	1.966	1.957	1.978	1.981	1.975
Fe								
Mn								
Mg	0.014	0.026		0.020	0.029	0.010	0.023	0.030
Sr	0.015	0.016	0.011	0.020	0.020	0.016	0.003	0.002
Ba								
Zn								
Sum	2.005	2.010	2.006	2.006	2.008	2.004	2.007	2.007

1 authigenic carbonate
2 authigenic carbonate
3 authigenic carbonate
4 authigenic carbonate
5 authigenic carbonate
6 authigenic carbonate
7 small early carbonate
8 small early carbonate

SAMPLE: 7

	1	2	3	4	5	6	7	8
$CaCO_3$	100.41	100.93	101.68	99.51	100.05	59.12	55.92	52.77
$SrCO_3$	0.60	2.19	0.56	ND	ND	0.27	0.37	0.22
$BaCO_3$	ND	ND	ND	ND	ND	ND	ND	ND
$ZnCO_3$	ND	ND	ND	ND	ND	ND	ND	ND
$FeCO_3$	ND	ND	ND	ND	ND	ND	ND	ND
$MnCO_3$	ND	ND	ND	ND	ND	ND	ND	ND
$MgCO_3$	ND	ND	ND	0.38	ND	43.59	44.56	45.20
Total	101.01	103.12	102.24	99.89	100.05	102.98	100.85	98.19

Atomic proportions based on six oxygens.

Ca	1.994	1.976	1.993	2.003	2.005	1.067	1.027	0.995
Fe								
Mn								
Mg				0.009		0.934	0.972	1.012
Sr	0.008	0.029	0.007			0.003	0.005	0.003
Ba								
Zn								
Sum	2.002	2.005	2.000	2.012	2.005	2.004	2.004	2.010

1 massive carbonate
2 massive carbonate
3 massive carbonate
4 horizontal vein
5 horizontal vein
6 cleat
7 cleat
8 cleat

SAMPLE: 7

	9	10	11
$CaCO_3$	55.84	100.32	103.87
$SrCO_3$	0.29	4.41	ND
$BaCO_3$	ND	ND	ND
$ZnCO_3$	ND	ND	ND
$FeCO_3$	ND	ND	ND
$MnCO_3$	ND	ND	ND
$MgCO_3$	41.32	ND	ND
Total	97.45	104.73	103.87

Atomic proportions based on six oxygens.

Ca	1.066	1.947	2.006
Fe			
Mn			
Mg	0.936		
Sr	0.004	0.058	
Ba			
Zn			
Sum	2.006	2.005	2.006

9 cleat
10 cell fill
11 cell fill

SAMPLE: 8

	1	2	3	4	5	6	7	8
$CaCO_3$	100.22	100.16	98.48	98.48	100.44	99.42	97.65	101.31
$SrCO_3$	0.40	ND	0.21	0.36	0.27	ND	0.25	0.27
$BaCO_3$	ND	ND	ND	ND	ND	ND	ND	ND
$ZnCO_3$	ND	ND	ND	ND	ND	ND	ND	ND
$FeCO_3$	ND	0.90	ND	ND	ND	ND	ND	ND
$MnCO_3$	ND	ND	ND	ND	ND	ND	ND	ND
$MgCO_3$	0.76	0.49	0.68	1.31	0.42	1.96	0.56	ND
Total	101.38	101.55	99.37	100.15	101.13	101.38	98.46	101.58

Atomic proportions based on six oxygens.

Ca	1.984	1.979	1.983	1.969	1.992	1.958	1.989	2.000
Fe		0.015						
Mn								
Mg	0.018	0.012	0.016	0.031	0.010	0.046	0.014	
Sr	0.005		0.003	0.005	0.004		0.003	0.004
Ba								
Zn								
Sum	2.007	2.006	2.002	2.005	2.006	2.004	2.006	2.004

1 massive carbonate
2 massive carbonate, edge
3 massive carbonate, centre
4 massive carbonate, centre
5 massive carbonate, centre
6 massive carbonate, centre
7 massive carbonate, edge
8 cleat

SAMPLE: 8

	9	10	11	12	13	14	15	16
$CaCO_3$	99.92	99.41	101.90	100.53	101.03	101.39	98.86	94.26
$SrCO_3$	0.70	0.24	ND	ND	ND	0.21	ND	ND
$BaCO_3$	ND	ND	ND	ND	ND	ND	ND	ND
$ZnCO_3$	ND	ND	ND	ND	ND	ND	ND	ND
$FeCO_3$	ND	ND	ND	ND	ND	ND	0.61	ND
$MnCO_3$	ND	ND	ND	ND	ND	ND	ND	ND
$MgCO_3$	0.86	2.45	ND	ND	ND	ND	ND	0.61
Total	101.48	102.10	101.90	100.53	101.03	101.60	99.47	94.87

Atomic proportions based on six oxygens.

Ca	1.974	1.941	2.008	2.002	2.007	1.998	1.998	2.000
Fe							0.011	
Mn								
Mg	0.020	0.057						0.015
Sr	0.009	0.003				0.003		
Ba								
Zn								
Sum	2.003	2.001	2.008	2.002	2.007	2.001	2.009	2.015

9 cleat
10 cleat
11 cleat
12 cleat
13 cleat
14 horizontal cleat
15 horizontal cleat
16 horizontal vein

SAMPLE: 8

17

$CaCO_3$	99.91
$SrCO_3$	0.36
$BaCO_3$	ND
$ZnCO_3$	ND
$FeCO_3$	ND
$MnCO_3$	ND
$MgCO_3$	0.79
Total	101.06

Atomic proportions based on six oxygens.

Ca	1.979
Fe	
Mn	
Mg	0.018
Sr	0.005
Ba	
Zn	
Sum	2.002

17 horizontal vein

SAMPLE: 9

	1	2	3	4	5	6	7	8
$CaCO_3$	98.65	97.77	95.98	99.52	99.96	98.41	99.65	99.45
$SrCO_3$	0.67	2.75	1.89	1.08	ND	0.70	0.16	0.24
$BaCO_3$	0.27	ND	ND	ND	ND	0.32	ND	ND
$ZnCO_3$	ND	ND	ND	ND	ND	ND	ND	ND
$FeCO_3$	ND	ND	ND	ND	ND	ND	ND	ND
$MnCO_3$	ND	ND	ND	ND	ND	ND	ND	ND
$MgCO_3$	ND	ND	ND	ND	ND	ND	ND	ND
Total	99.59	100.52	97.87	100.60	99.96	99.43	99.81	99.69

Atomic proportions based on six oxygens.

Ca	1.991	1.965	1.977	1.987	2.009	1.992	2.002	2.003
Fe								
Mn								
Mg								
Sr	0.009	0.037	0.026	0.015	0.010	0.002	0.003	
Ba	0.003				0.003			
Zn								
Sum	2.003	2.002	2.003	2.002	2.009	2.005	2.004	2.006

1 - 6 massive carbonate
7 - 8 cleat in vitrinite included in above

SAMPLE: 10

	1	2	3
$CaCO_3$	54.66	53.44	55.27
$SrCO_3$	ND	ND	ND
$BaCO_3$	ND	ND	ND
$ZnCO_3$	ND	ND	ND
$FeCO_3$	15.43	14.74	16.61
$MnCO_3$	0.48	ND	ND
$MgCO_3$	26.48	27.14	27.00
Total	97.05	95.32	98.88

Atomic proportions based on six oxygens.

Ca	1.140	1.085	1.086
Fe	0.319	0.262	0.286
Mn	0.066		
Mg	0.680	0.656	0.633
Sr			
Ba			
Zn			
Sum	1.999	2.002	2.006

1 - 3 carbonate cement

SAMPLE: 11

	1	2	3	4	5	6	7	8
$CaCO_3$	92.67	93.95	94.93	94.39	93.04	96.54	94.27	96.66
$SrCO_3$	ND	ND	0.16	0.20	ND	0.42	0.21	0.17
$BaCO_3$	ND	ND	ND	ND	ND	ND	ND	ND
$ZnCO_3$	ND	ND	ND	ND	ND	ND	ND	ND
$FeCO_3$	1.25	ND	ND	ND	0.75	0.63	0.51	ND
$MnCO_3$	0.78	0.97	0.55	0.51	0.72	ND	0.68	0.52
$MgCO_3$	4.67	4.72	0.93	2.36	2.19	ND	0.41	0.55
Total	99.37	99.64	96.57	97.46	96.70	97.59	96.08	97.90

Atomic proportions based on six oxygens.

Ca	1.854	1.888	1.974	1.937	1.923	1.989	1.966	1.977
Fe	0.022				0.013	0.011	0.009	
Mn	0.014	0.017	0.010	0.009	0.013		0.012	0.009
Mg	0.111	0.112	0.023	0.057	0.054		0.010	0.013
Sr			0.002	0.003		0.006	0.003	0.002
Ba								
Zn								
Sum	2.001	2.010	2.010	2.006	2.003	2.006	2.000	2.002

1 - 6 cleat
7,8 massive carbonate

SAMPLE: 11

	9	10
$CaCO_3$	99.04	97.73
$SrCO_3$	ND	ND
$BaCO_3$	ND	ND
$ZnCO_3$	ND	ND
$FeCO_3$	ND	ND
$MnCO_3$	0.69	0.49
$MgCO_3$	1.17	1.36
Total	100.90	99.58

Atomic proportions based on six oxygens.

Ca	1.967	1.958
Fe		
Mn	0.012	0.012
Mg	0.028	0.035
Sr		
Ba		
Zn		
Sum	2.007	2.005

9, 10 horizontal vein

SAMPLE: 12B

	1	2	3	4	5	6	7	8
$CaCO_3$	96.89	95.45	94.65	96.91	93.65	55.61	94.64	94.72
$SrCO_3$	0.44	0.31	ND	ND	0.39	ND	0.66	0.51
$BaCO_3$	ND	ND	ND	ND	ND	ND	ND	ND
$ZnCO_3$	ND	ND	ND	ND	ND	ND	ND	ND
$FeCO_3$	0.83	1.23	1.55	0.93	2.63	2.10	0.70	0.71
$MnCO_3$	ND	ND	ND	ND	ND	0.42	ND	0.37
$MgCO_3$	1.39	2.22	3.46	2.12	1.71	41.62	1.88	1.87
Total	99.55	99.21	99.66	99.96	98.38	99.75	97.88	98.17

Atomic proportions based on six oxygens.

Ca	1.950	1.930	1.898	1.939	1.913	1.038	1.936	1.930
Fe	0.015	0.022	0.027	0.016	0.046	0.034	0.012	0.012
Mn						0.007		0.007
Mg	0.033	0.053	0.082	0.050	0.041	0.922	0.046	0.045
Sr	0.006	0.004			0.005		0.009	0.007
Ba								
Zn								
Sum	2.004	2.010	2.007	2.006	2.006	2.001	2.003	2.007

1 - 4 small early carbonate
5,7,8 massive carbonate
6 cleat

SAMPLE: 12C

	1	2	3	4	5	6
$CaCO_3$	97.60	96.68	95.59	97.60	82.17	70.83
$SrCO_3$	0.86	0.37	0.37	0.19	ND	ND
$BaCO_3$	ND	ND	ND	ND	ND	ND
$ZnCO_3$	ND	ND	ND	ND	1.07	ND
$FeCO_3$	0.85	1.06	0.54	1.04	1.55	2.53
$MnCO_3$	ND	ND	ND	0.52	ND	ND
$MgCO_3$	1.47	0.69	3.07	1.38	14.69	23.50
Total	100.78	98.80	99.57	100.73	99.48	96.86

Atomic proportions based on six oxygens.

Ca	1.945	1.966	1.919	1.939	1.619	1.410
Fe	0.015	0.019	0.009	0.049	0.026	0.044
Mn				0.009		
Mg	0.035	0.017	0.073	0.032	0.344	0.555
Sr	0.012	0.005	0.005	0.003		
Ba						
Zn					0.017	
Sum	2.007	2.007	2.006	2.001	2.006	2.009

1 - 6 massive carbonate

SAMPLE: 12D

	1	2	3	4	5	6	7
$CaCO_3$	99.15	96.70	95.15	90.71	96.34	96.91	98.40
$SrCO_3$	0.27	0.17	0.20	ND	0.19	0.22	0.25
$BaCO_3$	ND	ND	ND	ND	ND	ND	ND
$ZnCO_3$	ND	ND	ND	ND	ND	ND	ND
$FeCO_3$	ND	ND	0.49	0.57	ND	ND	ND
$MnCO_3$	0.49	0.47	ND	0.55	0.50	0.52	0.70
$MgCO_3$	2.48	1.53	3.11	5.58	2.24	1.91	2.06
Total	102.39	98.87	98.95	97.41	99.27	99.56	101.41

Atomic proportions based on six oxygens.

Ca	1.936	1.960	1.924	1.848	1.941	1.945	1.942
Fe			0.009	0.010			
Mn	0.008	0.008		0.010	0.009	0.009	0.012
Mg	0.057	0.037	0.075	0.135	0.054	0.046	0.048
Sr	0.004	0.002	0.003		0.003	0.003	0.003
Ba							
Zn							
Sum	2.005	2.007	2.009	2.003	2.006	2.003	2.005

1 - 7 cleat

SAMPLE: 13

1

$CaCO_3$	90.70
$SrCO_3$	ND
$BaCO_3$	ND
$ZnCO_3$	ND
$FeCO_3$	3.45
$MnCO_3$	0.55
$MgCO_3$	6.49
Total	101.19

Atomic proportions based on six oxygens.

Ca	1.783
Fe	0.059
Mn	0.009
Mg	0.151
Sr	
Ba	
Zn	
Sum	2.002

1 vein

SAMPLE: 14A

	14	15
$CaCO_3$	70.58	67.82
$SrCO_3$	ND	0.17
$BaCO_3$	ND	ND
$ZnCO_3$	ND	ND
$FeCO_3$	5.38	4.67
$MnCO_3$	ND	ND
$MgCO_3$	22.88	26.59
Total	98.84	99.25

Atomic proportions based on six oxygens.

Ca	1.381	1.294
Fe	0.092	0.084
Mn		
Mg	0.531	0.606
Sr		0.009
Ba		
Zn		
Sum	2.005	1.994

14 - 15 cleat

SAMPLE: 15

	1	2	3	4	5	6	7	8
$CaCO_3$	99.75	3.90	94.29	100.80	88.32	2.43	4.56	4.95
$SrCO_3$	0.19	ND	0.63	ND	0.69	ND	ND	ND
$BaCO_3$	ND	ND	0.24	ND	0.24	ND	ND	ND
$ZnCO_3$	ND	ND	ND	ND	ND	ND	ND	ND
$FeCO_3$	1.00	81.96	1.98	1.07	1.06	84.88	81.44	78.97
$MnCO_3$	ND	0.89	ND	0.34	ND	0.67	1.64	1.91
$MgCO_3$	0.90	12.95	5.39	0.62	12.41	13.54	12.59	14.97
Total	101.84	99.70	102.53	102.83	102.72	101.52	100.23	100.80

Atomic proportions based on six oxygens.

Ca	1.962	0.086	1.835	1.963	1.692	0.053	0.100	0.107
Fe	0.017	1.558	0.033	0.018	0.018	1.587	1.542	1.475
Mn		0.017		0.002		0.013	0.031	0.036
Mg	0.021	0.338	0.124	0.014	0.282	0.348	0.327	0.384
Sr	0.003		0.008		0.009			
Ba			0.002		0.002			
Zn								
Sum	2.003	1.999	2.002	2.001	2.003	2.001	2.000	2.002

1 - 8 massive carbonate

SAMPLE: 15

	9	10	11	12	13	14	15	16
$CaCO_3$	96.00	92.01	59.56	95.85	84.88	99.71	56.89	99.23
$SrCO_3$	0.81	0.52	0.30	0.71	0.22	0.32	0.19	0.30
$BaCO_3$	0.24	0.28	ND	ND	ND	ND	ND	ND
$ZnCO_3$	ND	ND	ND	ND	ND	ND	ND	ND
$FeCO_3$	2.85	0.55	29.19	0.60	1.58	ND	0.93	ND
$MnCO_3$	ND	ND	0.58	ND	0.46	ND	ND	ND
$MgCO_3$	2.47	9.00	10.91	4.55	10.59	1.94	38.20	1.69
Total	102.37	102.36	100.54	101.71	97.73	101.97	96.21	101.22

Atomic proportions based on six oxygens.

Ca	1.885	1.777	1.211	1.879	1.710	1.961	1.105	1.966
Fe	0.048	0.009	0.513	0.010	0.028		0.016	
Mn			0.010		0.008			
Mg	0.057	0.206	0.263	0.106	0.253	0.045	0.881	0.040
Sr	0.011	0.007	0.004	0.009	0.003	0.004	0.002	0.004
Ba								
Zn								
Sum	2.003	2.002	2.001	2.004	2.002	2.010	2.004	2.010

9 - 12 horizontal cleats
13- 16 cleats

SAMPLE: 15

	17	18	19	20	21	22
$CaCO_3$	99.82	98.27	99.94	96.71	5.98	4.73
$SrCO_3$	0.27	0.25	ND	0.25	ND	ND
$BaCO_3$	ND	ND	ND	ND	ND	ND
$ZnCO_3$	ND	ND	ND	ND	ND	ND
$FeCO_3$	ND	ND	0.51	0.47	77.90	85.45
$MnCO_3$	ND	0.46	ND	ND	0.88	1.07
$MgCO_3$	1.72	2.34	ND	4.46	15.72	9.71
Total	101.81	101.32	100.45	101.89	100.48	100.96

Atomic proportions based on six oxygens.

Ca	1.963	1.942	1.993	1.891	0.129	0.104
Fe			0.009	0.008	1.453	1.623
Mn		0.008			0.017	0.020
Mg	0.040	0.055		0.103	0.403	0.253
Sr	0.004	0.003		0.003		
Ba						
Zn						
Sum	2.007	2.008	2.002	2.005	2.002	2.000

17 - 18 cleats
19 - 20 veins
21 - 22 clear carbonate

SAMPLE: 30

	1	2	3	4	5	6	7	8
$CaCO_3$	63.39	64.95	53.81	56.81	58.73	65.22	57.32	61.13
$SrCO_3$	0.31	0.73	0.32	0.26	0.28	0.38	0.24	0.39
$BaCO_3$	ND	0.27	ND	ND	ND	0.24	ND	ND
$ZnCO_3$	ND	ND	ND	ND	ND	ND	ND	ND
$FeCO_3$	0.43	0.99	2.73	ND	ND	ND	0.34	0.42
$MnCO_3$	0.47	ND	ND	0.42	0.12	ND	ND	ND
$MgCO_3$	34.81	32.92	41.43	39.12	39.40	30.46	38.20	34.90
Total	99.41	99.86	98.29	96.62	98.83	96.34	96.10	96.84

Atomic proportions based on six oxygens.

Ca	1.201	1.235	1.021	1.098	1.112	1.289	1.116	1.188
Fe	0.007	0.016	0.045				0.006	0.007
Mn	0.008			0.007	0.007			
Mg	0.783	0.743	0.933	0.898	0.885	0.714	0.883	0.805
Sr	0.004	0.009	0.004	0.003	0.001	0.005	0.003	0.005
Ba		0.003				0.003		
Zn								
Sum	2.003	2.006	2.003	2.006	2.008	2.011	2.008	2.005

1 cleat
2 cleat
3 small early carbonate
4 cleat
5 cleat
6 cleat
7 cleat
8 cleat

SAMPLE: 30

	9	10	11	12	13	14	15	16
$CaCO_3$	56.43	60.35	63.13	83.09	57.99	59.76	63.57	68.48
$SrCO_3$	0.34	0.35	0.27	0.58	0.28	0.30	0.30	0.29
$BaCO_3$	ND	ND	0.22	ND	ND	ND	ND	ND
$ZnCO_3$	ND	ND	ND	ND	ND	ND	ND	ND
$FeCO_3$	ND	ND	ND	ND	ND	ND	ND	ND
$MnCO_3$	ND	ND	ND	ND	ND	ND	ND	ND
$MgCO_3$	39.61	35.69	33.66	13.37	37.94	36.24	33.30	31.91
Total	96.38	96.39	97.28	97.04	96.21	96.30	97.17	96.68

Atomic proportions based on six oxygens.

Ca	1.097	1.179	1.226	1.676	1.131	1.165	1.237	1.262
Fe								
Mn								
Mg	0.913	0.828	0.776	0.320	0.878	0.839	0.769	0.741
Sr	0.005	0.005	0.004	0.008	0.004	0.004	0.004	0.004
Ba			0.002					
Zn								
Sum	2.015	2.012	2.008	2.004	2.013	2.008	2.010	2.007

9 cleat
10 cleat
11 cleat
12 cleat
13 cleat
14 cleat
15 vein
16 vein

SAMPLE: 32

	1	2	3	4	5	6	7	8
$CaCO_3$	98.31	93.89	95.70	97.90	96.96	97.08	97.61	100.41
$SrCO_3$	0.61	3.95	2.37	0.38	0.27	0.20	0.18	0.43
$BaCO_3$	ND	ND	ND	ND	ND	ND	ND	ND
$ZnCO_3$	ND	ND	ND	ND	ND	ND	ND	ND
$FeCO_3$	ND	ND	ND	ND	ND	ND	ND	ND
$MnCO_3$	ND	ND	ND	ND	ND	ND	ND	ND
$MgCO_3$	ND	ND	ND	ND	3.17	3.50	2.09	ND
Total	98.92	97.84	98.07	98.28	100.40	100.78	99.88	100.84

Atomic proportions based on six oxygens.

Ca	1.994	1.948	1.969	2.001	1.927	1.920	1.960	1.996
Fe								
Mn								
Mg					0.075	0.082	0.050	
Sr	0.008	0.056	0.033	0.005	0.004	0.003	0.002	0.006
Ba								
Zn								
Sum	2.002	2.004	2.002	2.006	2.006	2.005	2.012	2.002

1 massive carbonate
2 massive carbonate
3 lenticular carbonate
4 cleat
5 lenticular carbonate
6 lenticular carbonate
7 lenticular carbonate
8 massive carbonate edge

SAMPLE: 32

	9	10	11	12	13	14	15	16
$CaCO_3$	99.60	95.50	64.74	94.98	63.06	99.83	100.31	102.23
$SrCO_3$	0.35	0.24	0.26	0.30	0.24	0.17	0.79	0.60
$BaCO_3$	ND	ND	ND	ND	ND	ND	ND	ND
$ZnCO_3$	ND	ND	ND	ND	ND	ND	ND	ND
$FeCO_3$	0.42	ND	0.74	ND	ND	ND	ND	ND
$MnCO_3$	ND	0.47	ND	ND	ND	ND	ND	ND
$MgCO_3$	0.74	3.71	34.70	6.53	34.50	0.90	ND	ND
Total	101.11	99.92	100.44	101.81	97.80	100.90	101.10	102.83

Atomic proportions based on six oxygens.

Ca	1.977	1.904	1.214	1.855	1.214	1.978	1.992	1.992
Fe	0.007		0.012					
Mn		0.008						
Mg	0.017	0.088	0.772	0.151	0.789	0.021		
Sr	0.005	0.003	0.003	0.004	0.003	0.002	0.011	0.008
Ba								
Zn								
Sum	2.006	2.003	2.001	2.010	2.006	2.001	2.003	2.000

9 massive carbonate
10 cleat
11 cleat
12 cleat
13 cleat
14 cleat
15 massive carbonate
16 massive carbonate

SAMPLE: 34

	1	2
$CaCO_3$	94.05	96.58
$SrCO_3$	0.25	0.49
$BaCO_3$	ND	ND
$ZnCO_3$	ND	ND
$FeCO_3$	ND	ND
$MnCO_3$	1.12	0.85
$MgCO_3$	3.54	4.83
Total	98.96	102.75

Atomic proportions based on six oxygens.

Ca	1.893	1.858
Fe		
Mn	0.020	0.014
Mg	0.085	0.123
Sr	0.003	0.006
Ba		
Zn		
Sum	2.001	2.001

1 - 2 carbonate

SAMPLE: 35,36

	1	2	3	4	5	6	7	8
$CaCO_3$	98.98	100.08	99.91	96.52	101.74	100.57	92.21	93.41
$SrCO_3$	0.86	2.38	2.14	2.14	1.22	0.91	2.17	1.95
$BaCO_3$	ND	ND	ND	0.27	ND	ND	ND	0.37
$ZnCO_3$	ND	ND	ND	ND	ND	ND	ND	ND
$FeCO_3$	0.99	ND	ND	1.29	ND	ND	2.88	2.88
$MnCO_3$	ND	ND	ND	ND	ND	ND	0.41	ND
$MgCO_3$	0.55	ND	ND	0.93	ND	ND	0.50	0.83
Total	101.38	102.46	102.05	101.15	102.96	101.48	98.17	99.44

Atomic proportions based on six oxygens.

Ca	1.960	1.973	1.975	1.928	1.988	1.994	1.908	1.902
Fe	0.017			0.022			0.051	0.051
Mn							0.007	
Mg	0.013			0.022			0.012	0.020
Sr	0.012	0.032	0.029	0.029	0.016	0.012	0.030	0.027
Ba				0.003				0.004
Zn								
Sum	2.002	2.005	2.004	2.004	2.004	2.006	2.008	2.004

1 star carbonate, centre
2 star carbonate, base
3 star carbonate, centre
4 star carbonate, edge
5,6 star carbonate, centre
7,8 small star carbonate at sand contact

SAMPLE: 35,36

	9	10	11	12	13	14	15	16
$CaCO_3$	97.37	96.36	53.97	55.38	51.40	62.25	101.15	49.54
$SrCO_3$	1.01	1.67	0.99	0.87	0.84	0.87	ND	1.02
$BaCO_3$	ND	ND	ND	ND	ND	ND	ND	ND
$ZnCO_3$	ND	ND	ND	ND	ND	ND	ND	ND
$FeCO_3$	ND	ND	1.53	1.39	4.86	8.45	ND	22.38
$MnCO_3$	ND	ND	ND	ND	0.48	ND	ND	0.61
$MgCO_3$	ND	0.41	43.23	42.23	39.61	26.50	ND	25.51
Total	98.38	98.44	99.72	99.87	97.19	98.07	101.15	99.06

Atomic proportions based on six oxygens.

Ca	1.998	1.965	1.009	1.037	0.994	1.230	2.017	0.990
Fe			0.025	0.022	0.081	0.144		0.386
Mn					0.008			0.011
Mg		0.014	0.959	0.938	0.909	0.622		0.605
Sr	0.014	0.028	0.013	0.011	0.011	0.012		0.014
Ba								
Zn								
Sum	2.012	2.008	2.006	2.008	2.003	2.008	2.017	2.006

9 - 14 cleat
15,16 vein

SAMPLE: 35,36

	17	18	19	20	21	22	23	24
$CaCO_3$	98.83	97.58	98.24	99.10	96.81	94.74	99.73	97.37
$SrCO_3$	0.41	2.54	1.60	1.64	1.67	2.00	2.44	1.73
$BaCO_3$	ND	ND	ND	ND	0.35	0.53	ND	ND
$ZnCO_3$	ND	ND	ND	ND	ND	ND	ND	ND
$FeCO_3$	ND	ND	ND	ND	1.67	2.27	ND	ND
$MnCO_3$	ND	ND	ND	ND	ND	ND	ND	ND
$MgCO_3$	ND	ND	ND	ND	ND	0.74	ND	0.33
Total	99.24	100.12	99.85	100.74	100.49	100.28	102.17	99.44

Atomic proportions based on six oxygens.

Ca	2.005	1.972	1.984	1.983	1.950	1.912	1.972	1.978
Fe					0.029	0.040		
Mn								
Mg						0.018		0.008
Sr	0.006	0.034	0.022	0.022	0.023	0.027	0.033	0.024
Ba					0.004	0.006		
Zn								
Sum	2.011	2.006	2.006	2.005	2.006	2.003	2.005	2.010

17 vein
18 - 24 star carbonate

SAMPLE:	35,36 25	26	27	28
$CaCO_3$	95.58	94.76	98.47	99.08
$SrCO_3$	2.16	2.20	1.42	1.62
$BaCO_3$	0.37	0.29	ND	ND
$ZnCO_3$	ND	ND	ND	ND
$FeCO_3$	1.61	1.87	ND	ND
$MnCO_3$	ND	ND	ND	ND
$MgCO_3$	0.46	0.61	ND	ND
Total	100.17	99.74	99.89	100.70

Atomic proportions based on six oxygens.

Ca	1.930	1.919	1.983	1.981
Fe	0.028	0.033		
Mn				
Mg	0.011	0.015		
Sr	0.030	0.030	0.019	0.022
Ba	0.004	0.003		
Zn				
Sum	2.003	2.000	2.002	2.003

25 - 28 star carbonate

SAMPLE: 37

1

$CaCO_3$	53.14
$SrCO_3$	0.27
$BaCO_3$	ND
$ZnCO_3$	ND
$FeCO_3$	2.64
$MnCO_3$	ND
$MgCO_3$	40.95
Total	97.00

Atomic proportions based on six oxygens.

Ca	1.024
Fe	0.044
Mn	
Mg	0.937
Sr	0.004
Ba	
Zn	
Sum	2.009

1 cleat

SAMPLE: 38

	1	2	3	4	5	6
$CaCO_3$	57.31	56.88	59.10	57.61	55.80	55.67
$SrCO_3$	ND	0.44	0.38	0.34	0.51	NF
$BaCO_3$	ND	ND	ND	ND	ND	ND
$ZnCO_3$	ND	ND	ND	ND	ND	ND
$FeCO_3$	4.93	2.58	3.05	2.14	2.46	3.47
$MnCO_3$	1.15	ND	0.41	ND	ND	0.50
$MgCO_3$	39.78	40.79	39.96	42.25	40.82	39.38
Total	103.17	100.69	102.90	102.34	99.59	99.02

Atomic proportions based on six oxygens.

Ca	1.046	1.057	1.078	1.051	1.048	1.053
Fe	0.078	0.041	0.048	0.034	0.040	0.057
Mn	0.018		0.007			0.008
Mg	0.861	0.900	0.865	0.915	0.910	0.884
Sr		0.006	0.005	0.004	0.006	
Ba						
Zn						
Sum	2.003	2.004	2.003	2.004	2.004	2.002

1 cleat
2 cleat
3 cleat
4 cleat
5 cleat
6 cell fill

SAMPLE: 39

	1	2	3	4	5	6	7	8
$CaCO_3$	57.40	42.39	43.98	3.64	3.40	4.34	7.72	87.99
$SrCO_3$	ND	0.45	0.41	ND	ND	ND	ND	1.60
$BaCO_3$	ND	ND	ND	ND	ND	ND	ND	1.35
$ZnCO_3$	ND	ND	ND	ND	ND	ND	ND	ND
$FeCO_3$	1.31	33.01	30.59	82.39	84.72	82.53	73.73	5.10
$MnCO_3$	ND	ND	ND	1.23	1.18	1.31	0.65	ND
$MgCO_3$	42.87	23.35	23.98	8.06	6.28	8.33	16.98	1.04
Total	101.58	99.20	98.96	95.32	95.58	96.51	99.08	97.08

Atomic proportions based on six oxygens.

Ca	1.051	0.860	0.890	0.085	0.080	0.100	0.168	1.848
Fe	0.021	0.579	0.535	1.668	1.723	1.648	1.387	0.093
Mn				0.025	0.024	0.026	0.012	
Mg	0.932	0.563	0.576	0.224	0.175	0.229	0.439	0.026
Sr		0.006	0.006					0.023
Ba								0.014
Zn								
Sum	2.004	2.008	2.007	2.002	2.002	2.003	2.006	2.004

1,2 small carbonate, centre
3 small carbonate, edge
4 - 6 small carbonate, centre
7, 8 small carbonate, edge

SAMPLE: 39

	9	10	11	12	13	14	15	16
$CaCO_3$	2.93	4.69	63.18	53.74	2.09	61.52	63.70	56.10
$SrCO_3$	ND	ND	0.82	0.69	ND	0.59	ND	ND
$BaCO_3$	ND	ND	ND	ND	ND	ND	ND	ND
$ZnCO_3$	ND	ND	ND	ND	ND	ND	ND	ND
$FeCO_3$	87.27	88.26	5.83	16.67	86.20	6.22	2.53	3.13
$MnCO_3$	1.02	0.99	ND	ND	0.74	ND	ND	ND
$MgCO_3$	5.81	6.47	30.90	31.77	9.61	32.07	37.14	42.08
Total	97.03	100.41	100.73	102.87	98.64	100.40	103.37	101.31

Atomic proportions based on six oxygens.

Ca	0.068	0.105	1.201	1.015	0.047	1.172	1.161	1.034
Fe	1.758	1.709	0.096	0.272	1.687	0.102	0.040	0.050
Mn	0.021	0.019			0.015			
Mg	0.161	0.172	0.697	0.713	0.258	0.725	0.803	0.921
Sr			0.011	0.009		0.008		
Ba								
Zn								
Sum	2.008	2.005	2.005	2.009	2.007	2.007	2.004	2.005

9, 10	small carbonate, centre
11,12	small carbonate, edge
13	small carbonate, centre
14	small carbonate, edge
15,16	massive carbonate

SAMPLE: 39

	17	18
$CaCO_3$	81.49	73.77
$SrCO_3$	ND	ND
$BaCO_3$	ND	ND
$ZnCO_3$	ND	ND
$FeCO_3$	5.32	7.84
$MnCO_3$	ND	ND
$MgCO_3$	11.94	18.15
Total	98.75	99.76

Atomic proportions based on six oxygens.

Ca	1.630	1.449
Fe	0.092	0.133
Mn		
Mg	0.283	0.423
Sr		
Ba		
Zn		
Sum	2.005	2.005

17, 18 massive carbonate

SAMPLE: 41

	1	2	3
$CaCO_3$	59.71	55.17	56.94
$SrCO_3$	ND	ND	ND
$BaCO_3$	ND	ND	ND
$ZnCO_3$	ND	ND	ND
$FeCO_3$	0.54	0.54	0.91
$MnCO_3$	0.77	0.91	0.91
$MgCO_3$	37.04	41.64	38.99
Total	98.06	98.26	97.75

Atomic proportions based on six oxygens.

Ca	1.146	1.046	1.089
Fe	0.009	0.009	0.015
Mn	0.013	0.015	0.015
Mg	0.844	0.937	0.885
Sr			
Ba			
Zn			
Sum	2.012	2.007	2.004

1 - 3 vein

SAMPLE: 42

	1	2	3	4	5	6	7
$CaCO_3$	99.27	97.21	93.58	99.25	97.86	53.43	53.57
$SrCO_3$	ND	ND	ND	ND	ND	ND	ND
$BaCO_3$	ND	ND	ND	ND	ND	ND	ND
$ZnCO_3$	ND	ND	ND	ND	ND	ND	ND
$FeCO_3$	1.45	1.11	ND	0.43	ND	3.85	4.91
$MnCO_3$	ND	ND	ND	ND	ND	ND	0.41
$MgCO_3$	2.97	2.15	3.84	2.92	0.39	42.16	43.23
Total	103.69	100.47	97.42	102.60	98.25	99.44	102.14

Atomic proportions based on six oxygens.

Ca	1.912	1.935	1.915	1.933	1.997	1.004	0.978
Fe	0.024	0.019		0.007		0.062	0.078
Mn							0.007
Mg	0.068	0.051	0.093	0.068	0.010	0.940	0.937
Sr							
Ba							
Zn							
Sum	2.004	2.005	2.008	2.008	2.007	2.006	2.000

1 - 5 massive carbonate
6, 7 cleat

SAMPLE: 43

	1	2	3	4	5	6	7
$CaCO_3$	91.74	94.41	56.81	87.17	90.83	91.15	92.95
$SrCO_3$	ND	ND	ND	ND	ND	ND	ND
$BaCO_3$	ND	ND	ND	ND	ND	ND	ND
$ZnCO_3$	ND	ND	ND	ND	ND	ND	ND
$FeCO_3$	2.34	1.50	18.05	3.09	2.12	2.03	2.36
$MnCO_3$	0.32	ND	0.50	ND	ND	ND	0.40
$MgCO_3$	1.79	2.02	26.02	6.35	4.91	5.92	3.27
Total	96.19	97.93	101.38	96.61	97.06	99.10	98.98

Atomic proportions based on six oxygens.

Ca	1.913	1.924	1.091	1.796	1.852	1.837	1.881
Fe	0.042	0.027	0.302	0.055	0.037	0.035	0.041
Mn	0.006		0.011				0.007
Mg	0.044	0.050	0.595	0.155	0.119	0.142	0.079
Sr							
Ba							
Zn							
Sum	2.005	2.008	1.998	2.006	2.008	2.014	2.008

1, 2	massive carbonate
3	cleat
4 - 7	massive carbonate

SAMPLE: 44

	9	10
$CaCO_3$	56.13	67.72
$SrCO_3$	ND	ND
$BaCO_3$	ND	ND
$ZnCO_3$	ND	ND
$FeCO_3$	8.27	4.19
$MnCO_3$	ND	ND
$MgCO_3$	38.00	27.72
Total	102.40	99.64

Atomic proportions based on six oxygens.

Ca	1.037	1.302
Fe	0.132	0.070
Mn		
Mg	0.833	0.632
Sr		
Ba		
Zn		
Sum	2.002	2.004

9, 10 cleat

SAMPLE: 44

	1	2	3	4	5	6	7	8
$CaCO_3$	59.52	59.40	98.40	57.68	58.74	69.36	65.32	57.15
$SrCO_3$	ND	ND	ND	ND	ND	ND	ND	ND
$BaCO_3$	ND	ND	ND	ND	ND	ND	ND	ND
$ZnCO_3$	ND	ND	ND	ND	ND	ND	ND	ND
$FeCO_3$	12.84	11.73	0.80	15.18	4.16	3.26	3.04	2.54
$MnCO_3$	ND	ND	ND	ND	ND	ND	ND	ND
$MgCO_3$	28.39	29.51	0.67	27.43	35.88	28.88	32.31	39.23
Total	100.73	100.72	99.87	100.29	98.78	101.50	100.67	98.92

Atomic proportions based on six oxygens.

Ca	1.144	1.141	1.977	1.120	1.123	1.307	1.230	1.080
Fe	0.213	0.194	0.014	0.255	0.069	0.053	0.049	0.041
Mn								
Mg	0.647	0.672	0.016	0.632	0.814	0.646	0.722	0.880
Sr								
Ba								
Zn								
Sum	2.004	2.007	2.007	2.007	2.006	2.006	2.001	2.001

1 - 6 massive carbonate
7 vein
8 massive carbonate

APPENDIX E

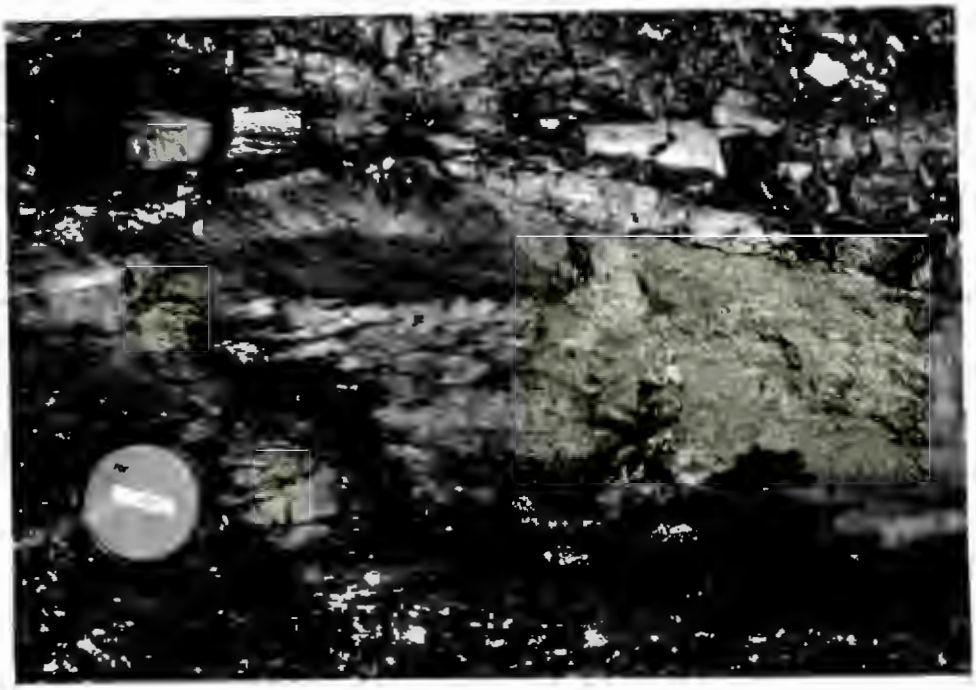

Plate:1a - Macroscopic view of a massive carbonate body in situ, sample 2. Lens cap is 4cm in diameter.

Plate:1b - Macroscopic view of a massive carbonate in situ, sample 9. Lens cap is 4cm in diameter.

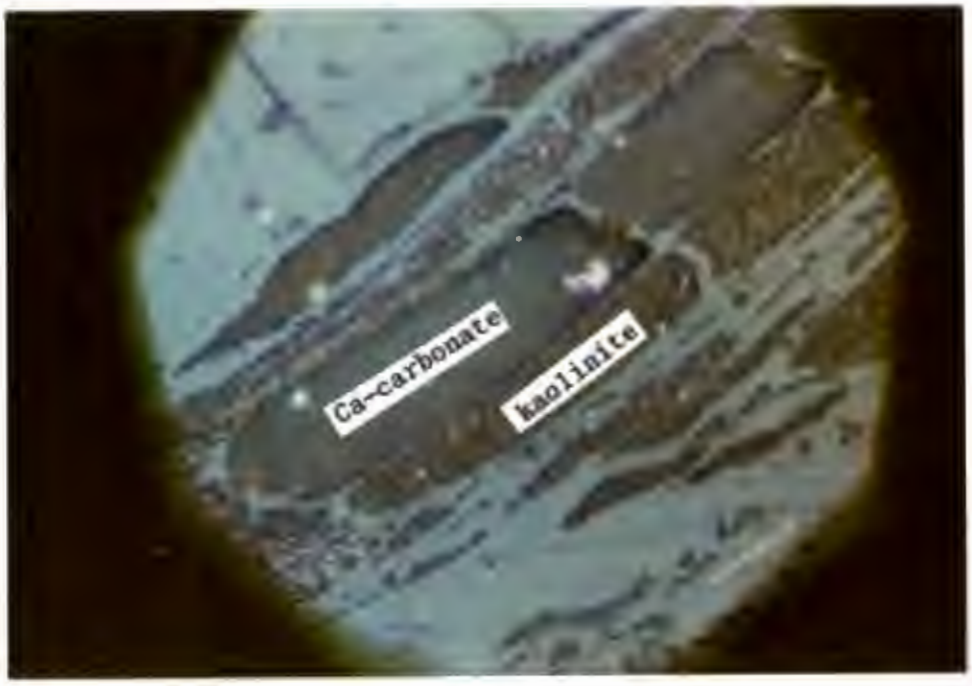

Plate:2 - Ca-carbonate and kaolinite cell-fill in adjacent cells. Note the tiny pyrite crystals within the carbonate and the deformation of the kaolinite filled cells. Reflected white light (RWL), photo long dimension 700 microns.

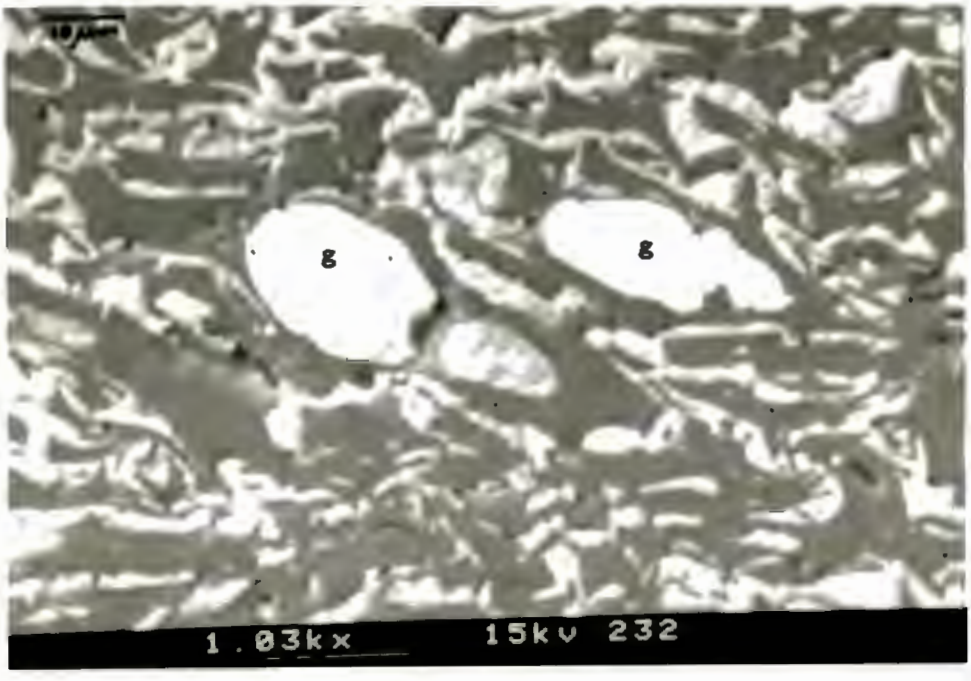

Plate:3a - Gorceixite (g) filling undeformed cells within a massive carbonate. Back-scattered electron image (BSEI) 1030x, 15kV.

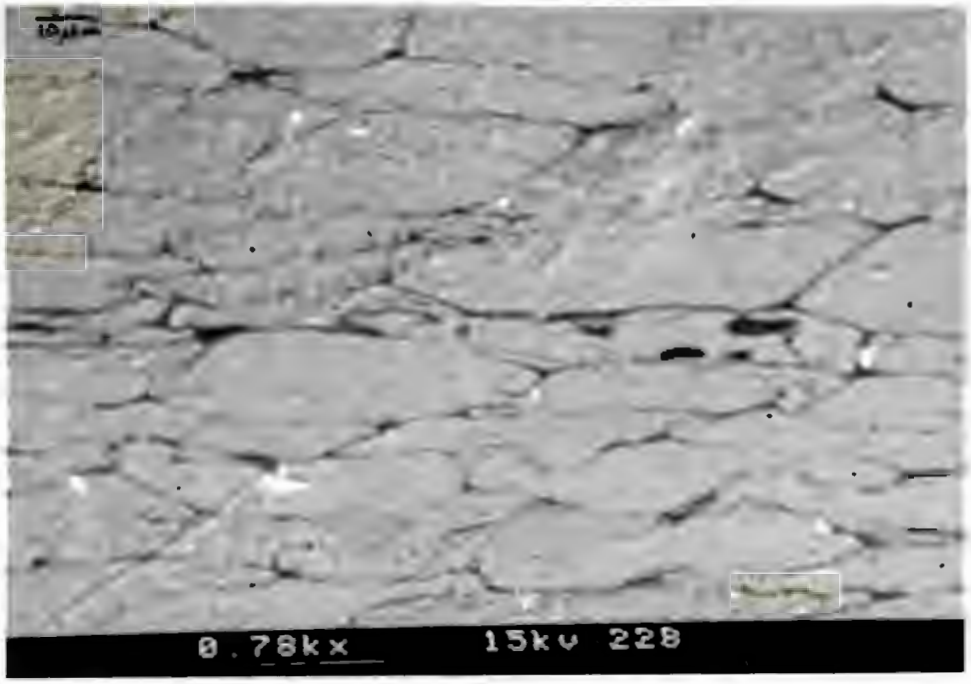

Plate:3b - Kaolinite filling cell lumens. BSEI 780x, 15kV

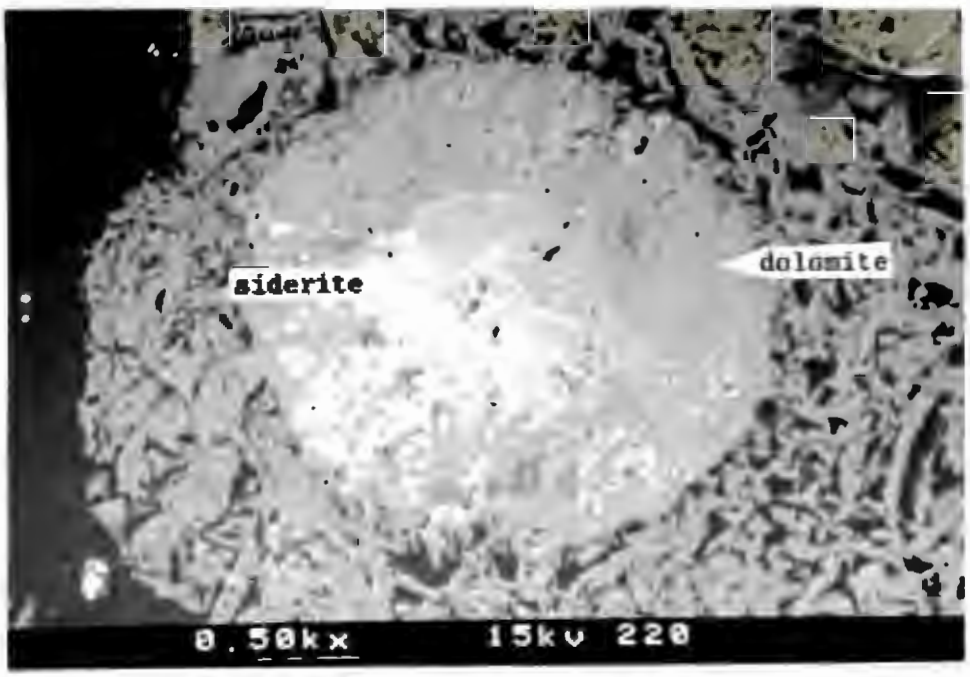

Plate:4 - Sample 39, compositional zoning of an early spherulite. Sideritic centre with dolomitic rim. BSEI, 500x, 15kV.

Plate:5 - Spherulite draped by surrounding organic matter. BSEI, 1020x, 15kV.

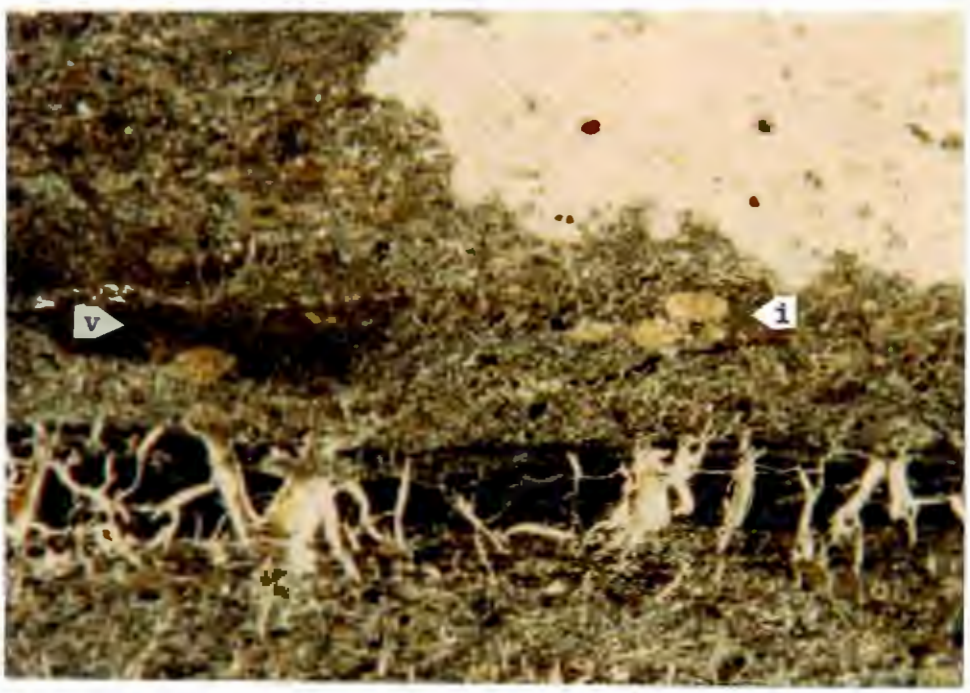

Plate:6 - Sample 12, spherulites in both vitrinite (v), and inertinite (i), RWL, 10x.

Plate:7 - Sample 3 - close association of siderite (s) and kaolinite (k) in a spherulite. BSEI, 770x, 15kV. Siderite identified by SEM-EDS and transmitted light microscopy.

Plate:8 - Tiny apatite grains included in vitrinite. WRL, photo long axis 700 microns.

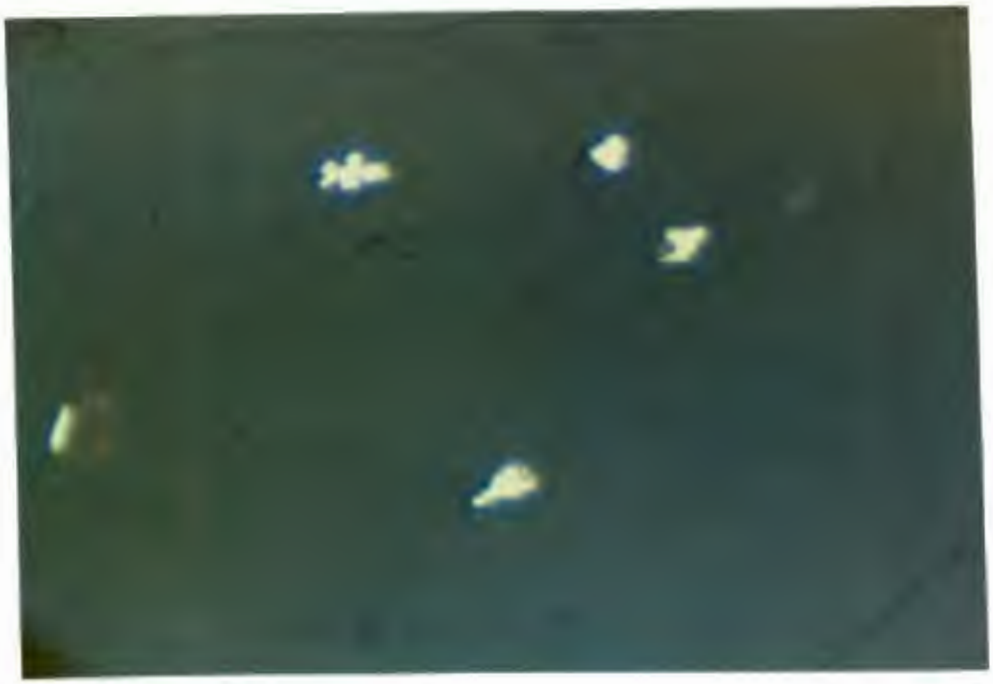

Plate:9 - Pyrite grains included in vitrinite. RWL, photo long axis 700 microns.

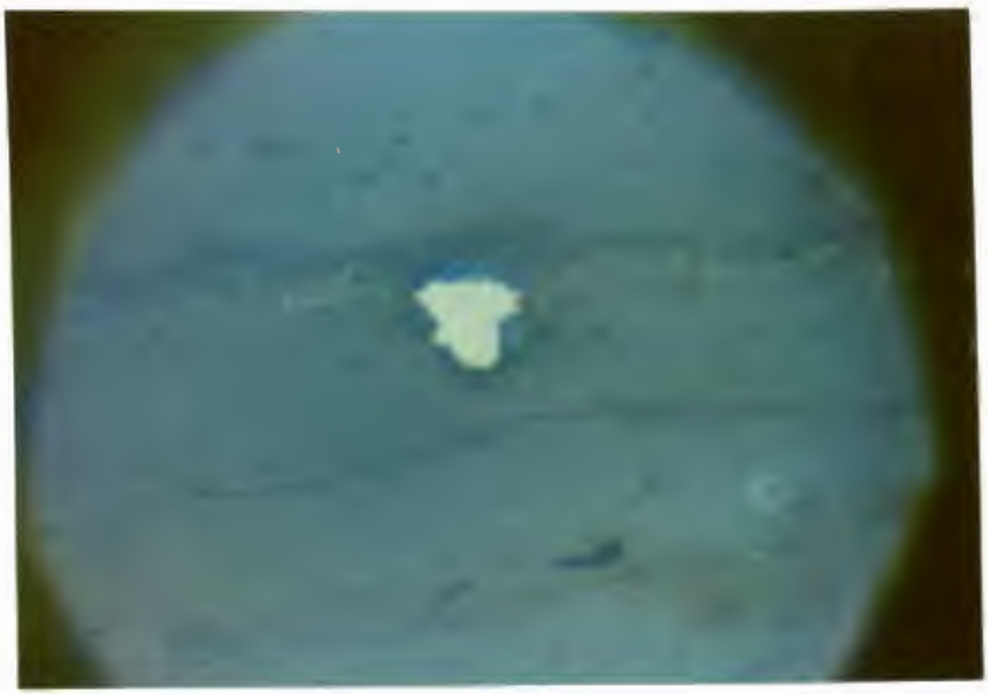

Plate:10 - TiO_2 included in vitrinite. WRL, photo long axis 700 microns.

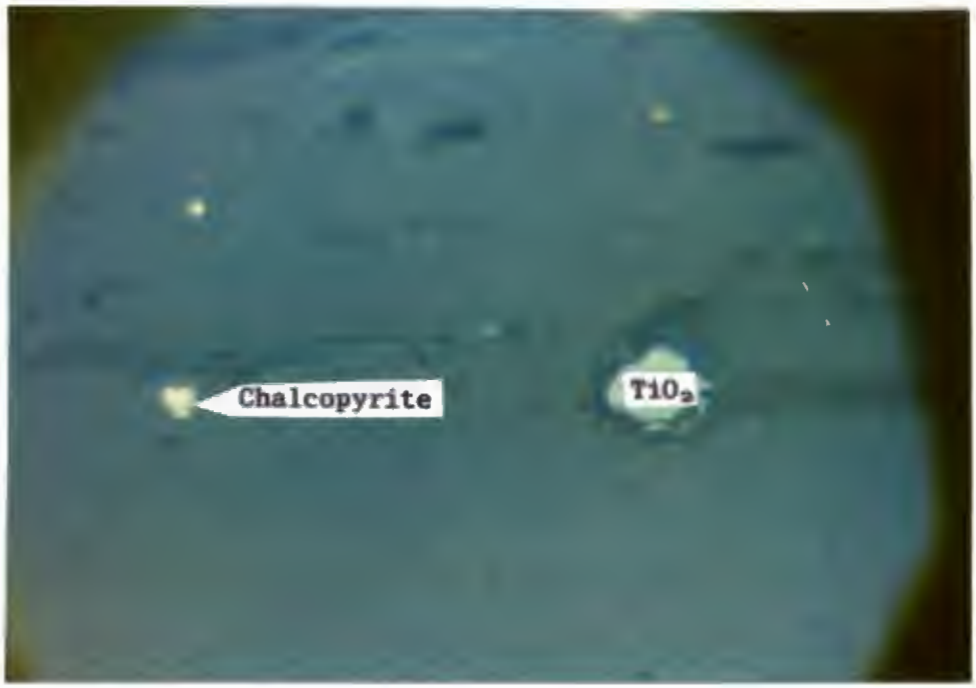

Plate:11 - Chalcopyrite included in vitrinite. WRL, photo long axis 700 microns.

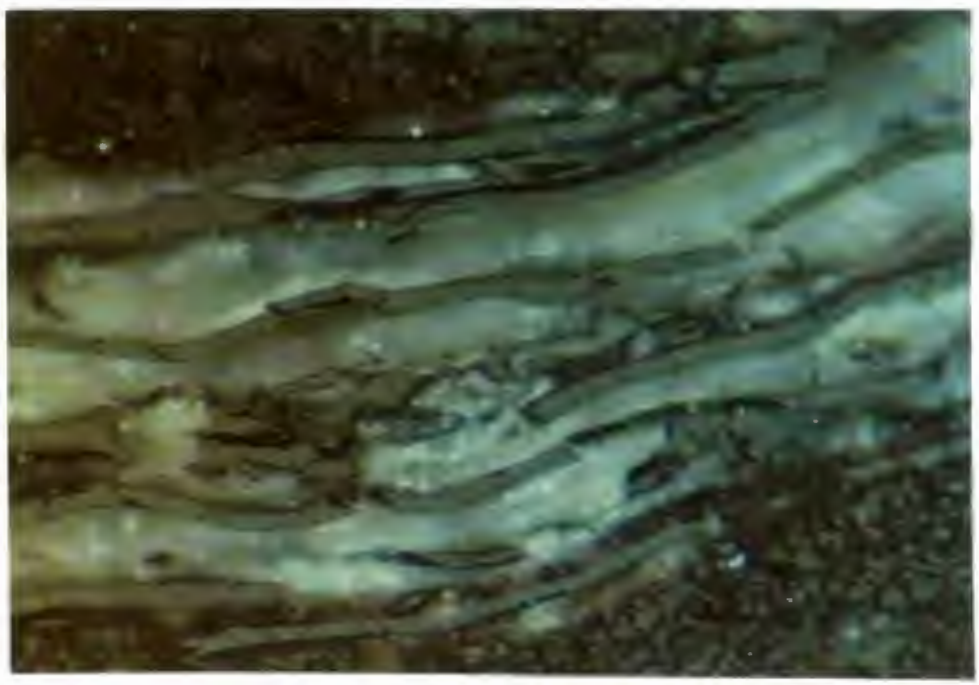

Plate:12 - Non-destructive massive carbonate. WRL, photo long axis 700 microns.

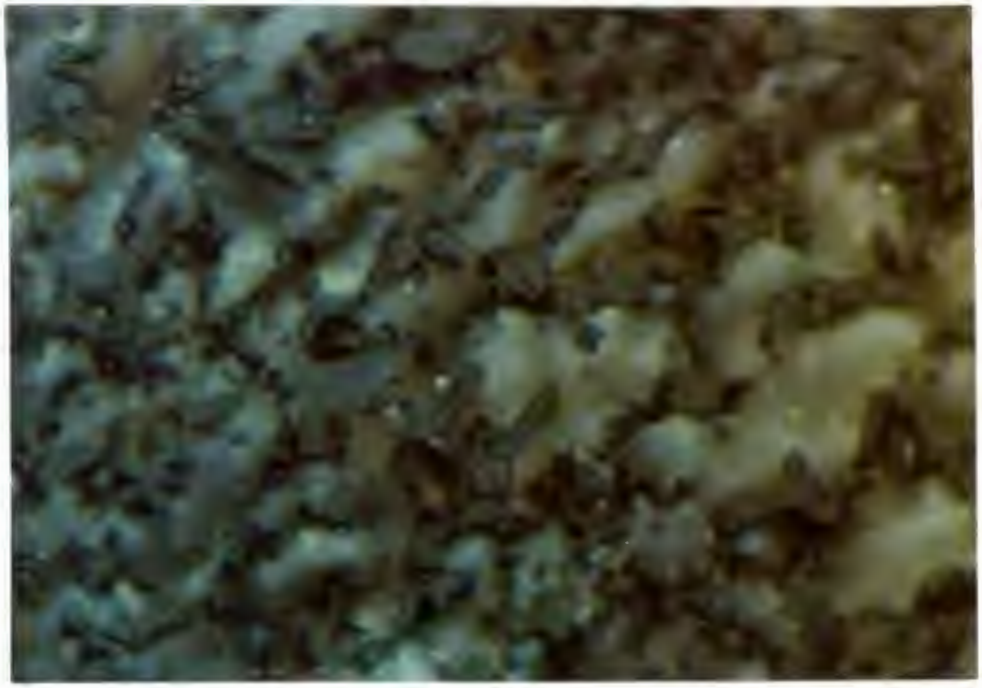

Plate:13 - Destructive massive carbonate. WRL, photo long axis 700 microns.

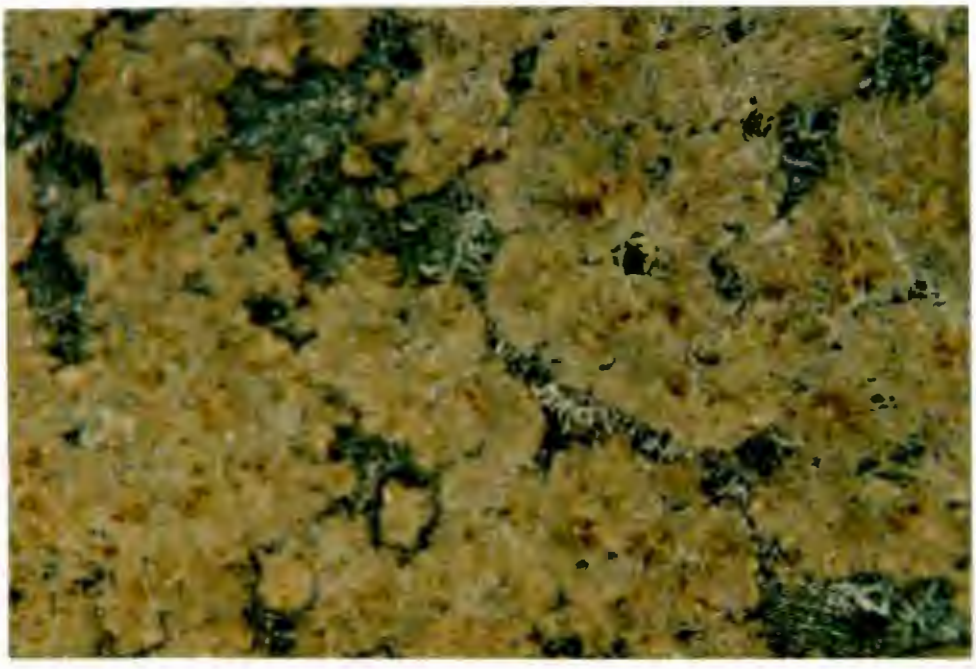

Plate:14 - small authigenic sideritic spherulites forming an amalgamated body (s). WRL, 10x.

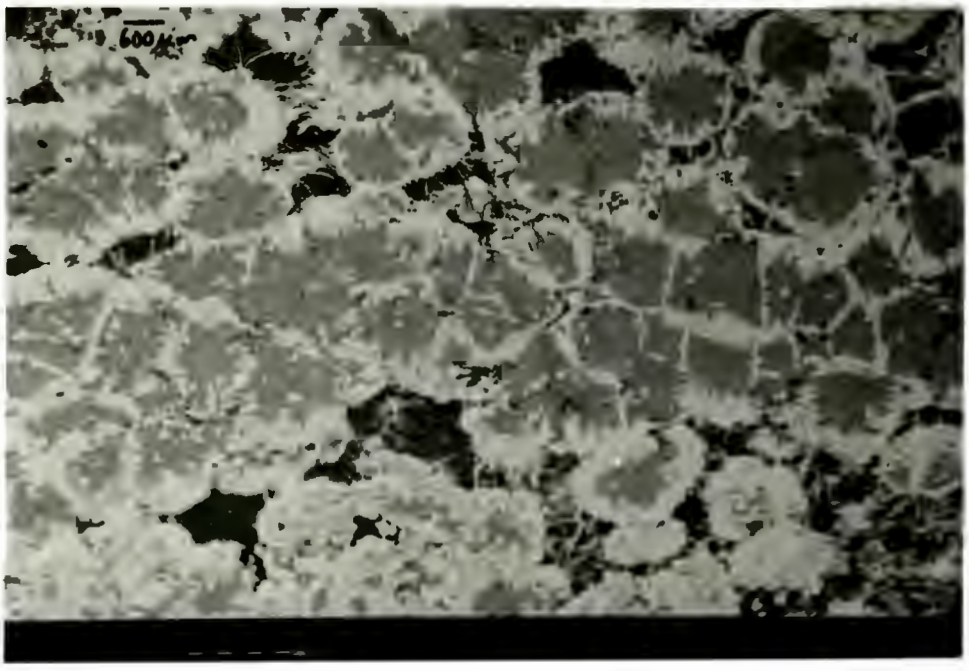

Plate:15 - Small authigenic spherulites with pyrite rims forming an amalgated body. BSEI, 50x, 15kV.

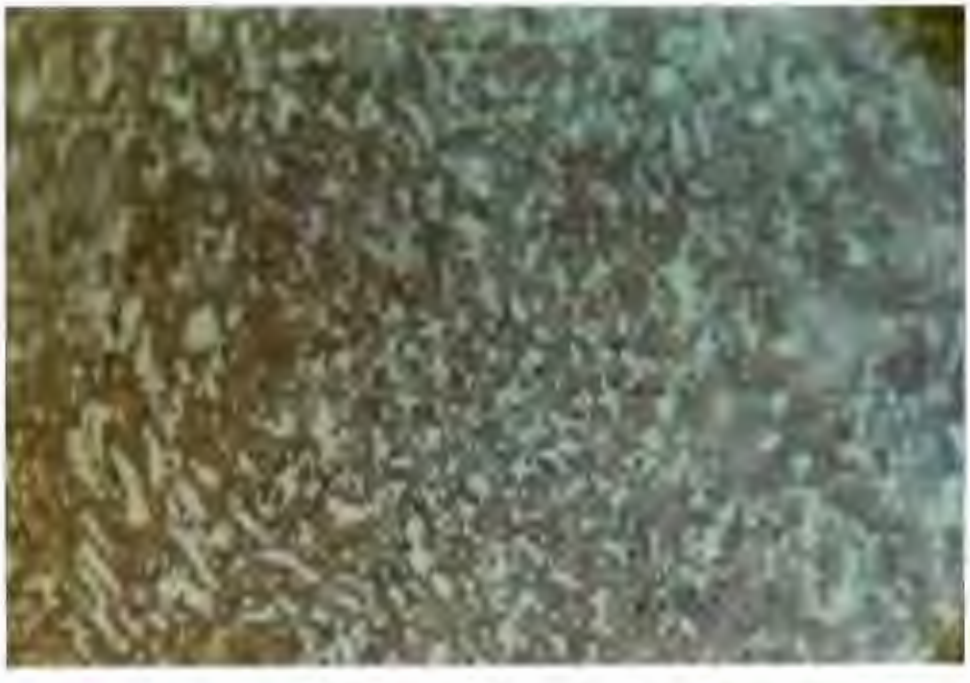

Plate:16 - Destruction of organic matter in a massive carbonate due to either chemical or bacterial attack. WRL, photo long axis 270 microns.

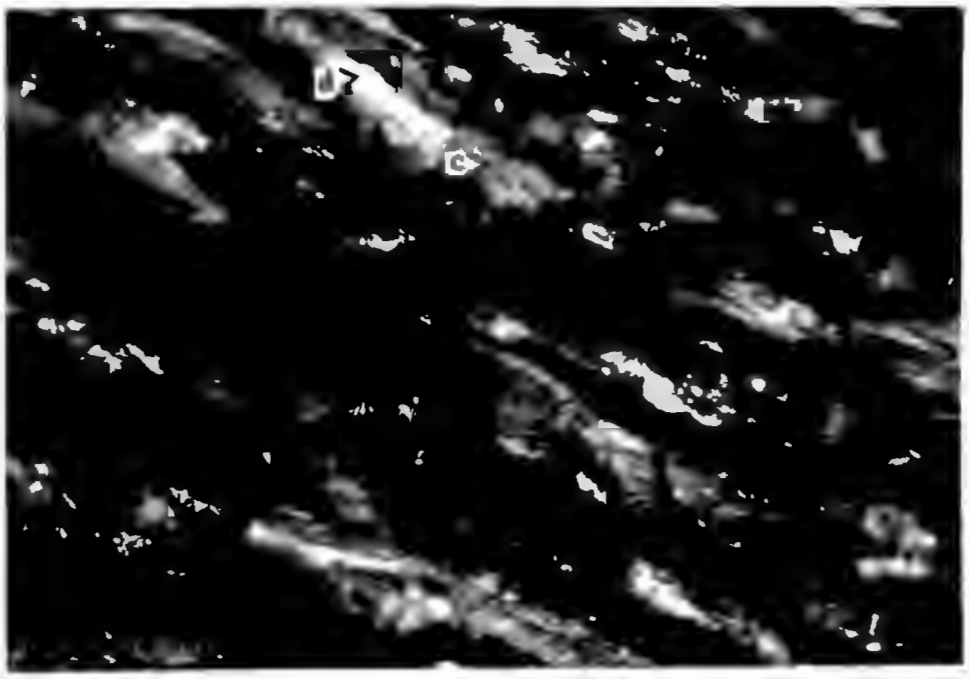

Plate:17 - Dolomite (d), and calcite (c), in close association in a massive carbonate body. White transmitted light, photo long axis 700 microns.

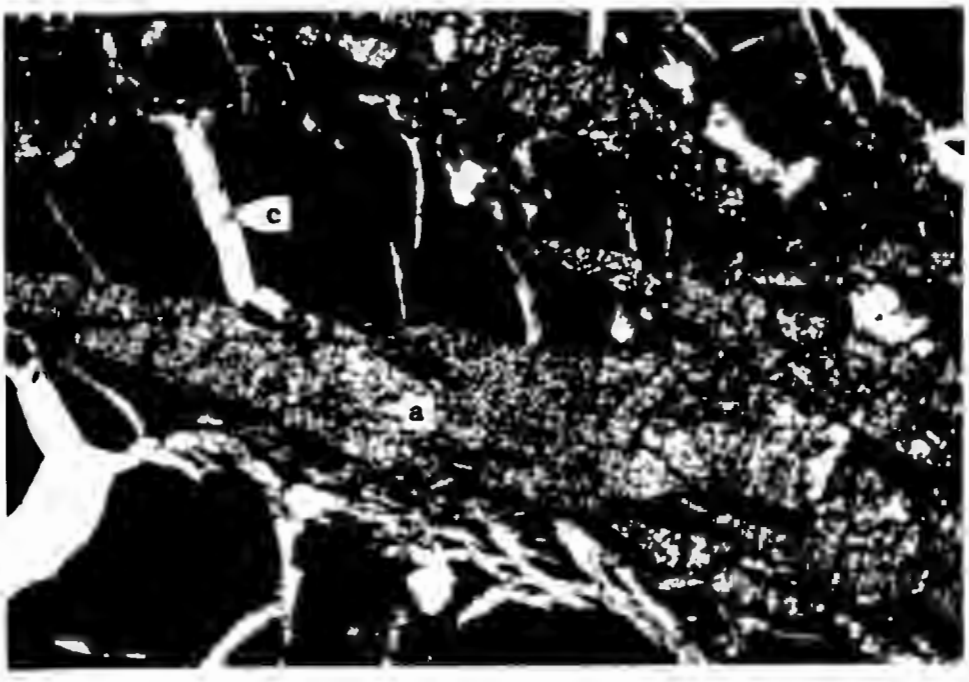

Plate:18 - Aragonitic (stained), massive carbonate with inclusions of vitrinite showing calcite (unstained)filled cleats. Aragonite (a), calcite (c). Transmitted white light, photo long axis 700 microns.

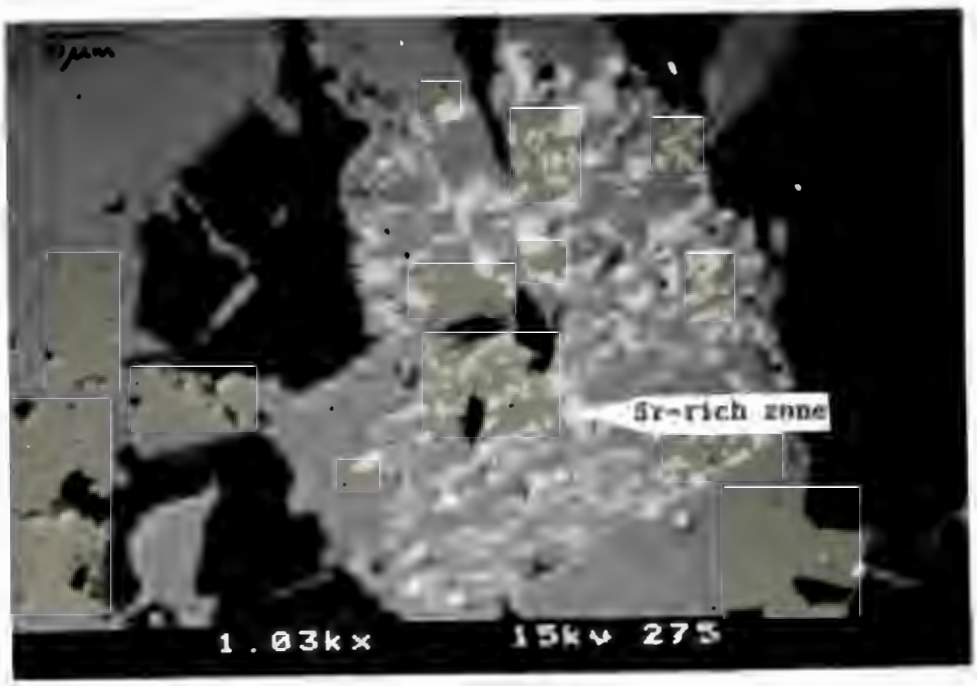

Plate:19 - Sr- rich "exsolution lamellae" in a massive carbonate, sample 35. BSEI, 1030x, 15kV.

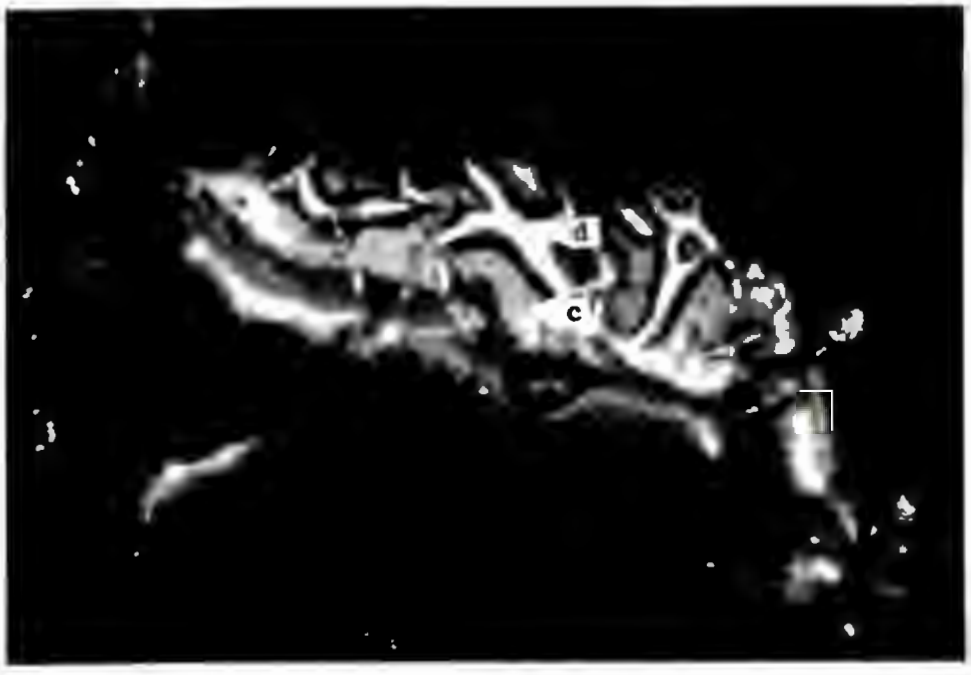

Plate:20 - Calcite (c) and dolomite (d), in cleats. Transmitted white light, photo long axis 700 microns.

Plate:21 - Cleat-fill with edges rich in inclusions of apatite grains. WRL, photo long axis 700 microns.

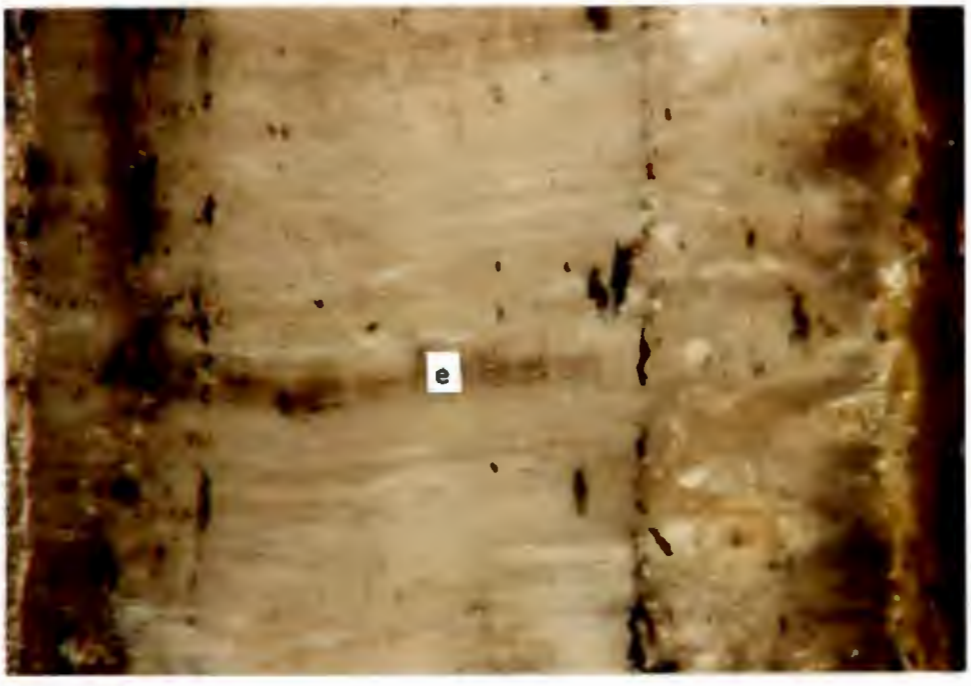

Plate:22 - Exinite (e) stretched across a fracture-filling carbonate. WRL, photo long axis 700 microns.

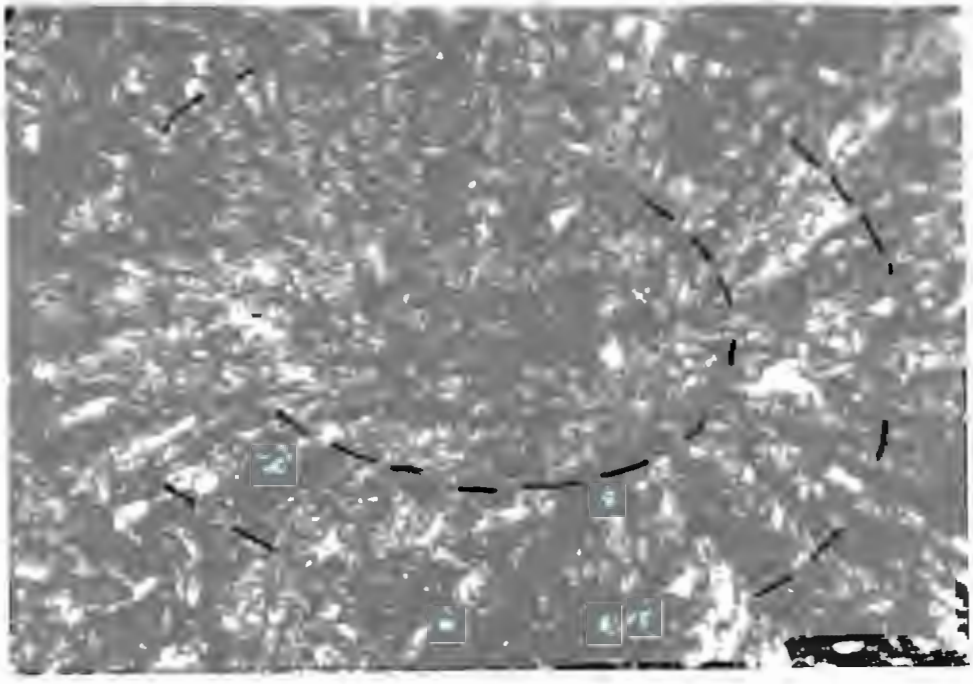

Plate:23 - Ovoid shape in a massive aragonitic carbonate - sample 9. Transmitted white light, photo long axis 700 microns.

APPENDIX E

The occurrence of aragonite in carbonate lenses in coals from the Witbank area

D. van der Spuy

SOEKOR, Pty. Ltd., P.O. Box 307, Parow, 7500,
Republic of South Africa

and

J.P. Willis

Geochemistry Department, University of Cape Town,
Private Bag, Rondebosch, 7700, Republic of South Africa

Abstract

XRD analyses of carbonate lenses from some coal mines in the Witbank area indicate that particular carbonate mineral assemblages are characteristic of carbonate lenses from particular mines. While aragonite is a major mineral in some of these assemblages, it is shown that its presence in small quantities can easily be masked in X-ray diffraction traces by diffraction peaks of other commonly occurring minerals (pyrite, kaolinite, quartz).

XRD-analises van karbonaatlense vanaf enkele steenkoolmyne in die Witbankgebied dui daarop dat definitiewe karbonaat mineraal groepe kenmerkend van karbonaatlense van sekere myne is. Alhoewel aragoniet die hoofmineraal in sommige van hierdie groepe is, word aangetoon dat klein hoeveelhede aragoniet maklik in XRD-spore verberg kan word deur diffraksie pieke van ander minerale wat algemeen teenwoordig is (piriet, kaoliniet, kwarts).

Large lens-shaped carbonate bodies, generally termed "limestones" or "siderites", commonly occur in coal seams in the Witbank area. These bodies range in size from a few centimeters to over a meter in their longest section (parallel to bedding) and may be up to a few tens of centimetres in height. They are generally brownish in colour and are often associated with pyrite and carbonate veins at acute angles to bedding planes. They appear to occur preferentially in particular bands within seams and their relative abundance has been used as an aid in identification of particular bands on some mines.

Thirteen of these lenses, sampled from different localities at Rietspruit, Wolwekrans, Duvha and Arnot mines, were analysed by X-ray diffraction (XRD) to

determine their gross mineral compositions. Reflected light microscopy studies have shown that these lenses consist of mineral phases in intimate textural relationships with organic matter. Textures range from that which appears to be due to violent injection under pressure where plant cell walls are broken and deformed, to that due to non-destructive filling of cell cavities in fusinite-rich coals. It is this intimate relationship of carbonate and organic matter that results in the brownish macroscopic appearance of most of these samples. The results of the XRD analyses are listed in Table 1. Fig. 1 shows XRD traces for samples R4 and R6 together with those for pure calcite and aragonite.

Table 1 here

It is obvious from Table 1 that there is a pattern to the occurrence of carbonate minerals in these lenses that could be due to controls imposed by the environment of mineralisation. Carbonate assemblages for the Arnot and Rietspruit mines include aragonite, calcite and dolomite, while the Wolwekrans and Duvha assemblages contain no aragonite. Siderite occurs in lenses only from Duvha mine. However, in Fig. 2 it can be seen that the macroscopic appearance of aragonite and siderite lenses is very similar, and it is very difficult to distinguish between them in the field.

The unexpected occurrence of aragonite in a number of the samples led to an investigation into the detectability by XRD anlysis of small weight percentages of this mineral in mineral mixtures. In order to evaluate the detectability of aragonite, two quartz-calcite-aragonite mixtures were made up as follows: Mix A consisting of 80% quartz, 10% clean natural calcite and 10% biogenic aragonite (crushed Mactra glabrata shells); and Mix B of 90% quartz and 5% each of calcite and aragonite from the same sources. The XRD traces for these two mixtures are shown in Fig. 3. Separate XRD

scans of pure quartz, aragonite and calcite are superimposed in Fig. 4.

The two strongest aragonite peaks at 3.396 and 3.273 Å d-spacings, (100% and 52% relative intensity (RI), respectively, Brown, 1961) are completely obscured by, and appear as "shoulders" on either side of, the strongest quartz peak at 3.343 Å d-spacing (Figs 3 and 4). The aragonite (012) peak at 2.700 Å (RI = 46%) appears clean but could be masked if significant quantities of pyrite, which has an 84% RI peak at 2.709 Å d-spacing, were present (Fig. 4). The presence of kaolinite and quartz would effectively mask the 1.814 Å d-spacing aragonite peak due to the kaolinite 20% RI 1.810 Å d-spacing peak and the quartz 17% RI 1.817 Å d-spacing peak. Thus, it can be seen that all of the characteristic aragonite peaks are effectively masked by the presence of quartz, kaolinite and pyrite. Kaolinite and quartz are the two most commonly occurring minerals in Witbank coals, with pyrite an important accessory mineral. It is obvious from Figures 3 and 4 that the presence of these minerals would make the detection of small amounts of aragonite very difficult.

The visual differentiation between aragonite and calcite in hand specimens is very difficult, if not impossible. The simplest means of identifying the presence of aragonite is by XRD analysis, or optical microscopic examination of thin sections which is seldom done for coals. It has been shown that the presence of aragonite peaks in XRD scans of coals may be easily missed due to masking by peaks of more abundant minerals.

It is suggested, therefore, that aragonite may be a more commonly occurring mineral in coals, albeit in restricted areas, than has previously been thought. We suspect that many of the carbonate lenses in S.A. coal mines, that have in the past been glibly and visually identified as siderite (on the basis of their brown colouration) or calcite, may in fact often have been aragonitic. Indeed, since the brown colour of many of these

lenses is due not to the presence of iron oxides but to an intimate relationship between calcium carbonate and organic matter, many of the lenses visually identified as sideritic may in fact consist of calcium carbonate. The controls on the formation of aragonite in coal deposits and its implications for the evaluation of diagenetic environments require further study.

Reference

Brown, G., Ed. (1961) The X-ray diffraction and crystal structures of clay minerals, Mineralogical Society, London, 544pp.

TABLE 1 Mineral assemblages in carbonate lenses from coals in the Witbank area, as shown by XRD analysis.

SAMPLE	MINE	MINERALS PRESENT
A1	Arnot	Aragonite + trace calcite
R1	Rietspruit	Calcite
R3	Rietspruit	Calcite + trace dolomite
R4	Rietspruit	Aragonite, calcite, pyrite
R5	Rietspruit	Calcite + trace dolomite
R6	Rietspruit	Aragonite + calcite
W1	Wolwekrans	Calcite
W2	Wolwekrans	Calcite + dolomite
W3	Wolwekrans	Pyrite + calcite
W4	Wolwekrans	Calcite + dolomite
D1	Duvha	Siderite, pyrite, calcite
D2	Duvha	Siderite, pyrite, calcite
D3	Duvha	Calcite

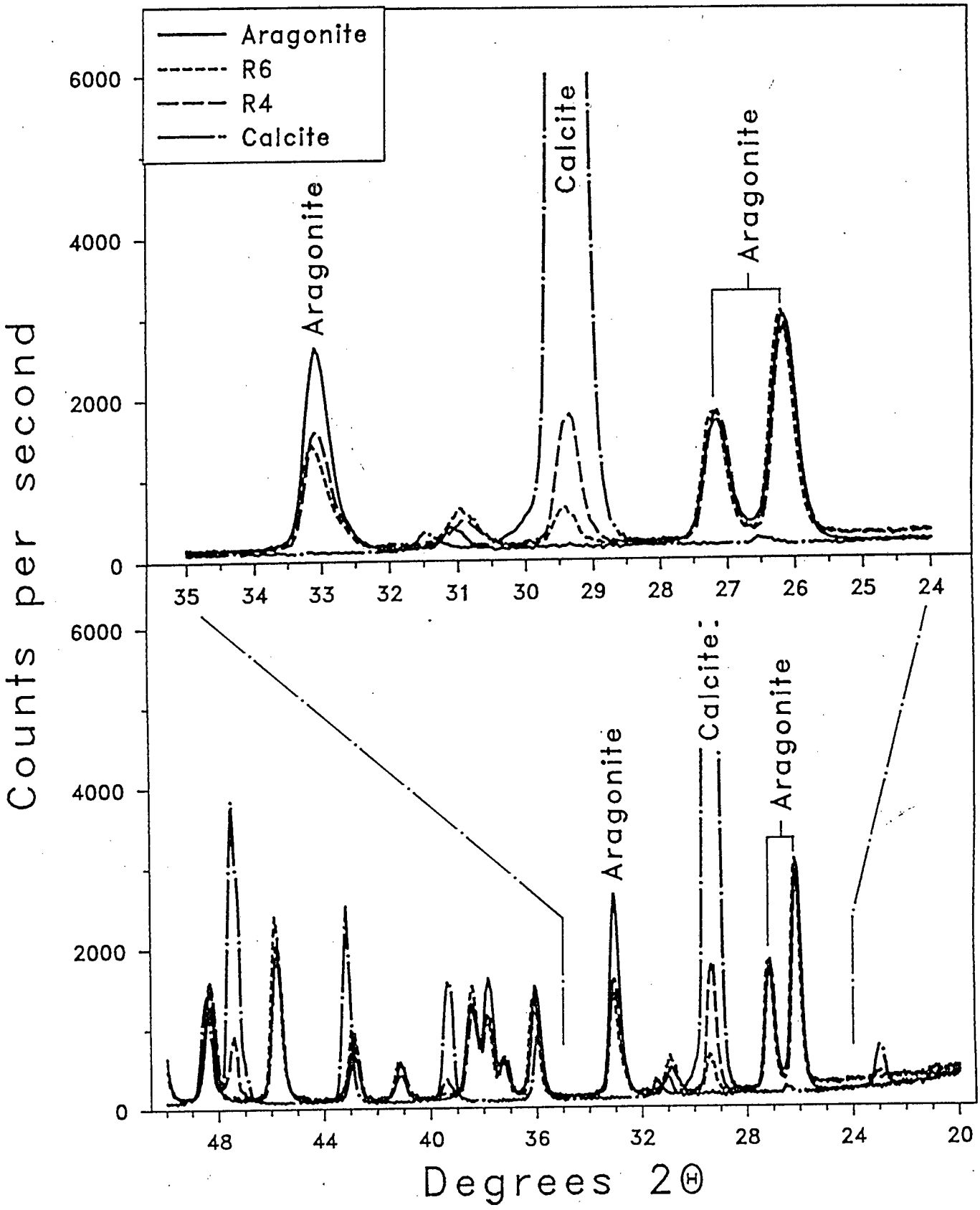

Figure 1. XRD traces for samples R4 and R6 together with those for pure calcite and aragonite.

Figure 2: See plates 1b (aragonite) and 1a (siderite) of main work.

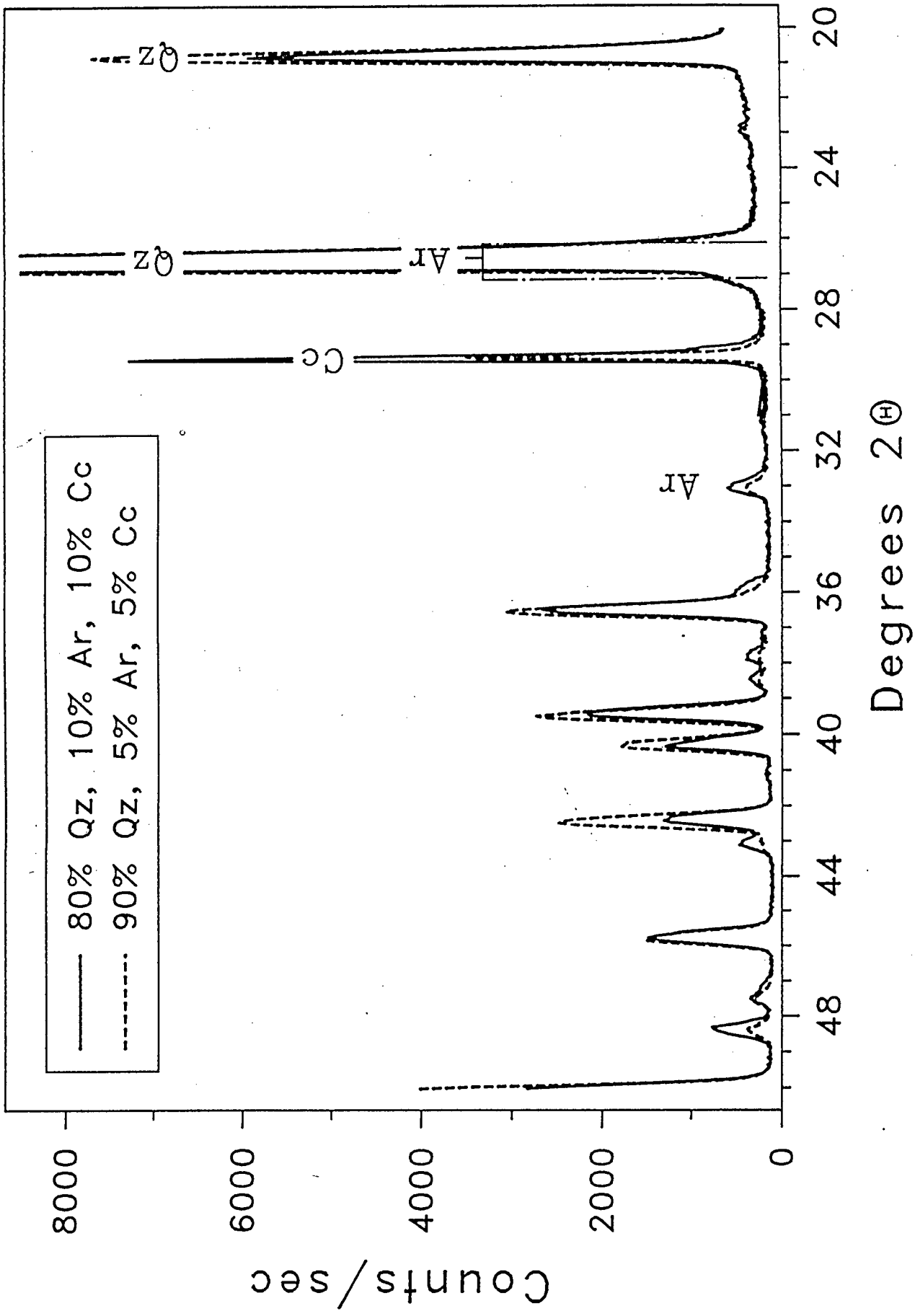

Figure 3. XRD traces for Mix A (80% quartz, 10% calcite, 10% aragonite and Mix B (90% quartz, 5% calcite, 5% aragonite).

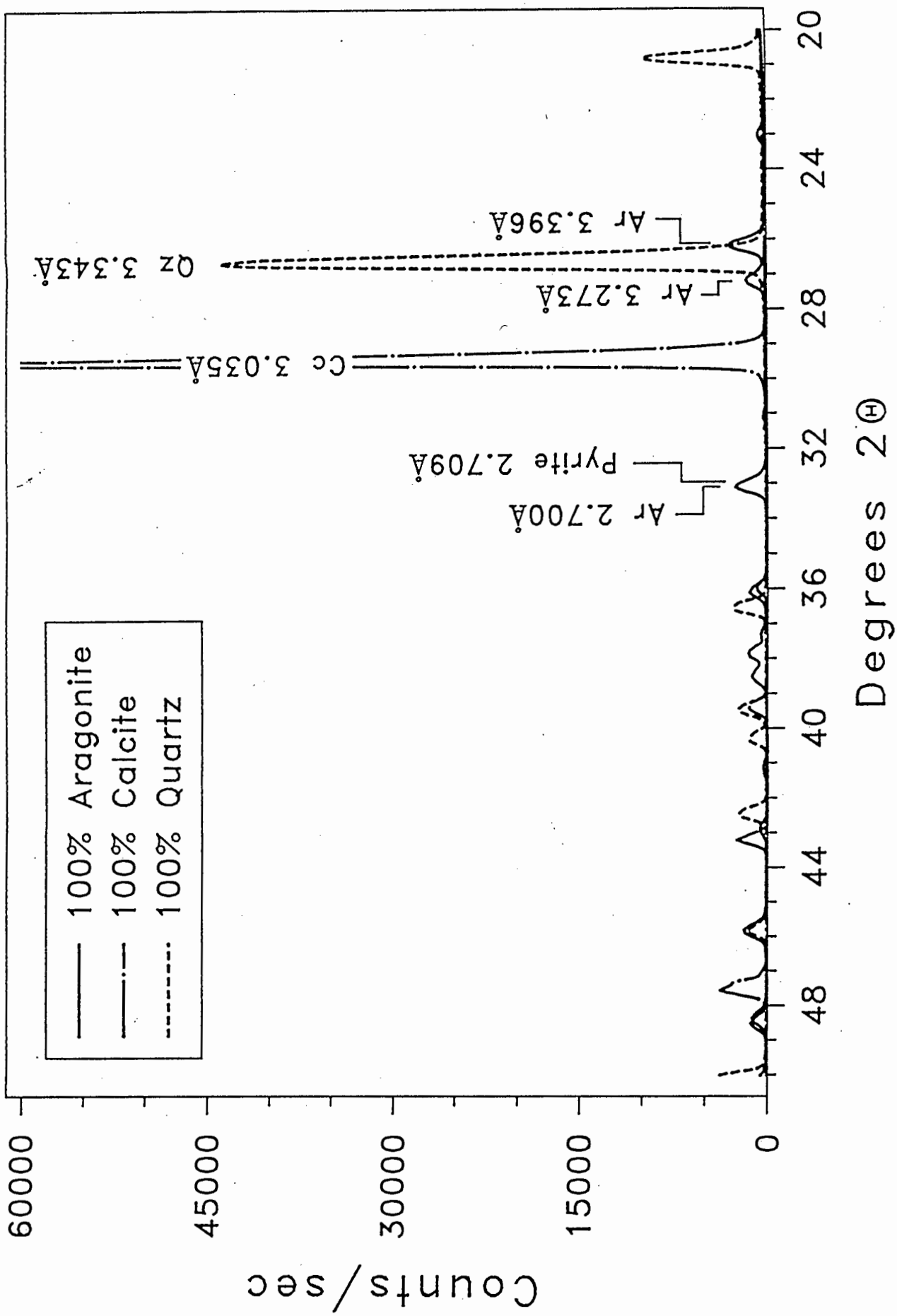

Figure 4. XRD traces for calcite, quartz and aragonite. Note how aragonite peaks are masked by peaks from other minerals.